

**NBSIR 73-415**

# **Noble Metal Constitution Diagrams: Part II**

---

R. M. Waterstrat and R. C. Manuszewski

Institute for Materials Research  
National Bureau of Standards  
Washington, D. C. 20234

Final Report September 1973

Issued August 1975

Prepared for  
**American Dental Association Research Unit  
at the National Bureau of Standards,  
Washington, D. C. 20234**



U.S. DEPT. OF COMM. BIBLIOGRAPHIC DATA SHEET	1. PUBLICATION OR REPORT NO.  NBSIR 73-415	2. Gov't Accession No.	3. Recipient's Accession No.
4. TITLE AND SUBTITLE  Noble Metal Constitution Diagrams: Part II		5. Publication Date	6. Performing Organization Code
7. AUTHOR(S) R. M. Waterstrat and R. C. Manuszewski		8. Performing Organ. Report No.	
9. PERFORMING ORGANIZATION NAME AND ADDRESS  NATIONAL BUREAU OF STANDARDS DEPARTMENT OF COMMERCE WASHINGTON, D.C. 20234		10. Project/Task/Work Unit No. 3110585	11. Contract/Grant No. DE02455
12. Sponsoring Organization Name and Complete Address (Street, City, State, ZIP) American Dental Association 211 East Chicago Avenue Chicago, Illinois 60611		13. Type of Report & Period Covered	14. Sponsoring Agency Code
15. SUPPLEMENTARY NOTES			
<p>16. ABSTRACT (A 200-word or less factual summary of most significant information. If document includes a significant bibliography or literature survey, mention it here.)</p> <p>Six binary constitution diagrams involving the noble metals are presented. These diagrams include the V-Ru, V-Rh, Nb-Os, Nb-Pd, Nb-Pt and Ta-Pd alloy systems.</p> <p>Experimental alloys were prepared from starting materials having a nominal purity of at least 99.9% and precautions were taken to insure that no significant contamination was introduced during alloy preparation and heat-treatment. Temperatures were measured to an accuracy within <math>\pm 20^{\circ}\text{C}</math>.</p>			
<p>17. KEY WORDS (six to twelve entries; alphabetical order; capitalize only the first letter of the first key word unless a proper name; separated by semicolons)</p> <p>Alloy phases; constitution diagrams; phase diagrams; phase equilibria; platinum group metals; noble metals</p>			
<p>18. AVAILABILITY <input type="checkbox"/> Unlimited</p> <p><input checked="" type="checkbox"/> For Official Distribution. Do Not Release to NTIS</p> <p><input type="checkbox"/> Order From Sup. of Doc., U.S. Government Printing Office Washington, D.C. 20402, SD Cat. No. C13</p> <p><input type="checkbox"/> Order From National Technical Information Service (NTIS) Springfield, Virginia 22151</p>		<p>19. SECURITY CLASS (THIS REPORT)</p> <p>UNCLASSIFIED</p>	<p>21. NO. OF PAGES</p> <p>170</p>
		<p>20. SECURITY CLASS (THIS PAGE)</p> <p>UNCLASSIFIED</p>	<p>22. Price</p>



NBSIR 73-415

**NOBLE METAL CONSTITUTION DIAGRAMS:  
PART II**

---

R. M. Waterstrat and R. C. Manuszewski

Institute for Materials Research  
National Bureau of Standards  
Washington, D. C. 20234

Final Report September 1973

Issued August 1975

Prepared for  
American Dental Association Research Unit  
at the National Bureau of Standards,  
Washington, D. C. 20234



---

**U.S. DEPARTMENT OF COMMERCE, Rogers C.B. Morton, *Secretary***  
**James A. Baker, III, *Under Secretary***  
**Dr. Betsy Ancker-Johnson, *Assistant Secretary for Science and Technology***  
**NATIONAL BUREAU OF STANDARDS, Ernest Ambler, *Acting Director***



SEPTEMBER 28, 1973

NOBLE METAL CONSTITUTION DIAGRAMS: PART II<sup>†</sup>

by

R. M. Waterstrat and R. C. Manuszewski\*

This investigation is supported by Grant DE02455 to the American Dental Association by the National Institute of Dental Research and is part of the dental research program conducted by the National Bureau of Standards in cooperation with the American Dental Association, the National Institute of Dental Research and the Dental Research Division of the U. S. Army Medical Research and Development Command.

† Noble Metal Constitution Diagrams, Part I, was issued April 20, 1971 as NBS Report 10571.

\* Research Associates, American Dental Association Research Program in the Dental Research Section, National Bureau of Standards, Washington, D. C. 20234.

NBS PROGRESS REPORT 73-415

NOBLE METAL CONSTITUTION DIAGRAMS :  
PART II

R. M. Waterstrat and R. C. Manuszewski

SEPTEMBER 1973

Performed under  
NIDR Research Grant DE02455 to  
the American Dental Association.

Conducted at the  
National Bureau of Standards  
Washington, D. C. 20234

## FOREWORD

This investigation was supported primarily by Research Grant DE02455 to the American Dental Association from the National Institute of Dental Research. The research was conducted at the National Bureau of Standards during the period from September 1, 1970 to August 31, 1973.

The electron probe microanalyses of two-phase alloys was performed at the National Bureau of Standards by Mrs. Martha Darr, Mr. Robert Myklebust and Mr. Charles Fiore under the direction of Dr. Kurt Heinrich.

Constitution diagrams for the binary Nb-Pd, Nb-Pt and Ta-Pd systems are partially based on unpublished experimental data which was generously made available to us by Prof. B. C. Giessen of Northeastern University, Boston, Mass.

Earlier work in this research program, conducted under the same Research Grant, is reported in NBS Report 10571 dated April 20, 1971.

## ABSTRACT

Six binary constitution diagrams involving the noble metals are presented. These diagrams include the V-Ru, V-Rh, Nb-Os, Nb-Pd, Nb-Pt and Ta-Pd alloy systems.

Experimental alloys were prepared from starting materials having a nominal purity of at least 99.9% and precautions were taken to insure that no significant contamination was introduced during alloy preparation and heat-treatment. Temperatures were measured to an accuracy within  $\pm 20^{\circ}\text{C}$ .

## TABLE OF CONTENTS

	<u>Page No.</u>
I. SUMMARY . . . . .	1
A. Constitution Diagrams . . . . .	1 and 2
B. Experimental Method . . . . .	3
II. INTRODUCTION . . . . .	5
A. Background . . . . .	5
B. Experimental Approach . . . . .	6
III. VANADIUM-RUTHENIUM CONSTITUTION DIAGRAM . . . . .	10
A. Previous Studies. . . . .	10
B. Materials. . . . .	10
C. Alloy Preparation . . . . .	11
D. Temperature Measurement . . . . .	11
E. Thermal Treatments . . . . .	13
F. Methods for Determination of Phase Boundaries. . . . .	14
G. Experimental Results . . . . .	16
H. Discussion. . . . .	24
REFERENCES. . . . .	25
IV. VANADIUM-RHODIUM CONSTITUTION DIAGRAM. . . . .	26
A. Previous Studies. . . . .	26
B. Materials. . . . .	26
C. Alloy Preparation . . . . .	26
D. Temperature Measurement . . . . .	28
E. Thermal Treatments . . . . .	28
F. Methods for Determination of Phase Boundaries. . . . .	30
G. Experimental Results. . . . .	31
H. Discussion. . . . .	44
REFERENCES. . . . .	51

## TABLE OF CONTENTS (Cont'd)

	Page No.
V. NIOBIUM-OSMIUM CONSTITUTION DIAGRAM . . . . .	53
A. Previous Studies . . . . .	53
B. Materials . . . . .	53
C. Alloy Preparation . . . . .	55
D. Temperature Measurement . . . . .	56
E. Thermal Treatments. . . . .	57
F. Methods for Determination of Phase Boundaries . . . .	59
G. Experimental Results. . . . .	62
H. Discussion. . . . .	73
REFERENCES. . . . .	77
VI. NIOBIUM-PALLADIUM CONSTITUTION DIAGRAM . . . . .	79
A. Previous Studies. . . . .	79
B. Materials. . . . .	80
C. Alloy Preparation . . . . .	81
D. Temperature Measurement . . . . .	81
E. Thermal Treatments. . . . .	82
F. Methods for Determination of Phase Boundaries. . . .	84
G. Experimental Results. . . . .	85
H. Discussion. . . . .	97
REFERENCES. . . . .	102

## TABLE OF CONTENTS (Cont'd)

	Page No.
VII. NIOBIUM-PLATINUM CONSTITUTION DIAGRAM . . . . .	104
A. Previous Studies. . . . .	104
B. Materials. . . . .	105
C. Alloy Preparation . . . . .	105
D. Temperature Measurement . . . . .	106
E. Thermal Treatments . . . . .	106
F. Methods for Determination of Phase Boundaries. . . . .	107
G. Experimental Results . . . . .	109
H. Discussion . . . . .	118
REFERENCES. . . . .	122
VIII. TANTALUM-PALLADIUM CONSTITUTION DIAGRAM. . . . .	123
A. Previous Studies. . . . .	123
B. Materials. . . . .	124
C. Alloy Preparation . . . . .	124
D. Temperature Measurement . . . . .	125
E. Thermal Treatments . . . . .	125
F. Methods for Determination of Phase Boundaries. . . . .	127
G. Experimental Results . . . . .	128
H. Discussion. . . . .	139
REFERENCES. . . . .	143
APPENDIX I. METALLOGRAPHIC PROCEDURES . . . . .	144
APPENDIX II. X-RAY DIFFRACTION PROCEDURES . . . . .	146
APPENDIX III. ELECTRON MICROPROBE ANALYSIS. . . . .	148
APPENDIX IV. ATOMIC VOLUME RELATIONSHIPS. . . . .	150

## LIST OF ILLUSTRATIONS

<u>Figure</u>	<u>Page No.</u>
1. Constitution diagrams of V-Ru, V-Rh, Nb-Os and Nb-Pd. . . . .	1
2. Constitution diagrams of Nb-Pt and Ta-Pd. . . . .	2
3. Vanadium-Ruthenium constitution diagram. . . . .	17
4. Microstructures of vanadium-ruthenium alloys . . . . .	19
5. Microstructures of vanadium-ruthenium alloys . . . . .	22
6. Microstructures of vanadium-ruthenium alloys . . . . .	23
7. Vanadium-Rhodium constitution diagram . . . . .	32
8. Microstructures of vanadium-rhodium alloys. . . . .	35
9. Microstructures of vanadium-rhodium alloys. . . . .	36
10. Microstructures of vanadium-rhodium alloys . . . . .	37
11. Microstructures of vanadium-rhodium alloys. . . . .	39
12. Microstructures of vanadium-rhodium alloys. . . . .	40
13. Microstructures of vanadium-rhodium alloys. . . . .	42
14. Niobium-Osmium constitution diagram . . . . .	61
15. Microstructures of niobium-osmium alloys . . . . .	68
16. Microstructures of niobium-osmium alloys . . . . .	71
17. Microstructures of niobium-osmium alloys . . . . .	72

## LIST OF ILLUSTRATIONS

<u>Figure</u>	<u>Page No.</u>
18. Niobium-Palladium constitution diagram. . . . .	86
19. Microstructures of niobium-palladium alloys . . .	88
20. Microstructures of niobium-palladium alloys . . .	89
21. Microstructures of niobium-palladium alloys . . .	90
22. Microstructures of niobium-palladium alloys . . .	91
23. Microstructures of niobium-palladium alloys . . .	95
24. Microstructures of niobium-palladium alloys . . .	96
25. Niobium-Platinum constitution diagram . . . . .	110
26. Microstructures of niobium-platinum alloys . . .	112
27. Microstructures of niobium-platinum alloys . . .	113
28. Microstructures of niobium-platinum alloys . . .	116
29. Microstructures of niobium-platinum alloys . . .	117
30. Tantalum -Palladium constitution diagram . . . . .	129
31. Microstructures of tantalum -palladium alloys . .	131
32. Microstructures of tantalum-palladium alloys . .	133
33. Microstructures of tantalum-palladium alloys . .	134
34. Microstructures of tantalum-palladium alloys . .	135
35. Microstructures of tantalum-palladium alloys . .	137
36. Microstructure of a tantalum -palladium alloy . .	138

## LIST OF ILLUSTRATIONS

	<u>Page No.</u>
37. Atomic volumes of V-Ru alloys . . . . .	151
38. Atomic volumes of V-Rh alloys . . . . .	152
39. Atomic volumes of Nb-Os alloys . . . . .	153
40. Atomic volumes of Nb-Pd alloys . . . . .	154
41. Atomic volumes of Nb-Pt alloys . . . . .	155
42. Atomic volumes of Ta-Pd alloys . . . . .	156

## LIST OF TABLES

<u>TABLE</u>	<u>Page No.</u>
1. Typical Analyses of the Materials Used in Preparing the Experimental Alloys . . . . .	12
2. Summary of Equilibration Treatments for Vanadium-Ruthenium Alloys. . . . .	14
3. Lattice Parameters of V-Ru Alloys . . . . .	20
4. Typical Analyses of the Materials Used in Preparing the Experimental Alloys . . . . .	27
5. Schedule of Typical Heat Treatments for Vanadium-Rhodium . . . . .	29
6. Relative Intensities (I) and Interplaner Spacings (d) for $\alpha$ 3 Phase Lines Compared with Equivalent Values Reported for the Phase $\alpha$ VIr <sup>(5)</sup> . . . . .	46 & 47
7. Invariant Reactions in the Vanadium-Rhodium System . . . . .	48
8. Crystallographic Data for Vanadium-Rhodium Intermediate Phases . . . . .	49
9. Lattice Parameters of Intermediate Phases and Terminal Solid Solutions for Vanadium-Rhodium .	50
10. Typical Analyses of the Materials Used in Preparing the Experimental Alloys . . . . .	54
11. Summary of Typical Equilibration Treatments for Niobium-Osmium Alloys . . . . .	58
12. Crystallographic Data for Niobium-Osmium Intermediate Phases . . . . .	63

## LIST OF TABLES

<u>TABLE</u>	<u>Page No.</u>
13. Lattice Parameters of Intermediate Phases and Terminal Solid Solutions for Niobium-Osmium. . . . .	64
14. Observed and Calculated Relative Intensities for Nb <sub>36</sub> Os <sub>64</sub> $\chi$ -Phase . . . . .	65, 66 & 67
15. Comparison of Site Occupancies for the $\chi$ , $\sigma$ and $\beta$ Phases . . . . .	75
16. Typical Equilibration Treatments for Niobium-Palladium Alloys . . . . .	83
17. Crystallographic Data for Niobium-Palladium Intermediate Phases . . . . .	100
18. Lattice Parameters of Intermediate Phases and Terminal Solid Solutions for Niobium-Palladium . . . . .	101
19. Typical Equilibration Treatments for Niobium-Platinum Alloys . . . . .	108
20. Crystallographic Data for Niobium-Platinum Intermediate Phases . . . . .	120
21. Lattice Parameters of Intermediate Phases and Terminal Solid Solutions for Niobium-Platinum . . . . .	121
22. Typical Equilibration Treatments for Tantalum-Palladium Alloys . . . . .	126
23. Crystallographic Data for Tantalum-Palladium Intermediate Phases . . . . .	141
24. Lattice Parameters of Intermediate Phases and Terminal Solid Solutions for Tantalum -Palladium . . . . .	142

# I. SUMMARY

## A. Constitution Diagrams

The constitution diagrams which have been determined are presented in Figures 1 and 2.

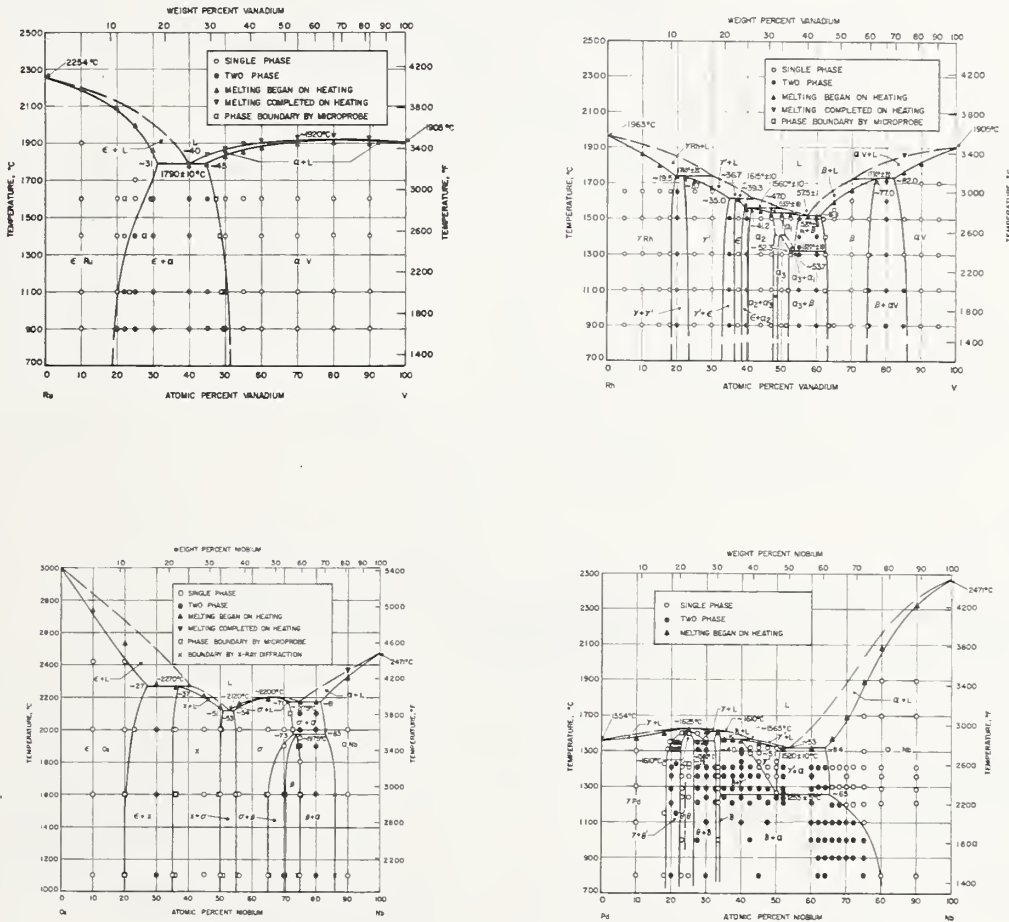


Fig. 1 - Constitution diagrams of vanadium-ruthenium; vanadium-rhodium; niobium-osmium; and niobium-palladium.

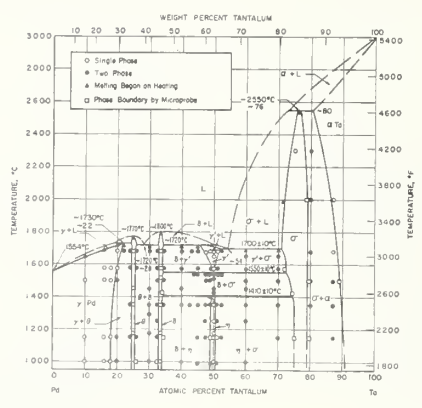
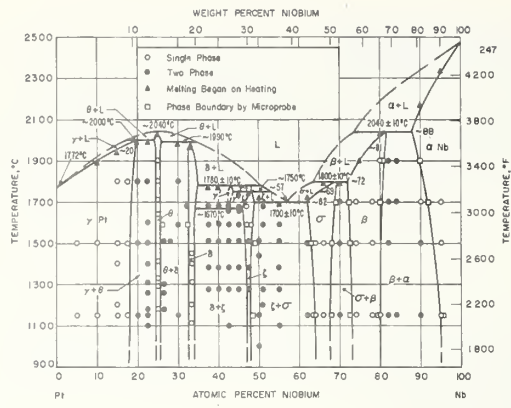


Fig. 2 - Constitution diagrams of niobium-platinum and tantalum-palladium.

## B. Experimental Method

### 1. Materials

The purity of all the starting materials used in this study was at least 99.9%. This purity was considered to be adequate to insure a reliable constitution diagram within the accuracy limits imposed by uncertainties in temperature and composition measurements.

### 2. Alloy Preparation

The experimental alloys were prepared by non-consumable arc-melting of the pure metals. The pure metals were submitted to melting in various forms. Vanadium was in the form of electrolytic dendrites which were compacted into 1/2-inch diameter cylinders of the appropriate weight. Mixed powders of niobium, tantalum, ruthenium, osmium and rhodium were compressed into 1/2-inch diameter cylinders. Platinum and palladium were in the form of 1/32-inch sheets cut to an appropriate size.

### 3. Composition Determination

The primary method of establishing the compositions of the experimental alloys was by monitoring weight changes at various stages of the alloy preparation. In addition, compositions were checked by wet chemical analysis, electron probe microanalysis, and lattice parameter measurements whenever these techniques were appropriate.

### 4. Temperature Measurement

Temperatures below 1500°C were measured using platinum versus platinum-10% rhodium thermocouples. Temperatures between 1500°C and 2200°C were measured using tungsten versus

tungsten-26% rhenium thermocouples. These thermocouples were calibrated against a standard platinum-6% rhodium versus platinum-30% rhodium thermocouple up to 1600°C. The standard thermocouple had been calibrated at the National Bureau of Standards. Secondary melting point standards were used to check the calibration of the tungsten versus tungsten-26% rhenium thermocouples at higher temperatures and to assist in extrapolating a furnace current versus temperature plot. The secondary melting point standards were high purity wires of nickel, platinum, rhodium, and iridium. The accuracy of the temperature measurements was believed to be within  $\pm 20^\circ\text{C}$ .

## 5. Phase Boundary Determinations

a. Solidus - A solidus technique was used which allows direct observation of a melting specimen and permits one to obtain its temperature reliably.<sup>(6)</sup> This technique was suitable for solidus determinations in alloys which melt congruently or are close to a eutectic composition. It is also reliable for alloys having a relatively small temperature increment between their solidus and liquidus temperatures. For other alloys, the technique of metallographic examination of quenched alloys to detect incipient fusion is a more accurate method and was used to supplement the method of direct observation.

b. Phase Boundaries - The methods used to locate phase boundaries include metallographic examination, x-ray diffraction studies, and electron probe microanalysis of equilibrated two-phase alloys. In each case the specimens were rapidly cooled or quenched from the equilibration temperature. The methods used detect changes in microstructure, crystal structure, and chemical composition which occur when an alloy is equilibrated at various temperatures or when its composition is varied at a fixed temperature.

## II. INTRODUCTION

### A. Background

This report terminates the investigation of some ten binary phase diagrams. The research program was a continuation of a previous investigation<sup>(9)</sup> of phase relationships among binary alloys containing a noble metal (i. e. , those metals which are exceptionally resistant to chemical corrosion or oxidation, such as gold and metals of the platinum group).

The existing metallurgical literature concerning binary or ternary constitution diagrams still contains only a relatively small percentage of alloy combinations involving the noble metals. The restricted industrial usage of the noble metals due to their limited availability and high cost may partly account for the scarcity of constitution diagrams. Another deterrent to such studies is the prohibitive cost of experimental samples, which should be of a sufficient number and size to permit measurements having the desired accuracy. It is probably not surprising, therefore, that the available noble metal constitution diagrams are sometimes inaccurate and in a few cases may even be considered to be essentially incorrect.

The importance of obtaining reliable constitution diagrams is widely recognized among those who are familiar with their uses. These diagrams may be directly used to predict equilibrium phase relationships and alloy microstructures for any given conditions of temperature, pressure, and alloy composition. With training and experience it is also possible to use these diagrams to predict the non-equilibrium microstructures which are produced when the alloy is cast, heat-treated, or subjected to various mechanical operations such as forging, drawing, rolling, etc. The existing microstructure is a highly important factor in determining the physical properties of an alloy.

The constitution diagram may be used to reveal other useful information. It is of considerable importance to know the temperature at which an alloy begins to melt (solidus temperature).

A knowledge of the solidus temperature permits one to estimate recovery temperatures, recrystallization temperatures, and the rates of atomic diffusion during annealing treatments. Accurate constitution diagrams may be used to determine various thermodynamic functions since the slopes of the phase boundaries are related to free energy relationships between the coexisting phases. Constitution diagrams are also helpful in studying the kinetics of phase transformations.

In recent years, there has been a considerable effort by alloy theorists to develop methods for predicting the extent of terminal solid solutions and the occurrence of intermediate phases having various crystal structures. Some attempts have been made to construct the entire binary constitution diagram on the basis of theoretical calculations. It appears that significant progress is being made in this direction, but such studies must continue to rely on experimental data in order to check the reliability of the theoretical calculations and to suggest new ways to improve their accuracy.

## B. Experimental Approach

In order to obtain reliable experimental data, it is necessary to take many precautions during the preparation and examination of the experimental alloys. Starting materials should be of high purity and care must be taken to insure that the alloys are not contaminated during melting or heat-treating. Particular attention must be given to the problems of temperature measurement and composition determination since the accuracy of these measurements is a major factor in the production of a reliable constitution diagram.

Temperatures below 1500°C were measured with platinum versus platinum-10% rhodium thermocouples because of the

high accuracy and reproducibility associated with this type of thermocouple. These thermocouples were periodically checked for accuracy against a standard platinum-6% rhodium versus platinum-30% rhodium thermocouple which had been calibrated at the National Bureau of Standards to 1600°C.

Temperatures above 1600°C are usually measured with an optical pyrometer, but this method did not yield satisfactory results in this study due to the formation of metallic films on the viewing windows. These films formed quite rapidly during the relatively brief time necessary for a temperature measurement, particularly when the experimental alloys contained chromium. It was impossible to make reliable corrections for this film absorption even by using a two-color pyrometer. Difficulties were also encountered in obtaining black-body radiation from within the hot zone of the furnace at a position which would yield a temperature corresponding to that of the experimental samples. Cylindrical black-bodies were fabricated of tantalum and designed to produce the necessary depth to diameter ratios, but it was found that these objects were unavoidably positioned within rather sharp temperature gradients and were, therefore, not at the uniform temperature which is essential for such black-body radiators.

In view of these difficulties with optical pyrometry, it was necessary to consider using high-temperature thermocouples for measuring the temperature between 1500°C and 2200°C. This method entails the risk of introducing errors due to thermocouple contamination by metal vapors. Metal vapors, in some cases, may even penetrate the refractory ceramics normally used to insulate the thermocouple, and for this reason it was decided to obtain thermocouples having an outer metallic sheath. Sheathed thermocouples are commercially available in a variety of sizes and also

with several alternative combinations of ceramic insulators and metallic sheaths. The combination selected as being most suitable under the conditions of this investigation was a tungsten versus tungsten-26% rhenium thermocouple insulated with beryllium oxide and having a tantalum sheath. The size of the thermocouple wires was 0.005" diameter and the entire assembly was enclosed in a sheath having a diameter of 0.040", thus minimizing errors due to heat conduction along the axis of the thermocouple.

The tungsten versus tungsten-26% rhenium thermocouples were calibrated against the standard platinum-6% rhodium versus platinum-30% rhodium thermocouple to 1600° C under the same experimental conditions used in the actual measurements on the alloy samples. Simultaneous readings of current in the furnace heating elements were obtained during the calibration runs so that a plot of temperature versus current was also obtained. This plot could be extended to higher temperatures with the help of standard emf versus temperature data for the tungsten versus tungsten-26% rhenium thermocouples, together with secondary fixed points obtained by observing the melting of high purity wires of nickel (1455° C), platinum (1772° C), rhodium (1963° C), and iridium (2447° C). In addition, many experimental runs were accompanied by an appropriate determination of a secondary fixed point obtained just prior to the temperature determination. This procedure is explained in greater detail in reference 6.

Alloy compositions were checked at various stages throughout this investigation. Considerable reliance was placed in the use of electron probe microanalysis to determine the compositions of coexisting phases in equilibrated two-phase alloys. In order to check the reliability of the probe data, however, it is

desirable to submit certain alloys to a complete wet chemical analysis. Alloys selected for this purpose were given a homogenization anneal at a temperature intended to produce a single phase sample. The compositions selected in each system were usually close to the equiatomic composition. The alloys were checked for homogeneity using the electron probe and then submitted to wet chemical analysis. The result of this chemical analysis was used not only to check the probe data, but also to check the nominal composition of the alloy and the feasibility of determining alloy compositions by monitoring weight losses during melting. Careful consideration was given to the possibility of alloy contamination during melting and annealing. Metallographic studies, particularly at the surfaces of the experimental samples, were quite helpful in detecting contamination.

Many other difficulties were encountered which posed a continual challenge to the success of these studies. Some of these problems are common to all such investigations while others are unique to a particular alloy system. These problems are discussed in connection with each system.

### III. VANADIUM-RUTHENIUM CONSTITUTION DIAGRAM

#### A. Previous Studies

Vanadium-ruthenium alloys have been studied in several previous investigations<sup>(1-3)</sup> but the information provided by these studies is still insufficient to permit the construction of a constitution diagram. A phase having a CsCl-type ordered structure has been observed in V-Ru alloys containing 54 to 75 at. % V and a tetragonal distortion of this structure has been observed very close to the equiatomic composition<sup>(1-3)</sup>. It is not known whether these structures form directly from the liquid state or whether they are produced by a solid-state reaction during cooling. The observation of banded microstructures at the equiatomic composition suggests a possible martensitic transformation.

Recent studies<sup>(3, 4)</sup> have revealed sharp changes in certain physical properties of vanadium-ruthenium alloys in the vicinity of the equiatomic composition. These anomalies were observed in measurements of the electronic specific heat coefficient<sup>(4)</sup>, superconducting transition temperature<sup>(4)</sup>, magnetic susceptibility<sup>(3)</sup>, NMR Knight shift<sup>(3, 5)</sup>, and electrical resistivity<sup>(3)</sup>. It has been reported that the transformation from the cubic (CsCl-type) structure to the tetragonal structure accompanies these anomalies at a critical temperature,  $T_k$ , which depends sensitively on the alloy composition<sup>(3)</sup>. The following investigation was undertaken in order to help clarify the phase relationships in the vanadium-ruthenium alloy system and to provide a constitution diagram.

#### B. Materials

The vanadium metal used in this study was obtained from the U.S. Bureau of Mines, Boulder City Metallurgy Research

Laboratory through the courtesy of Mr. T. A. Sullivan. The metal was in the form of electrolytic dendrites having a nominal purity of 99.95%. A typical analysis of the starting materials is shown in Table 1.

The ruthenium metal was in the form of powder or sponge and was obtained from Johnson-Matthey Chemicals Limited. Its purity was nominally 99.999%. The impurities detected by spectrographic analysis are shown in Table 1.

### C. Alloy Preparation

Carefully weighed amounts of each starting material were compressed in a 1/2-inch diameter cylindrical steel mold to produce small cylinders suitable for arc-melting. Each sample weighed 10 grams and was arc-melted at least four times in an atmosphere of 50% helium and 50% argon. Weight losses after melting were in all cases less than 1% and it was therefore assumed that the actual compositions of the samples were reasonably close to the intended compositions. This assumption was later verified for some of the alloys by electron-beam microanalyses.

### D. Temperature Measurement

A platinum versus platinum-10% rhodium thermocouple was used to measure temperatures up to 1500° C. This thermocouple and a standard platinum-6% rhodium versus platinum-30% rhodium thermocouple were used to obtain data on temperature versus furnace current in a high-vacuum furnace. The standard thermocouple had been calibrated on the International Practical Temperature Scale of 1968 (IPTS 68). Calibration was also made against

Table 1

Typical Analyses of the Materials Used in  
Preparing the Experimental Alloys<sup>+</sup>

Impurity	Vanadium	Ruthenium
	U. S. Bureau of Mines	Johnson-Matthey
C	80	-
Ca	ND	1
Cr	60	ND
Cu	32	<1
Fe	135	2
H	10	-
Mg	ND	<1
N	35	-
Na	ND	2
O	220	-
Si	ND	3

+ Values are given in ppm.

ND Not detected spectrographically.

No other elements were detected spectrographically.

secondary standards such as the melting temperatures of pure gold, nickel, platinum and rhodium. Temperatures above 1500<sup>o</sup>C were established by extrapolating the furnace current versus temperature plot through the points indicated by the secondary standards and then setting the furnace current to the appropriate value.

## E. Thermal Treatments

All alloys were homogenized by annealing at 1600° C for 6 hours except the alloy  $\text{Ru}_{90}\text{V}_{10}$  which was homogenized at 1900° C for 6 hours.

The homogenization treatments were carried out using all the precautions normally taken during an equilibration treatment and the samples were therefore considered as being equilibrated at the homogenization temperature. Equilibration annealing treatments subsequent to the initial homogenization were carried out consecutively at progressively decreasing temperatures.

The annealing was done in a tantalum-strip resistance furnace operating at pressures between  $5 \times 10^{-6}$  and  $5 \times 10^{-7}$  mm Hg. The samples were suspended in tantalum buckets using Ta wire. There was no detectable contamination revealed by subsequent electron probe studies. Samples annealed in this furnace were rapidly cooled by turning off the power to the heating elements. This cooling rate was not always rapid enough to prevent precipitation of lower-temperature phases but the structures formed could be readily identified. Thus, information on the prior high-temperature phases derived from these structures could be reliably deduced.

A summary of the equilibration treatments used for the various samples is shown in Table 2.

Table 2

Summary of Equilibration Treatments  
for Vanadium-Ruthenium Alloys

Temperatures (°C)	Time	Alloys (atomic %Ru)
1900	6 hrs	90
1700	3 hrs	80
1600	6 hrs	10, 20, 30, 40, 45, 50, 55, 60, 70, 75, 78, 80, 90
1400	1 day	10, 20, 30, 40, 50, 60, 70, 75, 78, 80, 90
1100	1 month	10, 20, 30, 40, 45, 50, 55, 60, 70, 75, 78, 80, 90
900	2 months	10, 20, 30, 40, 45, 50, 55, 60, 70, 75, 78, 80, 90

F. Methods for Determination of Phase Boundaries

1. Solidus Temperatures

The solidus temperatures of our alloys were determined by observations of incipient melting in alloys annealed at various temperatures above and below the solidus temperature. Metallographic examination was used to detect evidence of melting for some of the experimental alloys while in other cases it was possible to locate the solidus temperature with reasonable accuracy by direct observation of the sample during heating. This latter method has been described in detail in reference 6 and is a rather effective technique when working in the vicinity of the eutectic compositions or when the solidus and liquidus are

separated only by a small temperature interval as is the case for most of the V-Ru alloys. In most of our alloys, a sharp melting was observed at a fairly discrete temperature and the solidus temperature is therefore thought to be located with reasonable accuracy as indicated on the diagram of Fig. 3.

Losses of metal during a solidus determination were not excessive. The samples were supported in high-purity thoria crucibles during the solidus determinations and there was no appreciable reaction between the metal samples and the crucibles at the temperatures involved.

The temperatures indicated by our thermocouples during a solidus determination were in good agreement with temperatures deduced by reference to a plot of furnace current versus temperature provided that care was taken to insure that all operating conditions corresponded closely to those which prevailed during our calibration of furnace current versus temperature.

## 2. Liquidus Temperatures

The liquidus temperatures were not determined directly but were estimated from the general form of the solidus curves and the location of invariant reactions. Our metallographic examination of solidus samples was also helpful in locating the liquidus through the application of well known principles associated with the lever law. This was done by estimating the relative amounts of residual solid and chilled liquid phases in the microstructures of the partially melted alloys.

## 3. Other Phase Boundaries

The boundaries of intermediate phases were determined by metallographic studies of alloys annealed at tempera-

tures which would place them in close proximity to the boundary being determined. Alloys annealed within two-phase regions were particularly helpful in determining the location of phase boundaries. By estimating the relative amount of each phase in the microstructure and then applying the lever rule one can estimate the approximate location of the phase boundaries. This is particularly true if one of these boundaries is already known from some independent prior observations.

In some cases it was possible to determine the solid-state phase boundaries by quantitative electron probe microanalyses of two-phase ( $\epsilon + \alpha$ ) alloys annealed at various temperatures. The two-phase alloys, however, were not always reliable for electron probe microanalyses due to the presence of a fine precipitate in both the  $\epsilon$  phase and the  $\alpha$  phase regions. These precipitates apparently form during cooling. For these samples, therefore, the primary reliance was placed on metallographic studies in locating the phase boundaries.

## G. Experimental Results

### 1. General

The proposed constitution diagram for the vanadium-ruthenium system is shown in Fig. 3. All alloys were examined by x-ray diffraction or metallographic methods or both and the data obtained by the different methods were in good agreement. Quantitative electron probe microanalysis was rather helpful in locating the boundary of the  $\alpha$  and  $\beta$  phase regions but served only to set an upper limit on the solubilities of these phases at lower temperatures due to the presence of a fine precipitate in each phase. The electron beam

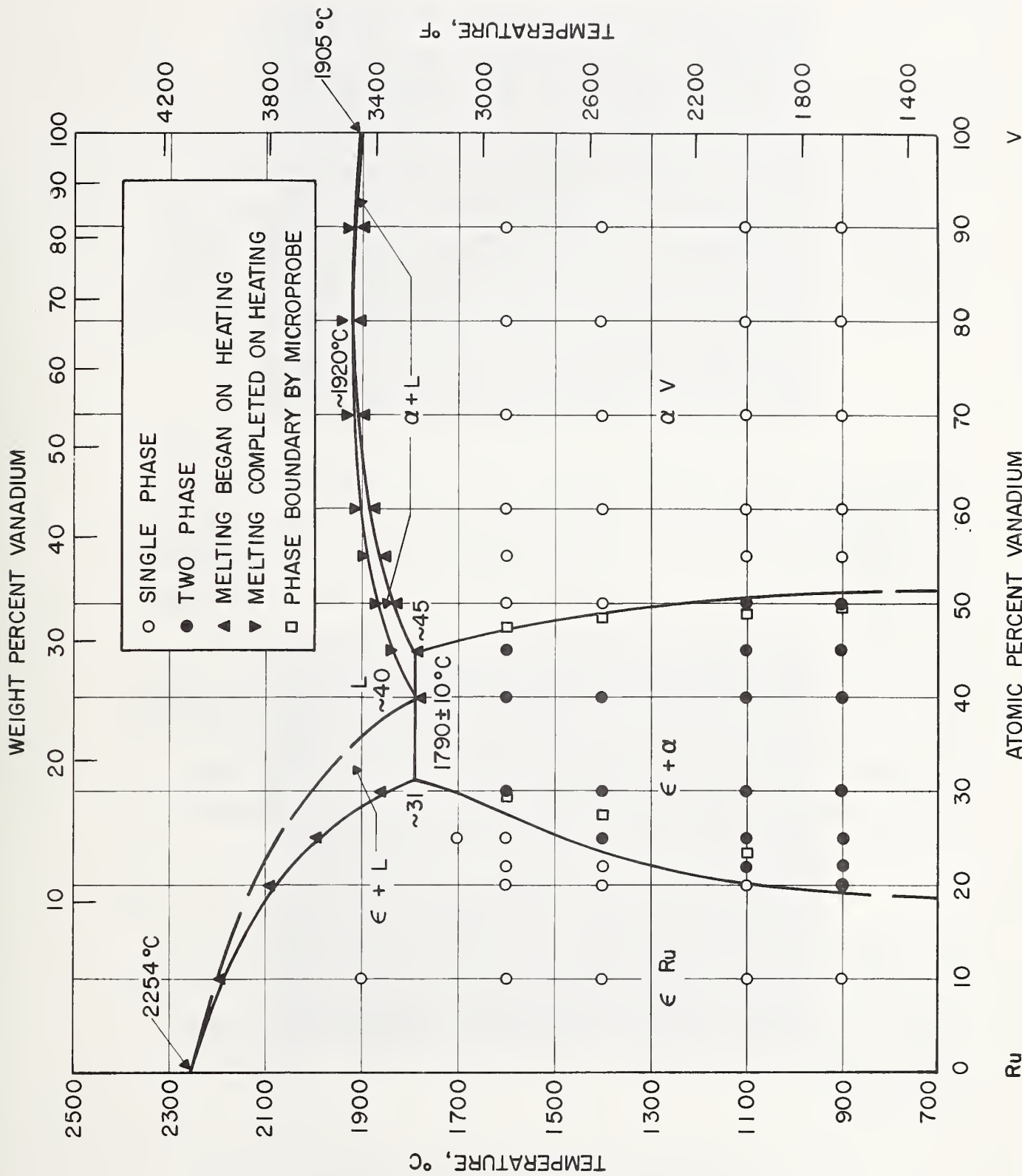


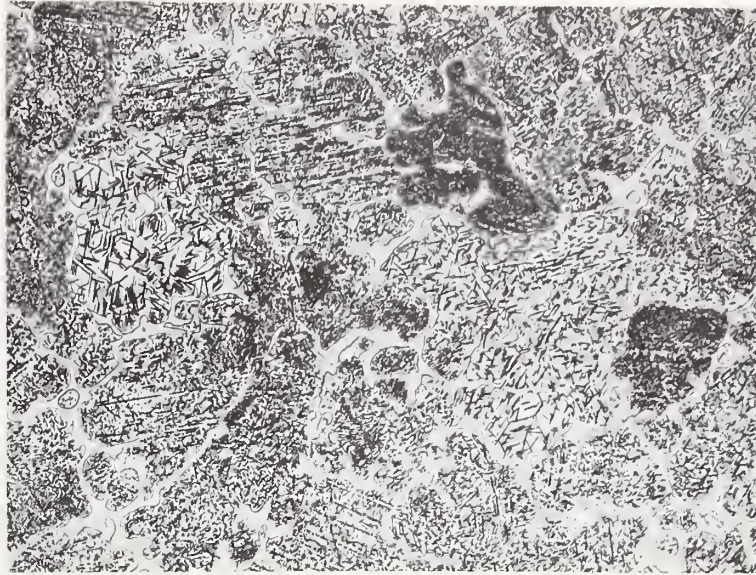
Fig. 3 - Vanadium-ruthenium constitution diagram

could not be positioned to avoid the precipitate particles due to the small interparticle spacing. Thus some of these particles are unavoidably positioned within the electron beam and this results in excessively high contents of one element (V or Ru) being recorded. Nevertheless, with this consideration in mind and utilizing supplementary metallographic and x-ray diffraction data it seems probable that the phase boundaries have been located with reasonable precision.

## 2. Ruthenium Terminal Solid Solution - $\epsilon$

The maximum solubility of vanadium in the close-packed hexagonal  $\epsilon$ -ruthenium terminal solid solution is about 31 at. % V at 1790°C. There is a significant decrease in solubility at lower temperatures, however, so that particles of  $\alpha$  phase are precipitated during cooling or after reannealing at lower temperatures (See Fig. 4a and 4b). At 900°C it appears that the maximum solubility of vanadium in the  $\epsilon$  phase is slightly less than 20 at. % V. The structure of the precipitated  $\alpha$  phase depends on the annealing temperature. Fig. 5a shows the structure observed in the alloy  $V_{25}Ru_{75}$  after annealing at 900°C for two months. This structure appears to be consuming a prior fine dispersoid structure which had apparently formed when this sample was previously annealed at 1100°C.

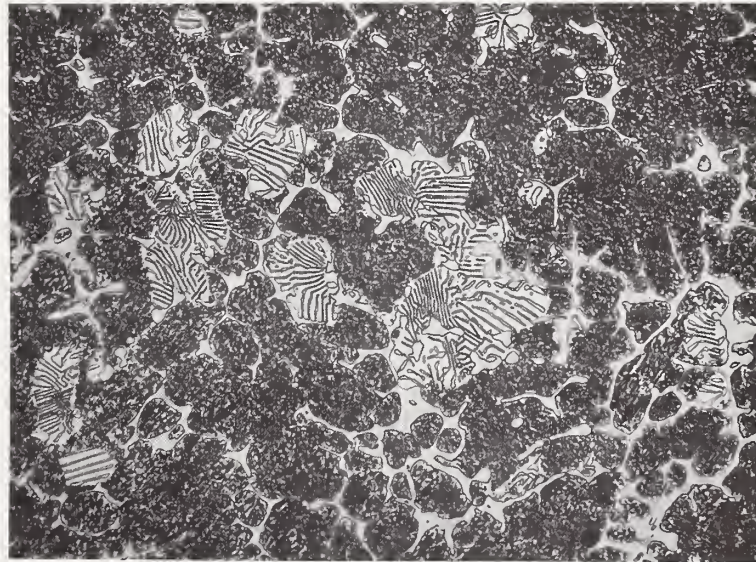
Lattice parameter measurements indicate that there is a slight decrease in  $a_0$ , and increase in  $c_0$  and an increase in the  $c/a$  ratio with increasing % V. The x-ray data, obtained at room temperature, are given in Table 3. These lattice parameter values are in reasonably good agreement with those reported by Raub and Fritzsche<sup>(2)</sup>.



208 X

(a)

30 at. % V, 70 at. % Ru equilibrated at 1400° C for one day and rapidly cooled. Large dendrites of  $\epsilon$ Ru containing an oriented precipitate of  $\alpha$ V phase.



208 X

(b)

30 at. % V, 70 at. % Ru equilibrated at 1100° C for one month. Prior fine structure now contains some cellular growth of  $\epsilon$ Ru and  $\alpha$ V phases.

Fig. 4 - Microstructures of vanadium-ruthenium alloys.

Table 3

Lattice Parameters of V-Ru Alloys

Alloy Composition	Structure	Lattice Parameters	
		a	c
V <sub>10</sub> Ru <sub>90</sub>	hcp	2.706	4.292
V <sub>20</sub> Ru <sub>80</sub>	hcp	2.701	4.295
V <sub>30</sub> Ru <sub>70</sub>	hcp	2.701	4.313
V <sub>50</sub> Ru <sub>50</sub>	tetr	2.944	3.126
V <sub>50</sub> Ru <sub>50</sub>	cub (CsCl)	3.003	
V <sub>60</sub> Ru <sub>40</sub>	cub (CsCl)	2.999	
V <sub>70</sub> Ru <sub>30</sub>	cub (CsCl)	2.999	
V <sub>80</sub> Ru <sub>20</sub>	bcc	2.998	
V <sub>90</sub> Ru <sub>10</sub>	bcc	3.017	

3. Vanadium Terminal Solid Solution -  $\alpha$

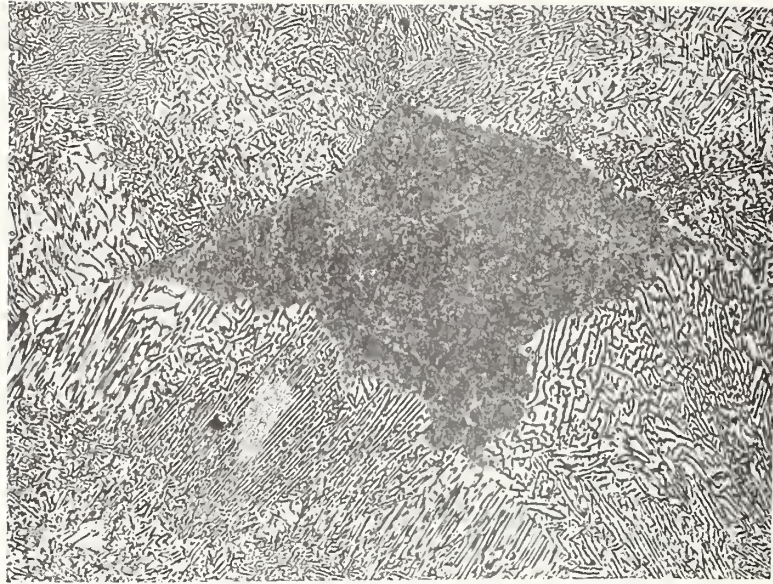
The maximum solubility of ruthenium in body-centered cubic vanadium is about 55 at. % Ru at 1790°C. The disordered body-centered cubic structure was observed in all samples containing up to 20 at. % Ru. The samples beginning at 30% Ru and extending to the maximum ruthenium contents showed evidence of atomic ordering. Superlattice lines characteristic of a CsCl-type structure were observed in the x-ray diffraction patterns of each of these higher Ru-content alloys.

It is not known whether an order-disorder transformation exists in these samples or whether ordering

persists up to the solidus temperature. The smooth continuous solidus curve containing no sharp discontinuities supports the view that the disordered body-centered cubic terminal solid-solution is stable at high temperatures up to the maximum Ru-contents. Raub and Fritzsche<sup>(2)</sup> suggest the possible existence of two-phase regions between the ordered and disordered bcc phases. However, we have found no evidence for the existence of such two-phase regions and the lack of convincing evidence is the principal reason why we have not indicated such features on the proposed diagram.

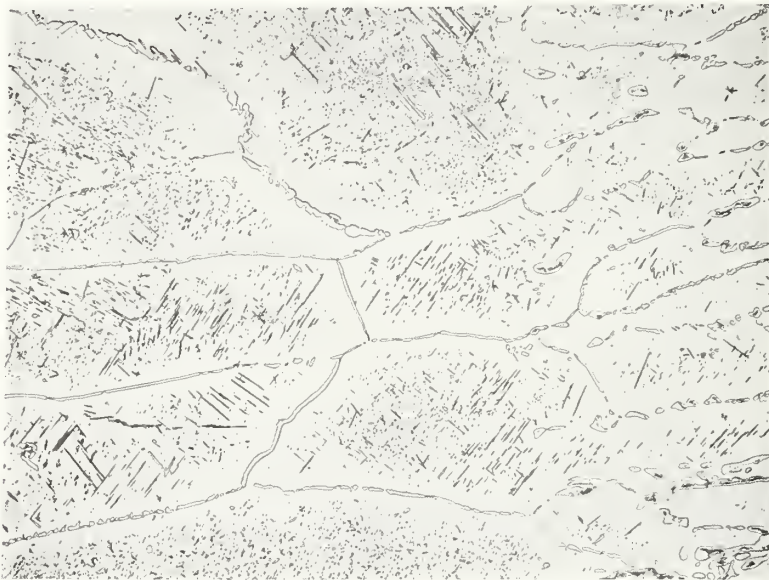
Tetragonality in the CsCl-type structure was observed only in our alloy  $V_{50}Ru_{50}$  and in this alloy only when the sample was annealed at or below  $1100^{\circ}C$ . According to Chu et al<sup>(3)</sup> the cubic to tetragonal transformation in such alloys occurs over a range of temperatures,  $T_k$ , which vary from about  $500^{\circ}K$  for  $V_{47}Ru_{53}$  to almost  $0^{\circ}K$  for  $V_{55}Ru_{45}$ . Our samples were examined only at or slightly above room temperature and it is consistent with these results<sup>(3)</sup> that we observed tetragonality only in our alloy  $V_{50}Ru_{50}$ . The existence of possible hysteresis effects on the critical temperature,  $T_k$ , have been considered<sup>(3)</sup> but it was concluded that any such effects would probably not exceed 0.5 K. Obviously further studies will be needed to elucidate the nature of this transformation.

Quantitative electron-probe microanalysis was helpful in determining the boundary of the  $\alpha$ -phase region at  $1600^{\circ}C$  and at  $1400^{\circ}C$  but the precipitation of a second phase in the  $\alpha$ -phase regions (Fig. 5b and 6a) reduced the reliability of this method for samples annealed at  $1100^{\circ}C$  and  $900^{\circ}C$ . Primary reliance was placed on metallographic studies for samples annealed at these lower temperatures.



272X (a)

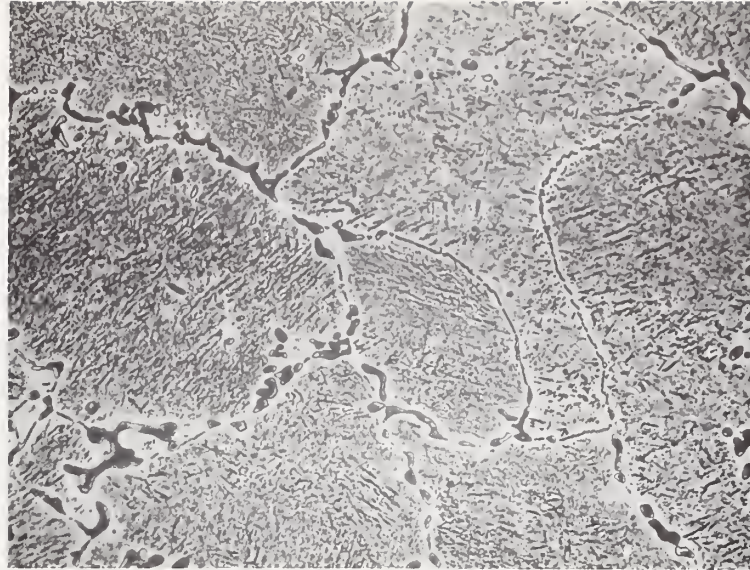
25 at. % V, 75 at. % Ru equilibrated at 900° C for two months. Prior fine structure is now largely consumed by a courser structure. Both structures consist of  $\epsilon$  Ru and  $\alpha$  V .



160 X (b)

45 at. % V, 55 at. % Ru equilibrated at 1100° C for one month. Large grains of  $\alpha$  V containing an oriented precipitate of  $\epsilon$  Ru phase together with a grain boundary network of  $\epsilon$  Ru.

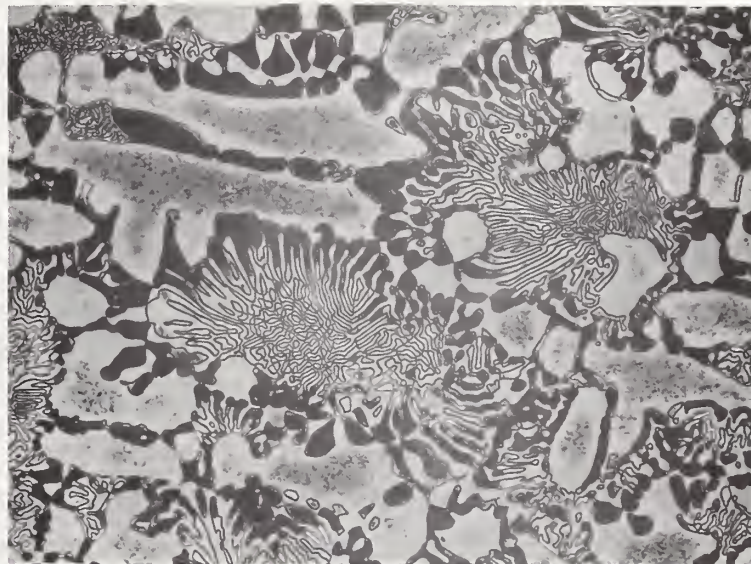
Fig. 5 - Microstructures of vanadium-ruthenium alloys.



272X

(a)

45 at. % V, 55 at. % Ru equilibrated at 900° C for two months. Large grains of  $\alpha$ V containing a precipitate of  $\epsilon$  Ru. Grain boundary network of  $\epsilon$  Ru contains a fine precipitate of  $\alpha$ V thus demonstrating a reduced solubility in both phases at this temperature.



272X

(b)

40 at. % V, 60 at. % Ru in the "as-cast" condition. Eutectic structure of  $\epsilon$  Ru and  $\alpha$ V with fine precipitates in both phases.

Fig. 6 - Microstructures of vanadium-ruthenium alloys.

#### 4. Eutectic $L \rightleftharpoons \epsilon + \alpha$

The existence of this eutectic reaction was established by our solidus data and supported by the observation of a typical eutectic structure in a melted sample having the composition  $V_{40}Ru_{60}$  (see Fig. 6b). Melting occurs in this alloy at  $1790 \pm 10^\circ C$ . This is in contradiction to the report by Raub and Fritzsche<sup>(2)</sup> that V-Ru alloys in this composition range are molten at  $1700^\circ C$ . The lower solidus temperatures of Raub and Fritzsche may perhaps be a result of alloy contamination. We have observed that the melting points of vanadium alloys can be seriously in error when crucible reactions are involved. All of our melting point determinations were done in thoria crucibles in order to prevent such reactions.

#### H. Discussion

The proposed V-Ru constitution diagram resembles the diagram which has been reported for the Nb-Ru system<sup>(6)</sup> except that no ordered hcp intermediate phase was observed in the V-Ru system. In both of these systems one observes an ordered CsCl-type structure and a tetragonal distortion of this structure which may possibly be the result of a martensitic transformation. Additional studies are needed in both systems to delineate the region of stability of these ordered phases and to elucidate their mode of formation. It is noteworthy that diffusion couples did not indicate the existence of any two-phase regions separating the disordered bcc, ordered (CsCl-type) and tetragonal phases for the Nb-Ru alloys<sup>(7)</sup>. High-temperature x-ray diffraction studies, however, will probably be needed to clarify the mode of formation of the ordered CsCl-type structure and its tetragonal transformation. These studies might also be extended to include the Ta-Ru alloys for which a similar behavior has been noted<sup>(8)</sup>.

## REFERENCES

1. Greenfield, P. and Beck, P. A., Intermediate Phases in Binary Systems of Certain Transition Elements, Trans. AIME 206, pp. 265-276 (1956).
2. Raub, E. and Fritzsche, W., The Ruthenium-Vanadium Alloys, Z. Met. 54, pp. 21-23 (1963).
3. Chu, C. W., Bucher, E., Cooper, A. S. and Maita, J. P., Electronic Transitions in Near-Equiatomic Vanadium-Ruthenium Alloys, Phys. Rev. B. 4, pp. 320-326 (1971).
4. Flükiger, R., Heiniger, F. and Müller, J., Electronic Specific Heat and Superconductivity in the Vanadium-Ruthenium Alloy System, Proc. LT 11, St. Andrews, Scotland, p. 1017 (1968).
5. Bernasson, M., Descouts, P., Donzé, P. and Treyvaud, A., Magnetic Susceptibilities and NMR Properties of V-Ru Alloys, J. Phys. Chem. Solids 30, p. 2453 (1969).
6. Waterstrat, R. M., The Vanadium-Platinum Constitution Diagram, Met. Trans. 4, pp. 455-466 (1973).
7. Hurley, G. F. and Brophy, J. H., A Constitution Diagram for the Niobium-Ruthenium System Above 1100°C, J. Less-Common Metals 7, pp. 267-277 (1964).
8. "Constitution of Binary Alloys" (First Supplement) edited by R. P. Elliott, McGraw-Hill Book Co., p. 786 (1965).
9. Waterstrat, R. M. and Manuszewski, R. C., Noble Metal Constitution Diagrams, NBS Report 10571 (1971).

## IV. VANADIUM-RHODIUM CONSTITUTION DIAGRAM

### A. Previous Studies

The only previous investigation of the vanadium-rhodium alloy system was that of Greenfield and Beck<sup>(1)</sup> who confined their study to four alloy compositions and identified two intermediate phases. The purpose of the present study was to acquire sufficient information on this system to permit the construction of a constitution diagram.

### B. Materials

The vanadium metal used in this study was obtained from the U. S. Bureau of Mines, Boulder City Metallurgy Research Laboratory through the courtesy of Mr. T. A. Sullivan. The metal was in the form of electrolytic dendrites having a nominal purity of 99.95%. A typical analysis of the starting materials is shown in Table 4.

The rhodium metal was in the form of powder (sponge) and was obtained from Johnson-Matthey Chemicals Limited. The impurities detected by spectrographic analysis are shown in Table 4.

### C. Alloy Preparation

Carefully weighed amounts of each starting material were compressed in a 1/2-inch diameter cylindrical steel mold to produce small cylinders suitable for arc-melting. Each sample weighed 10 grams and was arc-melted at least four times in an atmosphere of purified 50% argon and 50% helium. Weight losses

Table 4

Typical Analyses of the Materials Used in  
Preparing the Experimental Alloys<sup>+</sup>

Impurity	Vanadium	Rhodium
	U. S. Bureau of Mines	Johnson-Matthey
C	80	--
Ca	ND	1
Cr	60	ND
Cu	32	3
Fe	135	5
H	10	--
Mg	ND	<1
N	35	--
Na	ND	<1
O	220	--
Pd	ND	<1
Si	ND	2

+ Values given in ppm.

ND Not detected spectrographically.

No other elements were detected spectrographically.

after melting were in all cases less than 0.6% and it was therefore assumed that the actual compositions of the samples were close to the intended compositions. This assumption was later verified by electron beam microanalyses of several samples.

#### D. Temperature Measurement

A platinum versus platinum-10% rhodium thermocouple was used to measure temperatures up to 1500°C. This thermocouple and a standard platinum-6% rhodium versus platinum-30% rhodium thermocouple were used to obtain data on temperature versus furnace current in our high-vacuum furnace. The standard thermocouple had been calibrated on the International Practical Temperature Scale of 1968 (IPTS 68). Calibration was also made against secondary standards such as the melting temperatures of pure gold, nickel, platinum, and rhodium. Temperatures above 1500°C were obtained by extrapolating the furnace current versus temperature plot through the points established by the secondary standards and then setting the furnace current to the appropriate value.

#### E. Thermal Treatments

Rhodium-rich alloys containing up to 30 at. % V were homogenized by annealing at 1650°C for 2 hours. Vanadium-rich alloys containing up to 10 at. % Rh were homogenized by annealing at 1700°C for 2 hours. In addition, all of the alloys were annealed at 1500°C for 2 days before proceeding with any further heat treatments at lower temperatures.

The annealing treatments were accomplished in a tantalum-strip resistance furnace operating at pressures between

$5 \times 10^{-6}$  and  $5 \times 10^{-7}$  mm Hg. The samples were suspended in tantalum buckets using Ta wire. There was no significant Ta contamination detectable in subsequent electron probe studies. Samples to be annealed at temperatures up to  $1100^{\circ}\text{C}$  were sealed in evacuated quartz tubes which had been backfilled with a partial pressure of argon.

After annealing in the vacuum furnace the samples were rapidly cooled by turning off the furnace power. Alloys which had been sealed in quartz tubes were quenched in cold water.

A summary of the equilibration treatments used for the various samples is shown in Table 5.

Table 5  
Schedule of Typical Heat Treatments for Vanadium-Rhodium

Temperature, $^{\circ}\text{C}$	Time	Cooling
1700	2 hrs	Rapid cooling*
1650	2 hrs	Rapid cooling*
1500	2 days	Rapid cooling*
1300	5 days	Rapid cooling*
1100	3 weeks	Quenched
900	6 weeks	Quenched

\* Rapid cooling in the vacuum furnace was accomplished by turning off the furnace power.

## F. Methods for Determination of Phase Boundaries

### 1. Solidus Temperatures

The solidus temperatures of our alloys were determined by observations of incipient melting in alloys annealed at various temperatures above and below the solidus temperature. Metallographic examination was used to detect evidence of melting for some of the experimental alloys while in other cases it was possible to locate the solidus temperature with reasonable accuracy by direct observation of the sample during heating. This latter method has been described in detail<sup>(2)</sup> and is a rather effective technique when working in the vicinity of the eutectic compositions or when the solidus and liquidus are separated by a fairly small temperature interval as is the case for most of the V-Rh alloys. In most of our alloys, a sharp melting was observed at a fairly discrete temperature and the solidus temperature is therefore thought to be located with reasonable accuracy as indicated on the diagram of Fig. 7.

The samples were supported in high-purity thoria crucibles during the solidus determinations and there was no detectable reaction between the molten alloys and the crucibles.

### 2. Liquidus Temperatures

The liquidus temperatures were not determined directly but were estimated from the general form of the solidus curves and the location of invariant reactions. Our metallographic examination of solidus samples was also helpful in locating the liquidus through the application of well-known principles associated with the lever law. This was done by estimating the relative amounts of residual solid and chilled liquid phases in the microstructures of the partially melted alloys.

### 3. Other Phase Boundaries

The boundaries of intermediate phases were determined by metallographic studies of alloys annealed at temperatures which would place them in close proximity to the boundary being determined. Alloys annealed within two-phase regions were particularly helpful in determining the location of phase boundaries. By estimating the relative amount of each phase in the microstructure and then applying the lever rule one can estimate the approximate location of the phase boundaries. This is particularly true if one of these boundaries is already known from some independent prior observations such as electron microprobe analyses.

In some cases it was possible to determine the phase boundaries by quantitative electron probe microanalyses of two-phase alloys ( $\alpha_3 + \beta$  and  $\beta + \alpha$ ) annealed at various temperatures. Alloys annealed within other two-phase regions, however, could not be used for electron probe microanalyses due to the presence of fine structures or an insufficient amount of one phase. The fine structures are usually produced by decomposition during cooling. For these samples, therefore, the primary reliance was placed on metallographic studies in locating the phase boundaries.

#### G. Experimental Results

##### 1. General

The proposed constitution diagram for the vanadium-rhodium system is shown in Fig. 7. All alloys were examined by x-ray diffraction or metallographic methods or both and data obtained by the different methods are in good agreement.

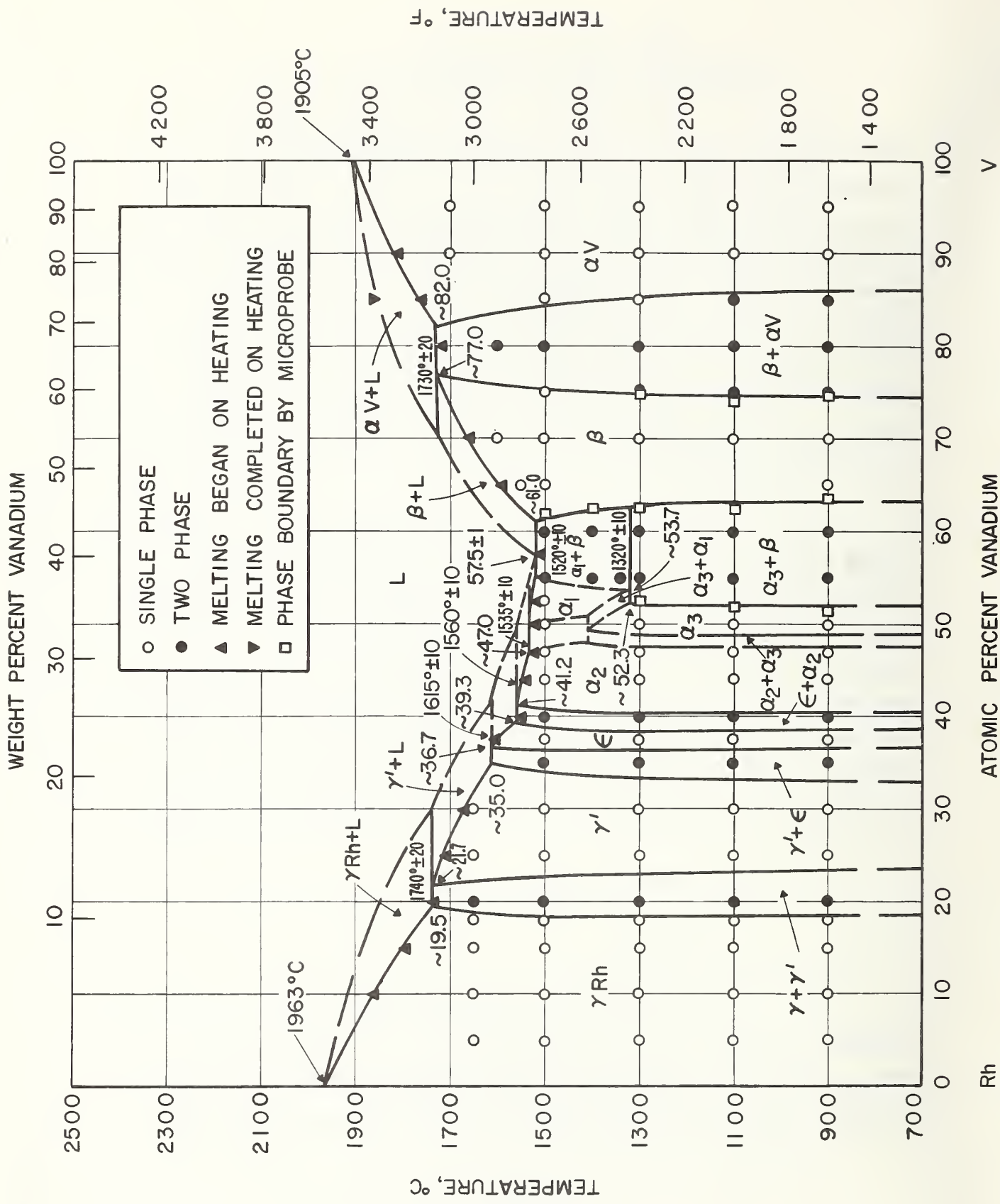


Fig. 7 - Vanadium-rhodium constitution diagram

The use of electron probe microanalysis in locating phase boundaries was limited to alloys containing the  $\beta$  phase. All other solid-state phase boundaries were located with sufficient accuracy by metallographic methods.

## 2. Rhodium Terminal Solid Solution - $\gamma$

The extent of the face-centered cubic rhodium terminal solid solution was established mainly by x-ray diffraction studies of annealed samples with increasing vanadium contents. The solubility of vanadium in fcc rhodium extends to about 19 atomic % vanadium and is nearly independent of temperature. X-ray diffraction patterns of alloys beginning at 20 atomic % vanadium contain the characteristic "superlattice lines" of the ordered  $\gamma'$  phase. The existence of a two-phase region between the  $\gamma$  and  $\gamma'$  phases could not be clearly demonstrated using metallographic or x-ray diffraction methods but its presence is suggested by a sharp break in the experimental solidus curve at about 20 atomic % vanadium.

## 3. Intermediate Phase - $\gamma'$

The ordered phase ( $\gamma'$ ) possesses a  $\text{Cu}_3\text{Au}(\text{L1}_2)$ -type structure. This confirms previous studies<sup>(1, 3)</sup>. The degree of ordering is revealed by comparing the relative intensities of certain lines in the x-ray diffraction pattern of this structure. Increasing degrees of ordering produce an increase in the intensity of the so-called "superlattice lines" relative to the intensities of the "fundamental lines". A visual comparison of these lines for samples annealed over a range of temperatures from 900°C to 1650°C reveals no pronounced changes in the degree of ordering. This suggests that the degree of ordering in the  $\gamma'$  phase

is not strongly temperature dependent. The relative intensities of the superlattice lines, however, are noticeably reduced at the compositions  $V_{20}Rh_{80}$  and  $V_{35}Rh_{65}$  but in these two cases the intensity reduction is probably due to the co-existence of two phases at these compositions with accompanying superpositions of some of the fundamental lines.

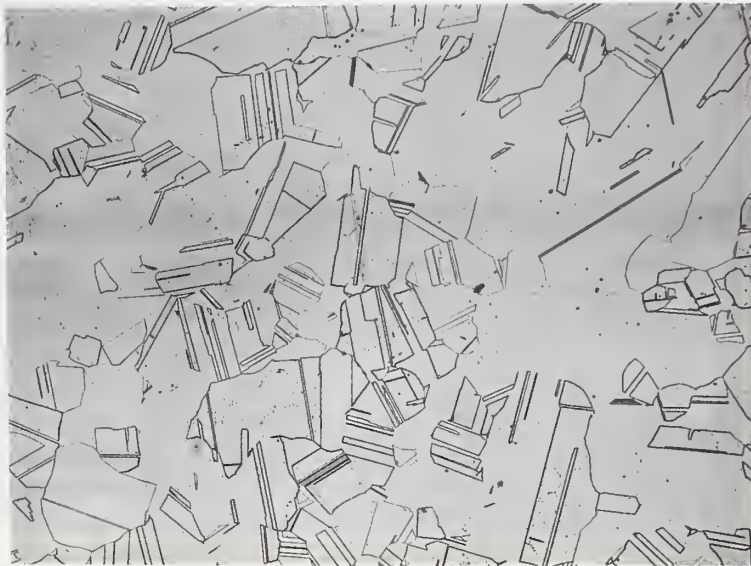
X-ray diffraction studies and solidus measurements indicate that the  $\gamma'$  phase (Fig. 8a) extends from about 22 atomic % vanadium where it forms from the liquid via a peritectic reaction at about  $1740^{\circ}C$  to 35 atomic % vanadium at  $1615^{\circ}C$  where it enters into the peritectic formation of the  $\epsilon$  phase. The composition range of the  $\gamma'$  phase is reduced at lower temperatures by slight reductions in solubility for both rhodium and vanadium (Fig. 8b).

#### 4. Intermediate Phase - $\epsilon$

The intermediate phase  $\epsilon$  is stable over a narrow composition range centered at the composition  $V_3Rh_5$ . Its crystal structure has been determined in a separate investigation<sup>(4)</sup> and may be described as a close-packed array of atoms having a two-layer stacking periodicity and containing both ordered and disordered atomic sites. It apparently forms by a peritectic reaction at about  $1615^{\circ}C$ . Its microstructure is characterized by the presence of extensive microtwinning (Fig. 9a).

#### 5. Intermediate Phase - $\alpha_2$

The intermediate phase  $\alpha_2$  is stable over a composition range from about 40.5 to 48.0 atomic % vanadium. It possesses a tetragonal crystal structure in which the close-packed rhodium and vanadium atoms are ordered in alternate layers along



80X (a)

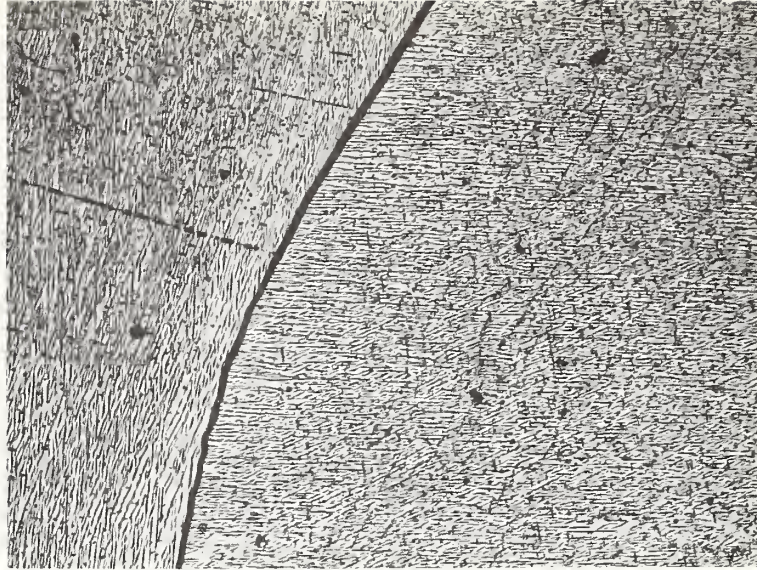
25 at. % V, 75 at. % Rh equilibrated at 1300 °C for five days. Twinning in large grains of  $\gamma'$  phase.



160X (b)

35 at. % V, 65 at. % Rh equilibrated at 900 °C for two months. Large grains of  $\gamma'$  phase containing oriented precipitates of  $\epsilon$  phase.

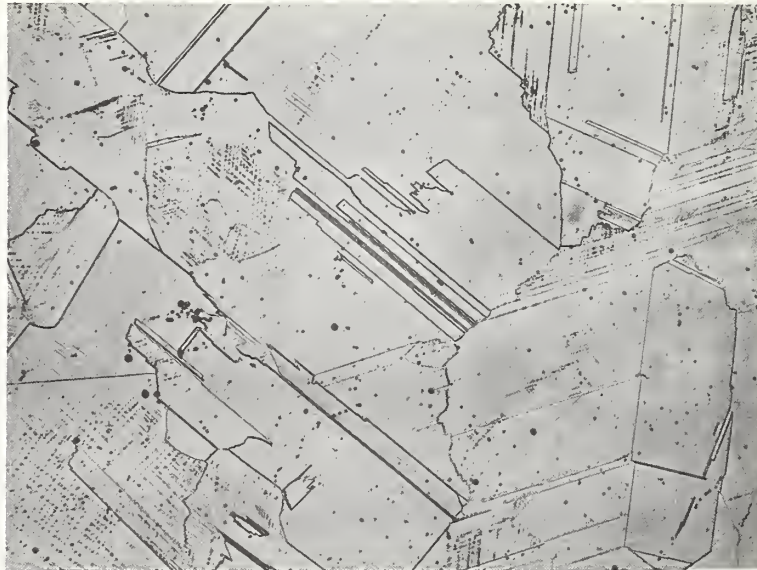
Fig. 8 - Microstructures of vanadium-rhodium alloys.



160X

(a)

37.5 at. % V, 67.5 at. % Rh equilibrated at 1300° C for five days. Large grains of  $\epsilon$  phase containing extensive micro-twinning.



160X

(b)

40 at. % V, 60 at. % Rh equilibrated at 900° C for two months. Large twins and fine deformation markings in  $\alpha_2$  phase.

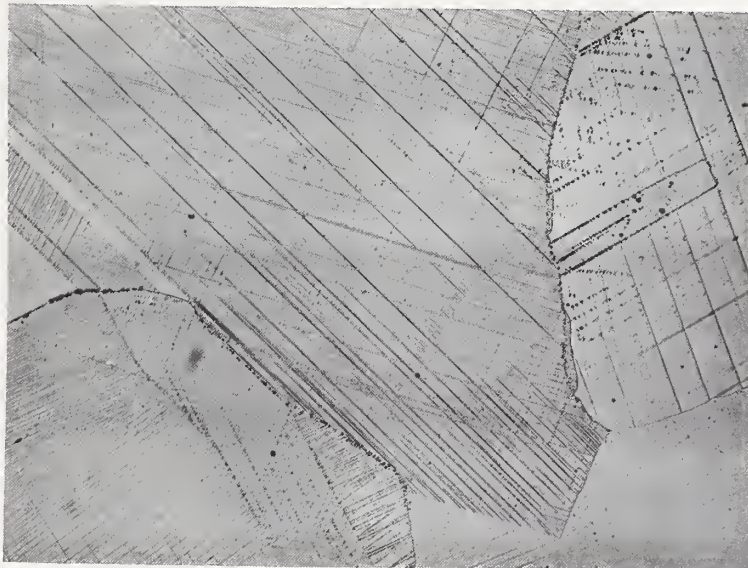
Fig. 9 - Microstructures of vanadium-rhodium alloys.



80X

(a)

44 at. % V, 56 at. % Rh equilibrated at 900°C for two months. Twins and fine deformation markings in  $\alpha_2$  phase together with a dispersion of etch pits.



160X

(b)

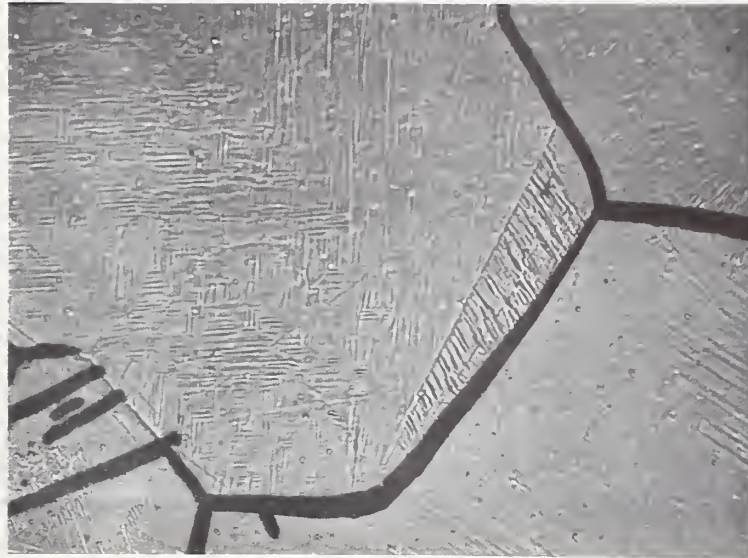
47 at. % V, 53 at. % Rh equilibrated at 900°C for two months. Large grains of  $\alpha_2$  phase with fine deformation lines.

Fig. 10 - Microstructures of vanadium-rhodium alloys.

the c-axis and the structure is isomorphous with the  $\text{CuAu(Ll}_0\text{)}$  type. The  $\alpha_2$  phase is apparently formed by a peritectic reaction at about  $1560^\circ\text{C}$ . The microstructure of this phase contains large twin bands and other fine deformation markings (Fig. 9b, 10a, 10b).

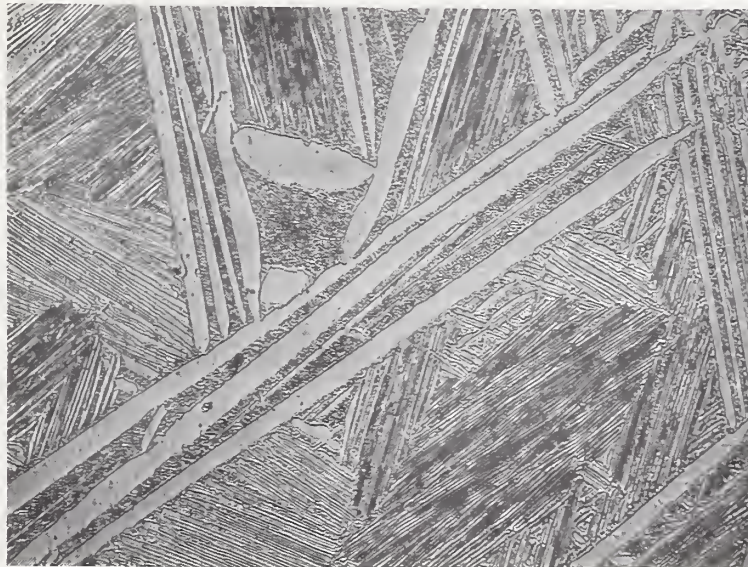
## 6. Intermediate Phase - $\alpha_3$

The intermediate phase  $\alpha_3$  is stable between about 49 and 52 atomic % vanadium and its crystal structure has been tentatively identified as being isomorphous with the  $\alpha\text{VIr}$  structure first reported by Giessen et al<sup>(5)</sup>. This structure is orthorhombic and may be considered as a distorted version of the ordered CsCl-type structure. Our identification of this structure is based mainly on the position and relative intensities of low-angle lines (Table 6) since at higher angles the lines become increasingly diffuse. High-temperature vacuum annealing of the powders did not produce any significant sharpening of the high-angle lines. Metallographic studies revealed the existence of relatively large crystals but each crystal was densely microtwinned (Fig. 11a). X-ray diffraction data obtained from each of several individual crystals produced unsatisfactory patterns suggesting the presence of multiple twinning. We have tentatively concluded that the  $\alpha_3$  phase probably forms by a solid-state reaction (compare Fig. 11b and 12a). This reaction may occur at about  $1400^\circ\text{C}$  and is probably a peritectoid reaction which we could not suppress by rapid cooling. Thus, high-temperature x-ray diffraction studies will probably be needed to conclusively identify the mode of formation of this phase. The lattice constants could not accurately be determined due to the diffuse character of the high-angle lines but "d-values" obtained from low-angle lines suggest lattice constants which are close to those reported for  $\alpha\text{VIr}$  (see Table 6).



400X (a)

50 at. % V, 50 at. % Rh equilibrated at 1100°C for three weeks. Large grains of  $\alpha_3$  phase containing extensive microtwinning.



400X (b)

55 at. % V, 45 at. % Rh equilibrated at 1340°C and rapidly cooled. Fine structure of  $\alpha_3$  and  $\beta$  phases formed from a prior matrix of  $\alpha_1$  and a trace of  $\beta$ .

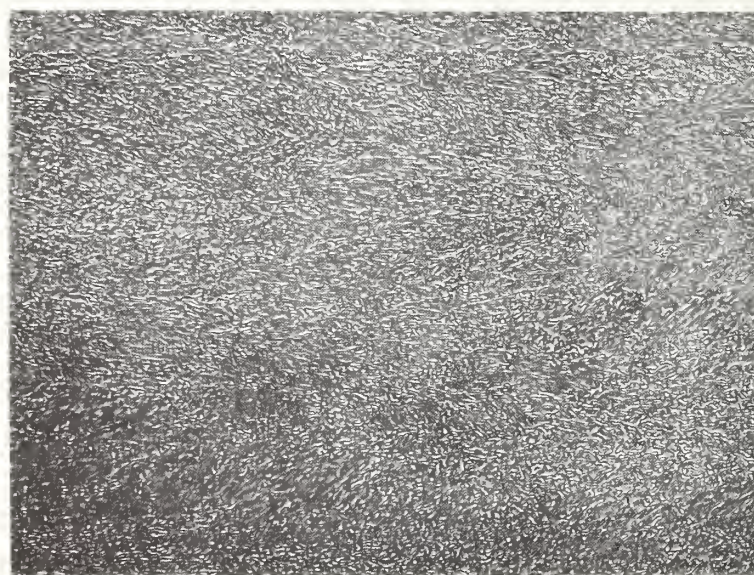
Fig. 11 - Microstructures of vanadium-rhodium alloys.



80X

(a)

55 at. % V, 45 at. % Rh equilibrated at 1100°C for three weeks. Matrix is  $\alpha_2$  phase and contains oriented, elongated islands of  $\beta$  phase.



680X

(b)

57.5 at. % V, 42.5 at. % Rh in the "as-cast" condition. Fine eutectic structure composed of  $\beta$  and decomposed  $\alpha_1$  phases.

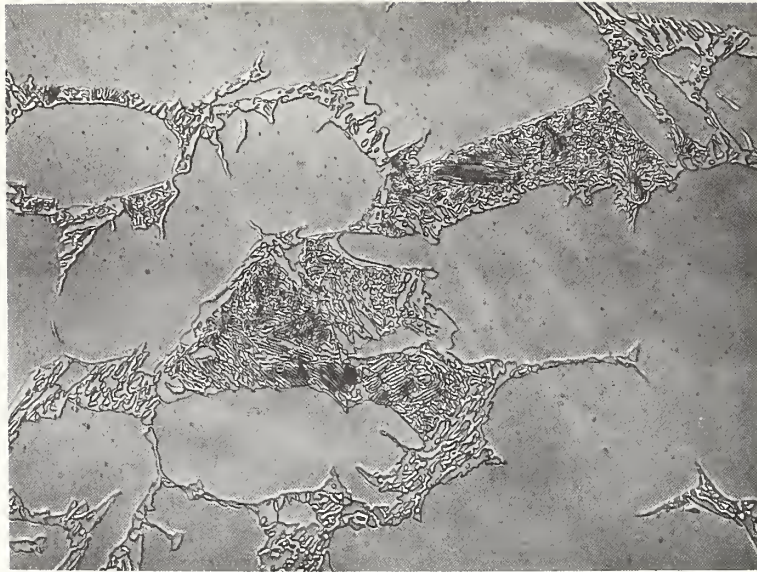
Fig. 12 - Microstructures of vanadium-rhodium alloys.

## 7. Intermediate Phase - $\alpha_1$

The existence of a high-temperature phase on the vanadium-rich side of the equiatomic composition is suggested by metallographic studies in which we observed the finely-decomposed structures (Fig. 11b, 13a) which are characteristic of a eutectoid decomposition. Metallographic examination of alloys quenched from various temperatures indicated that the eutectoid temperature was located at about 1325°C (see Fig. 11b and 12a). We were unable to retain the high-temperature phase in alloys which had been rapidly cooled from above this proposed eutectoid temperature and we were therefore unable to identify the crystal structure of the  $\alpha_1$  phase.

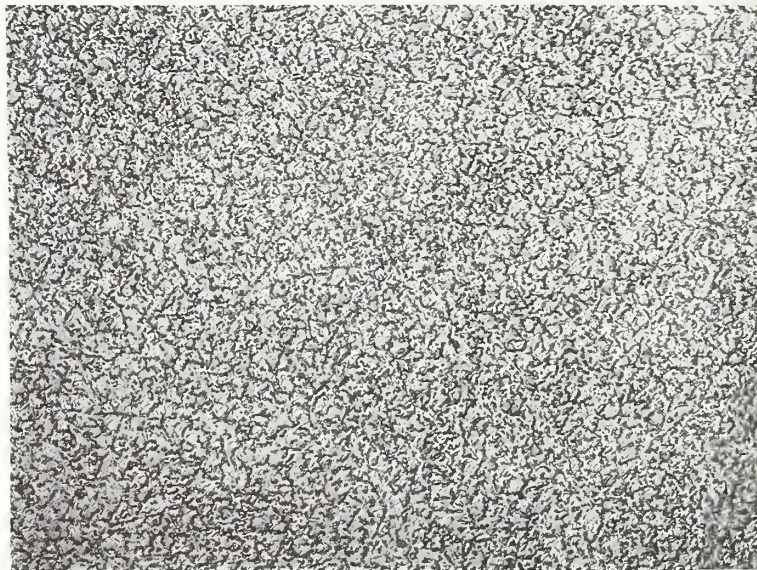
## 8. Intermediate Phase - $\beta$

Previous studies<sup>(1, 6)</sup> have established the existence of a phase having the Al<sub>5</sub> ( $\beta$ -W) structure in the V-Rh system at the "ideal" stoichiometric composition (A<sub>3</sub>B). We have confirmed these observations and, in addition, we find that this phase is stable over a substantial composition range extending toward the rhodium-rich side of the "ideal" composition. The  $\beta$  phase apparently forms by a peritectic reaction at 77 atomic % vanadium and at 1730°C. On the rhodium-rich side it enters into a eutectic reaction with  $\alpha_1$  at 1520°C. There is a slight reduction in solubility for both vanadium and rhodium at lower temperatures where the stability range extends from about 63.0 to 74.5 atomic % vanadium. A similar range of composition has been reported for this structure in the V-Ir alloy system where the superconducting transition temperatures have been reported to increase significantly with increasing iridium contents<sup>(7)</sup>. A similar effect has now been observed in our V-Rh  $\beta$ -phase samples. The  $\beta$ -phase alloy V<sub>65</sub>Rh<sub>35</sub> was found to have a superconducting transition



400X (a)

60 at. % V, 40 at. % Rh equilibrated at 1500°C for two days. Large islands of  $\beta$  phase interspersed with a fine structure of decomposed  $\alpha_1$  phase.



400X (b)

80 at. % V, 20 at. % Rh equilibrated at 1500°C for two days. Fine two-phase structure consisting of  $\beta$  and  $\alpha_V$ .

Fig. 13 - Microstructures of vanadium-rhodium alloys.

temperature of  $1.075\text{K}^{(8)}$  whereas the alloy  $\text{V}_{75}\text{Rh}_{25}$  remained in the normal state at  $0.015\text{K}^{(9)}$ . The extent of the  $\beta$ -phase region in the V-Rh system was established primarily by quantitative electron-beam microanalyses of alloys annealed and quenched from various temperatures.

#### 9. Vanadium Terminal Solid Solution - $\alpha$

The body-centered cubic vanadium solid solution was found to dissolve up to 18 atomic % rhodium at  $1730^\circ\text{C}$  where it enters into the peritectic formation of the  $\beta$  phase. The solubility of rhodium in the  $\alpha$  solid solution decreases to about 14 atomic % rhodium at lower temperatures. Two-phase ( $\alpha + \beta$ ) alloys reveal an unusually fine, uniform structure (Fig.13 b).

#### 10. Invariant Reactions

All invariant reactions found or assumed in the V-Rh system are listed in Table 7. Many of these were established by solidus measurements. Solid state reaction temperatures were determined by bracketing the reaction temperature with annealing runs and then examining the x-ray patterns and microstructures of these alloys. In some cases the reactions were only postulated from circumstantial evidence since it was not possible to detect them by the methods used in this study.

In many cases it was quite helpful to first establish the solid-state phase boundaries by x-ray microprobe analyses and by examining the microstructures of two-phase alloys. These solid-state boundaries were then extrapolated to the reaction horizontals established by the solidus measurements. Some applications of the lever law were necessary to establish the

eutectic or peritectic compositions. This was accomplished by metallographic examination of the samples used for the solidus measurements. The accuracy of such methods is difficult to estimate but errors would probably not exceed  $\pm 2$  at. %. Errors in temperature measurement are probably  $\pm 10^\circ \text{C}$ .

## H. Discussion

The vanadium-rhodium constitution diagram which emerges from the present investigation is similar in appearance to the vanadium-iridium constitution diagram tentatively presented by Giessen et al<sup>(5)</sup>. At least four of the six intermediate phases observed in the V-Rh system ( $\gamma'$ ,  $\alpha_2$ ,  $\alpha_3$  and  $\beta$ ) are structurally equivalent to phases observed in the V-Ir system<sup>(5)</sup> [ $\alpha$ -V<sub>3</sub>Ir,  $\beta$ -(V<sub>1-x</sub>Ir<sub>x</sub>)Ir,  $\alpha$ -V<sub>2</sub>Ir, and  $\alpha$ -V<sub>3</sub>Ir, respectively]. These four phases occur over similar ranges of composition in both systems. Other similarities may also exist but the data so far available on the V-Ir system are inadequate for a complete description of the constitution diagram and more data are needed, particularly at lower temperatures.

One may also observe similarities between the V-Rh constitution diagram and the Nb-Rh constitution diagram presented by Ritter et al<sup>(10)</sup>. In both systems one observes a high temperature phase ( $\alpha_1$ ) of unknown crystal structure which decomposes eutectoidally on cooling. In addition three other V-Rh intermediate phases ( $\gamma'$ ,  $\alpha_2$  and  $\beta$ ) have structural counterparts in the Nb-Rh system [ $\alpha$ NbRh<sub>3</sub>,  $\alpha_2$ (Nb<sub>0.96</sub>Rh<sub>0.04</sub>)Rh and  $\alpha$ Nb<sub>3</sub>Rh, respectively]. The  $\epsilon$  phase (V<sub>3</sub>Rh<sub>5</sub>) apparently resembles the phase  $\alpha_5$ (Nb<sub>3</sub>Rh<sub>5</sub>) since both structures contain close-packed atom layers having a mutually equivalent type of atomic ordering<sup>(4, 11)</sup>. The two

structures apparently differ only in the stacking of these layers<sup>(4)</sup> which follows a two-layer sequence in  $V_3Rh_5$  compared to a nine-layer sequence in  $Nb_3Rh_5$ . Another interesting feature of these two systems involves the existence of a broad sigma phase region in the Nb-Rh system which is apparently replaced by a similarly broad A15-type phase region in the V-Rh system. A plot of the atomic volumes of the V-Rh phases is shown in Fig. 38. It involves a slight negative departure from a linear relationship similar to the behavior observed in both V-Ir<sup>(5)</sup> and Nb-Rh<sup>(10)</sup> systems. Crystallographic data and lattice parameters for phases forming in the V-Rh system are summarized in Tables 8 and 9.

Table 6

Relative Intensities (I) and Interplanar Spacings (d) for  $\alpha_3$  Phase  
Lines Compared with Equivalent Values Reported for  
the Phase  $\alpha$ VIr<sup>(5)</sup>

hkl	$\alpha_3$ VRh		$\alpha$ VIr	
	d*	I	d	I
110	-	-	-	-
020	3.325	w	3.384	20
200	2.888	w	2.887	20
001	2.771	w	2.805	<20
111	2.340	w	2.361	10
220	2.183	s	2.200	100
021	2.136	s	2.154	60
130	2.073	w	2.102	40
201	2.005	s	2.017	80
310	1.853	vw	1.857	10
221	1.718	mw	1.726	50
040	1.666	m	1.693	30
131			1.682	30
311	-	-	-	-
330	-	-	1.467	<10
240	-	-	1.463	<10
400 } 041 }	1.449	mw	1.449	20
002	1.392	m	1.400	20
112 } 420 }	1.329	w	1.330	20
150	-	-	1.317	10

(Table 6 continued)

Table 6 (continued)

hkl	$\alpha_3\text{VRh}$		$\alpha\text{VIr}$	
	d*	I	d	I
331	1.284	m	1.294	60
241				
022				
401	1.253	w	1.287	10
202	-	-	1.260	< 5
421	1.199	m	1.202	30
151				
222	1.176	ms	1.181	35
132	1.157	vw	1.166	10
510	-	-	-	-
060	-	-	-	-
312	1.113	vw	1.118	< 5
350	1.098	w	1.108	15
440	1.070	w	1.099	15

\* Lines of  $\alpha_3\text{VRh}$  become increasingly broad with increasing Bragg angle and the accuracy of the values reported probably does not exceed  $\pm 0.02 \text{ \AA}$ . On the basis of the d values above, we would estimate that the lattice constants for  $\alpha_3\text{VRh}$  are:

$$a = 5.78 \qquad b = 6.65 \qquad c = 2.78$$

This may be compared with the lattice constants reported<sup>(5)</sup> for  $\alpha\text{VIr}$  which are:

$$a = 5.791 \qquad b = 6.756 \qquad c = 2.796$$

Table 7

## Invariant Reactions in the Vanadium-Rhodium System

No.	Type	Reaction, At. % Rh	Temp. °C	Method of Determination (See text)	Remarks
[1]	Peritectic	$\alpha V(18.0) + L(29.0) = \beta$	1730	Solidus measurement	-
[2]	Eutectic	$L(42.5) = \beta(39.0) + \alpha_1(45.0)$	1520	Liquid by observing eutectic constituent	-
[3]	Peritectic	$L + \alpha_2 = \alpha_1(50.0)$	1535	Solidus measurement	Postulated
[4]	Peritectic	$L + \epsilon = \alpha_2$	1560	Solidus measurements	Postulated
[5]	Peritectic	$L + \gamma' = \epsilon$	1615	Solidus measurements	Postulated
[6]	Peritectic	$L + \gamma Rh = \gamma'(\sim 78.0)$	1740	Solidus measurements	Temperature estimated
[7]	Peritectoid	$\alpha_1(49.5) + \alpha_2(52.0) = \alpha_3(50.5)$	$\sim 1410$	Metallographic and x-ray diffraction studies	Temperature estimated
[8]	Eutectoid	$\alpha_1(46.0) = \beta(37.5) + \alpha_3(47.5)$	$\sim 1325$	Metallographic studies	Temperature estimated

Table 8

## Crystallographic Data for Vanadium-Rhodium Intermediate Phases

Intermediate Phase	Crystal System	Space Group	Structure Type	No. Atoms Per Unit Cell	Composition Limits, At. %Rh
$\beta$ $V_3Rh$	Cubic	$O_h^3 - Pm\bar{3}n$	$Al_5, Cr_3O$	8	24.5 to 39.0 1520°C
$\alpha_1$ VRh	Unknown	-	Unknown	-	45.0 to 55.0 1520°C
$\alpha_2(V_{0.88}Rh_{0.12})Rh$	Tetragonal	$D_{4h}^1 - P4/mmm$	$Ll_0, AuCu$	4	52.5 to 59.5 1300°C
$\alpha_3$ VRh	Orthorhombic	$D_{2h}^{19} - Cmmm$	$\alpha-VIr$	8	48.0 to 51.0 1100°C
$\epsilon(V_{0.75}Rh_{0.25})Rh$ or $(V_3Rh_5)$	Orthorhombic	$Cm2m$ or $Cmcm^*$	$\epsilon(V-Rh)$	16	61.5 to 63.0 1300°C
$\gamma'$ VRh <sub>3</sub>	Cubic	$O_h^1 - Pm\bar{3}m$	$Ll_2, AuCu_3$	4	66.5 to 77.0 1300°C

\* The data available (ref. 4) do not permit a definite choice between these two space groups.

Table 9

Lattice Parameters of Intermediate Phases and Terminal Solid Solutions  
for Vanadium-Rhodium

At. % Rh	Phase	Lattice Parameter(s), Å			$c_0/a_0$
		a	b	c	
15.0	$\alpha V$	3.009			
25.0	$\beta$	4.784			
30.0	$\beta$	4.779			
35.0	$\beta$	4.788			
50.0	$\alpha_3$	5.78	6.65	2.78	
53.0	$\alpha_2$	3.895		3.599	.924
56.0	$\alpha_2$	3.870		3.657	.945
60.0	$\alpha_2$	3.855		3.599	.934
62.5	$\epsilon$	5.420	9.276	4.320	
70.0	$\gamma'$	3.787			
75.0	$\gamma'$	3.784			
82.0	$\gamma$	3.789			
85.0	$\gamma$	3.793			
90.0	$\gamma$	3.797			
95.0	$\gamma$	3.800			

## REFERENCES

1. Greenfield, P., and Beck, P. A., Intermediate Phases in Binary Systems of Certain Transition Elements, Trans. AIME 206, pp. 265-276 (1956).
2. Waterstrat, R. M., The Vanadium-Platinum Constitution Diagram, Met. Trans. 4, pp. 455-466 (1973).
3. Dwight, A. E. and Beck, P. A., Close-Packed Ordered Structures in Binary  $AB_3$  Alloys of Transition Elements Trans. AIME, 215, pp. 976-979 (1959).
4. Waterstrat, R. M., and Dickens, Brian, The Crystal Structure of  $V_3Rh_5$ , J. Less-Common Metals 31, pp. 61-67 (1973).
5. Giessen, B. C., Dangel, P. N., and Grant, N. J., New Phases in the Vanadium-Iridium System and a Tentative Constitution Diagram, J. Less-Common Metals 13, pp. 62-70 (1967).
6. Zegler, S. T., and Downey, J. W., Ternary  $Cr_3O$ -Type Phases with Vanadium, Trans. AIME 227, pp. 1407-1411 (1963).
7. Cox, J. E., Bostock, J., and Waterstrat, R. M., Superconducting Properties of Al5 Phase V-Ir Alloys. Proc. LT 13, Boulder, Colorado (1972).
8. Cox, J. E., and Waterstrat, R. M., unpublished results (1973).
9. Blaugher, R. D., Hein, R. E., Cox, J. E., and Waterstrat, R. M., Atomic Ordering and Superconductivity in Al5 Compounds, J. Low-Temp. Physics 1, pp. 539-561 (1969).

10. Ritter, D. L., Giessen, B. C., and Grant, N. J.,  
The Niobium (Columbium)-Rhodium Binary System, Part I:  
The Constitution Diagram, Trans. TMS-AIME 230,  
pp. 1250-1259 (1964).
11. Ritter, D. L., Giessen, B. C., and Grant, N. J.,  
The Niobium (Columbium)-Rhodium Binary System, Part II:  
Crystal Structure Relationships, Trans. TMS-AIME 230,  
pp. 1259-1267 (1964).

## V. NIOBIUM-OSMIUM CONSTITUTION DIAGRAM

### A. Previous Studies

Niobium-osmium alloys have been the subject of several previous investigations<sup>(1-3)</sup> but there has been no attempt to construct a constitution diagram for this system. In fact, one observes a disagreement among the various investigations regarding the location of some phase boundaries. Nevertheless, the existence of at least three intermediate phases in this system seems to be well-established. The present study represents an attempt to obtain sufficient data to permit the construction of a constitution diagram.

### B. Materials

The niobium metal used in this study was obtained from Leico Industries, Inc., in the form of powder (-325 mesh) having a nominal purity of 99.8%. A portion of this material was melted in our arc-furnace and then submitted to spectrographic and vacuum-fusion analyses with the results shown in Table 10.

The osmium metal was also obtained as powder (-325 mesh) from Engelhard Industries, Inc. and had a nominal purity of 99.9%.

A portion of each of these metals was arc-melted and then submitted to spectrographic analysis with the results shown in Table 10.

Table 10

Typical Analyses of the Materials Used in  
Preparing the Experimental Alloys<sup>†</sup>

Impurity	Niobium	Osmium
	Leico Industries Inc.	Engelhard Industries Inc.
Al	< 300	< 10
Au	-	< 10
C	53	
Ca	< 10	<100
Cr	*	<30
Cu	*	<10
Fe	<1000	<30
H	15	
Ir	-	< 300
Mg	<100	<30
N	95	
Ni	ND	<10
O	3866	
Pt	-	<100
Rh	-	<100
Si	<1000	<30
Ta	*	
V	ND	<10
W	ND	<30

\* Not determined due to niobium interferences.

† Values given in ppm.

ND Not detected spectrographically.

No other elements were detected spectrographically.

### C. Alloy Preparation

In preparing the experimental alloys we obtained helpful guidance from previous studies of the Mo-Os system<sup>(4)</sup> and the Nb-Ir system<sup>(5)</sup>. For example, special precautions were taken to insure that no residual unmelted portion of the osmium metal remained after arc-melting. This was accomplished by a thorough mixing of accurately weighed portions of niobium and osmium powders. The mixture was compressed in a 1/2-inch diameter cylindrical die of hardened steel to produce small cylinders suitable for subsequent melting. The cylindrical powder compacts were then sintered and degassed in a high-vacuum furnace operating at 1600°C and between  $10^{-5}$  and  $10^{-6}$  mm Hg. Previous experience in sintering pure Os had suggested that a weight loss of about 0.5% can be expected during this procedure and we, therefore, added a small excess of Os to each alloy compact in order to compensate for this small loss and thus produce an alloy which closely approximates the intended nominal composition. When the sintering had been completed, the alloys were removed from the high-vacuum furnace and each alloy composition was then melted at least four times in an arc-furnace under an inert atmosphere of high-purity 50% argon and 50% helium. The arc current was maintained at a high level during melting (~600 amperes) to insure complete melting of each alloy. Subsequent visual and metallographic studies indicated that all samples had been adequately melted and electron microprobe analyses of several alloys revealed that no significant contamination had occurred. Each alloy sample weighed about 20 grams and was given a homogenization anneal at high temperatures before sectioning the sample for internal examination and subsequent lower-temperature annealing.

#### D. Temperature Measurement

Temperatures up to 1500°C were measured with a platinum versus platinum-10% rhodium thermocouple. This thermocouple was calibrated with a standard thermocouple of platinum-6% rhodium versus platinum-30% rhodium which was itself calibrated at the National Bureau of Standards on the International Practical Temperature Scale of 1968 (IPTS 68). Both of these thermocouples were used to obtain data on temperature versus furnace current in our high-temperature vacuum furnace. The furnace was in this case equipped with a tungsten-mesh heating element and tungsten heat shields rather than the usual tantalum fixtures so that temperatures in excess of 2500°C could be obtained. Temperatures from 1500°C to 2200°C were measured with a tungsten versus tungsten-6% rhenium thermocouple. At all temperatures, and especially at temperatures above 2000°C, it was necessary to supplement our temperature versus furnace current plot with data obtained from the observed melting points (IPTS 68) of certain secondary standards. The secondary standards used in our calibration procedures were high-purity wires of gold (1064°C), nickel (1455°C), platinum (1772°C), rhodium (1963°C), iridium (2447°C), niobium (2472°C) and molybdenum (2625°C). In most cases the standard wires were placed in thoria crucibles using a technique described previously<sup>(6)</sup>. At about 2500°C, however, it appeared that there may have been some reaction between the thoria crucibles and their tantalum holder and, therefore, the niobium and molybdenum wires were simply suspended from fine tungsten wires extending part way into the hot zone of the furnace. Each standard wire was formed into a small (~1/8-inch diameter) loop at its tip to facilitate the observation of melting. The wires always melted first at this tip since the tip was accurately placed in the hot zone at the position of maximum temperature.

The accuracy of these procedures, however, can be no better than the accuracy to which one can specify the melting points of the secondary standards. At present it appears that an accuracy of  $\pm 10^\circ\text{C}$  would be the best that could be claimed for our Nb and Mo wires which had a nominal purity of at least 99.9%. Nevertheless, future work may produce more reliable values for wires of this purity and if more reliable values are obtained it should be possible to make appropriate corrections to our data. There is certainly an urgent need for accurate secondary temperature standards above  $2000^\circ\text{C}$  since many experiments are not conducive to the use of ideal "black-body" radiation cavities either because of interference with other objects in the hot zone or because the hot zone does not contain a region of reasonably constant temperature large enough to accommodate the "black-body" cavity. In such cases the use of radiation pyrometry techniques will suffer a substantial loss of accuracy even though the accuracy and sensitivity of some present photo-electric devices are quite good. The tungsten-rhenium thermocouples are, at best, only a partial solution to this problem since substantial changes in their calibration can occur during a measurement either as a result of contamination or because of strains introduced by thermal expansion and contraction during temperature cycling. Even with these thermocouples, however, secondary standards would be very helpful in improving measurements above  $2000^\circ\text{C}$ .

#### E. Thermal Treatments

Alloys containing 80% Os or more were homogenized by annealing at  $2420^\circ\text{C}$  for 6 hours. All of the alloys were annealed at  $2000^\circ\text{C}$  for 12 hours prior to any annealing at lower temperatures.

All annealing was performed in a tungsten-mesh resistance furnace operating at pressures between  $10^{-5}$  and  $10^{-6}$  mm Hg.

The samples were suspended in Ta buckets lined with Nb sheet and suspended with Ta wire. Samples to be annealed at 1100°C were sealed in evacuated quartz tubes which were back-filled with a partial pressure of argon gas.

Samples annealed in the vacuum furnace were "radiation-quenched" by turning off the furnace power. Alloys sealed in quartz tubes were quenched in cold water. The cooling rates appeared to be adequate for retaining structures formed at the respective annealing temperatures except for the  $\sigma$  phase containing over 68 at. % Nb which always transformed to the  $\beta$  phase during cooling. A summary of typical annealing treatments used in this study is given in Table 11.

Table 11  
Summary of Typical Equilibration Treatments  
for Niobium-Osmium Alloys

Temperature °C	Time	Alloys (atomic % Nb)
2420	6 hrs	10, 20
2000	12 hrs	10, 20, 30, 36, 45, 50, 56, 65, 70, 75, 80, 90
1600	1 week	10, 20, 30, 36, 45, 50, 56, 65, 70, 75, 80, 90
1100	6 weeks	10, 20, 30, 36, 45, 50, 56, 65, 70, 75, 80, 90

## F. Methods for Determination of Phase Boundaries

### 1. Solidus Temperatures

The solidus temperatures of the niobium-osmium alloys were determined mainly by direct observation of small (~1 g) samples during heating. The samples were tied in place at the end of a piece of fine (.005") tungsten wire or, particularly at the highest temperatures, with thicker (.010") tungsten wire. The tungsten wires were then suspended so that the sample would be located at the point of maximum temperature in the hot zone. Standard wires of Pt, Rh, and Nb were also suspended in this manner in preliminary experiments which established that the method was capable of yielding accurate melting point data.

The method was surprisingly successful. In many cases the sample melted to form a small molten droplet which remained fixed in the loop of tungsten wire presumably with some support provided by surface tension of the liquid droplet as it wetted the tungsten wire. One might expect that at these temperatures (>2000°C) there would be significant diffusion and chemical reaction between the niobium-osmium alloys and the tungsten wire but subsequent examination of the wires and the samples revealed little evidence of any reaction although the wire was indeed "wetted" by the molten alloys. The wire in contact with the sample essentially retained its original size and shape, as far as could be determined by visual observation, although recrystallization of the wires at these high temperatures did produce embrittlement. The absence of any significant reaction between the wires and the samples suggests that the method has probably yielded reasonably accurate solidus temperatures for the

niobium-osmium alloys. One must remember that the temperature is recorded at the first sign of melting and that reactions in the solid state are likely to be even more restricted than reactions with the liquid. Furthermore, it appears that, in this system, melting occurs rather sharply in most cases due to the small interval between the liquidus and solidus temperatures.

## 2. Liquidus Temperatures

The liquidus temperatures were estimated from the general form of the solidus boundaries and from the location of the invariant reactions. In some cases metallographic observations on samples used for solidus determinations were helpful in suggesting the location of the liquidus.

## 3. Other Phase Boundaries

The boundaries of the various phases were determined by metallographic and x-ray diffraction studies together with quantitative electron-probe microanalyses of the phases coexisting in two-phase alloys. The relatively narrow two-phase regions occurring in this system permit the location of phase boundaries with unusual accuracy through use of the well-known "lever rule". One first estimates the relative amounts of each phase coexisting in a two-phase alloy and then, by independent knowledge of one of these phase boundaries, it is possible to estimate the approximate position of the other boundary. A fortunate choice of alloy compositions lying very close to the phase boundaries in this system greatly facilitates this process since one phase boundary is thus already fairly well established. The accuracy of the phase boundaries determined in this study is estimated at about  $\pm 1$  atomic %.

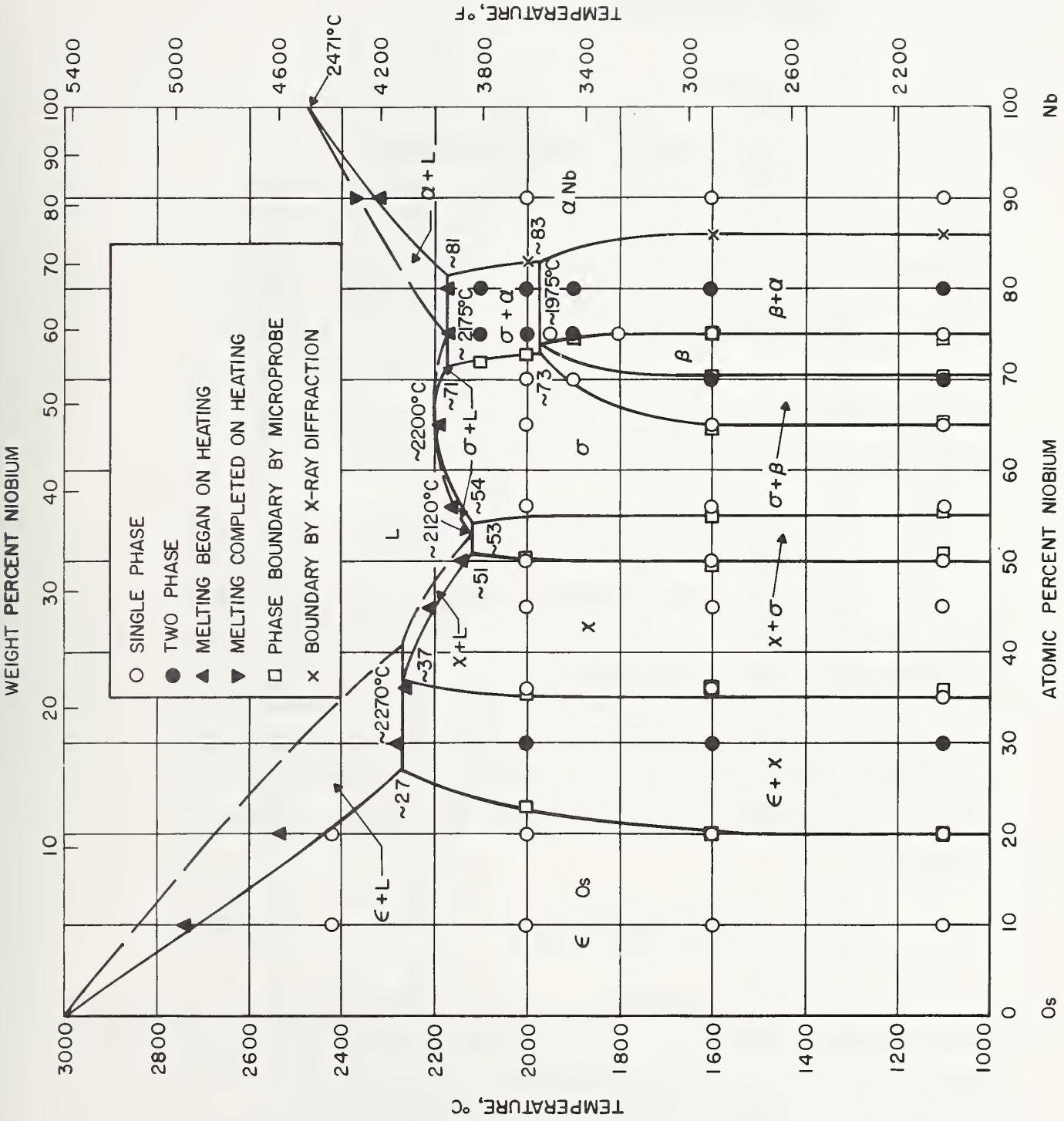


Fig. 14 - The niobium-osmium constitution diagram

## G. Experimental Results

### 1. General

The proposed constitution diagram for the niobium-osmium system is shown in Fig. 14. The number of alloy compositions represented by our experimental samples is relatively small but these were, fortunately, located in such a manner that considerable information on the location of the phase boundaries was obtained. The proposed diagram is, therefore, considered to be accurate to about  $\pm 1$  atomic % and  $\pm 20^\circ\text{C}$ . The crystal structures for each intermediate phase are given in Table 12 and lattice parameters are given in Table 13.

### 2. Osmium Terminal Solid Solution - $\epsilon$

The close-packed hexagonal osmium terminal solid solution dissolves up to about 27 at. % Nb at  $2270^\circ\text{C}$ . An increasing Nb content in this phase is accompanied by an increase in the lattice parameters ( $a_0$  and  $c_0$ ) with a nearly constant axial ratio ( $c/a$ ). The solubility limit is only moderately temperature dependent. Alloys containing more than 27 at. % Nb (Fig 15a) show that the  $\epsilon$  solid solution coexists with an intermetallic compound ( $\chi$  phase).

### 3. Intermediate Phase - $\chi$

The  $\chi$  phase was found to possess a cubic  $\alpha$ -Mn (Al<sub>2</sub>)-type structure, in confirmation of previous studies<sup>(1, 3)</sup>. It extends over a significant composition range from about 35 to 51 at. % Nb and apparently forms via a peritectic reaction at about  $2270^\circ\text{C}$ . Although previous studies suggested that atomic ordering was present in this structure, there has been little

Table 12

## Crystallographic Data for Niobium-Osmium Intermediate Phases

Intermediate Phase	Crystal System	Space Group	Structure Type	No. Atoms		Composition Limits, At. % Nb
				Per Unit Cell		
$\chi$	Cubic	$T_d^3 - \bar{1}43m$	Ordered Al2, $\alpha$ Mn	58		35 to 49 1600°C
$\sigma$	Tetragonal	$D_{4h}^{14} - P4/mnm$	$D8_p, \beta$ U	30		54 to 68 1600°C
$\beta$	Cubic	$O_h^3 - Pm3n$	Ordered Al5, $Cr_3Si$	8		71 to 76 1600°C

Table 13

Lattice Parameters of Intermediate Phases and Terminal  
Solid Solutions for Niobium-Osmium

At. % Os	Phase	Lattice Parameter(s), Å			c/a
		a	b	c	
10	α Nb	3.263			
14	α Nb	3.251			
17	α Nb	3.233			
25	β	5.135			
29	β	5.118			
35	σ	9.897		5.083	.514
44	σ	9.820		5.050	.514
50	χ	9.776			
55	χ	9.739			
64	χ	9.661			
80	ε Os	2.762		4.415	1.598
90	ε Os	2.752		4.368	1.587

Table 14

Observed and Calculated Relative Intensities  
for Nb<sub>36</sub>Os<sub>64</sub>  $\chi$ -Phase

hkl	I <sub>obs</sub>	I <sub>calc</sub>	
		Disordered	Ordered†
110	-	0	1
200	-	1	0
211	m	5	110
220	w	7	44
310	vw	2	10
222	vw	8	14
321	-	7	4
400	m	48	60
330 } 411 }	vs	1000	1000
420	vw	5	10
332	s	278	441
422	m	101	107
431 } 510 }	ms	140	262
521	mw <sup>+</sup>	12	24
440	w	2	6
433 } 530 }	mw	11	15
442 } 600 }	w	14	11
532 } 611 }	mw	20	13
620	w <sup>+</sup>	3	7
541	-	4	5

(Table 14 Continued)

Table 14 (Continued)

hkl	I <sub>obs</sub>	I <sub>calc</sub>	
		Disordered	Ordered†
622	m	27	32
631	vw	7	4
444	ms	71	85
543	s	83	112
550			
710			
640	-	0	0
552	vs	308	326
633			
721			
642	s	54	109
730	ms	36	51
732	s	54	72
651			
800	-	0	0
811	m	15	18
741			
554			
820	m	24	21
644			
653	m	17	22
822	vs	98	132
660			
831	m	31	26
750			
743			

(Table 14 Continued)

Table 14 (Continued)

hkl	I <sub>obs</sub>	I <sub>calc</sub>	
		Disordered	Ordered <sup>+</sup>
662	w	9	7
752	mw	11	14
840	-	1	1
910 } 833 }	ms	31	64
842	w	9	14
921 } 761 } 655 }	ms	25	63
664	w	19	18
930 } 851 } 754 }	ms	59	69

+ The model chosen was based on the composition  $Nb_{36}Os_{64}$  and therefore one must distribute approximately 21 Nb atoms among the 58 atomic sites in this structure. The large Nb atoms were assumed to be distributed so that 10 Nb atoms completely fill the sites of CN 16 [positions 2(a) and 8(c)]. The remaining 11 Nb atoms were assumed to partially fill the sites of CN 14 [position 24(g)] with Os atoms occupying the remainder of these sites. The sites of CN 12 [position 24(g)] are assumed to be completely filled with Os atoms.



160X (a)

30 at. % Nb, 70 at. % Os. Annealed at 2000°C for twelve hours. Globules of  $\chi$  phase in a matrix of  $\epsilon$  Os.



80X (b)

50 at. % Nb, 50 at. % Os. Annealed at 1600°C for one week. Grain boundary network of sigma phase surrounding large grains of  $\chi$  phase.

Fig.15 - Microstructures of niobium-osmium alloys.

information available on the nature and extent of this atomic ordering. We have, therefore, calculated the relative intensities to be expected for an x-ray diffraction pattern from what we considered to be the most likely ordered structure. This involves placing the larger Nb atoms preferentially in sites having the highest coordination number (CN 16). Observed and calculated intensities are presented in Table 14. The relative intensities have been calculated for both ordered and disordered models. The disordered model is clearly ruled out by significant differences between observed and calculated intensities. The ordered model which we chose, however, eliminates these differences and produces a reasonably good agreement between calculated and observed intensities. Thus it appears that the proposed model for the atomic ordering may be substantially correct. The  $\chi$  phase enters into a eutectic reaction with another intermetallic compound ( $\sigma$  phase) and a small two-phase region exists near the equiatomic composition (Fig.15b).

#### 4. Intermediate Phase - $\sigma$

The existence of a Nb-Os sigma phase was first reported by Knapton<sup>(1)</sup>. The sigma phase region extends from about 55 to 73 at. % Nb at 1975°C and it apparently melts congruently at about 2200°C. It possesses a tetragonal ( $D_{8h}$ )-type structure<sup>(1)</sup> similar to that of beta-uranium. The atomic ordering in this phase has been determined in a previous study<sup>(7)</sup>. The Os-rich boundary of the  $\sigma$  phase and the Nb-rich boundary of the  $\chi$  phase were located by microprobe analysis of the sample Nb<sub>50</sub>Os<sub>50</sub>. This sample was essentially single phase ( $\chi$ ) except for a surface layer which had apparently been depleted in Os during annealing and which, consequently, had transformed to the sigma phase. Microprobe analyses were made close to the boundary

between the  $\chi$  phase interior and the  $\sigma$  phase surface layer and on both sides of this boundary.

#### 5. Intermediate Phase - $\beta$

The beta phase region extends from about 70.5 to 75 at. % Nb and this phase forms via a peritectoid reaction at 1975°C. It possesses the cubic A15-type structure in which partial atomic long-range ordering occurs. The extent of the atomic ordering has been reported in a previous study<sup>(8)</sup>. This phase was apparently first discovered by Geller et al<sup>(9)</sup>. It coexists with the  $\sigma$  phase (Fig.16a) and the  $\alpha$ Nb phase (Fig.16b).

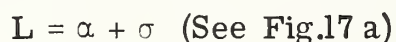
#### 6. Niobium Terminal Solid Solution - $\alpha$

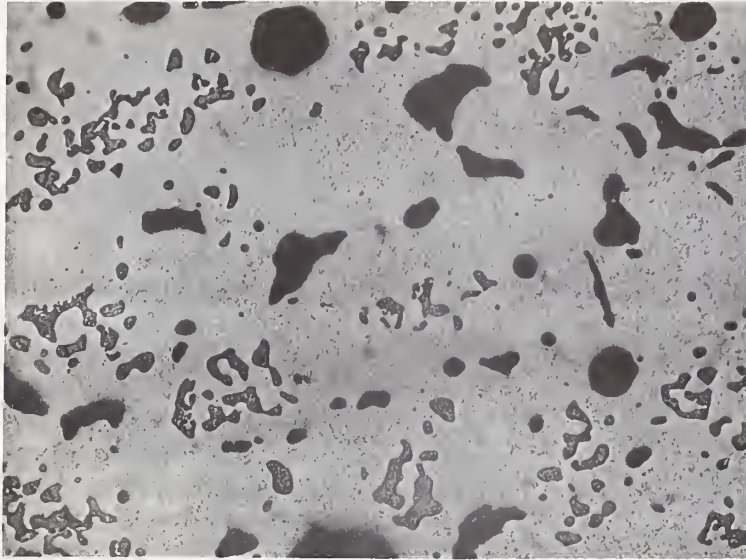
The body-centered cubic niobium solid solution may contain up to 19 at. % Os at 2175°C but a substantial decrease in solubility to about 14 at. % Os occurs at lower temperatures. This was established mainly by x-ray lattice parameters measurements since the presence of fine precipitates in this phase produced erroneous x-ray microanalyses. The addition of osmium to the  $\alpha$  phase produces decreasing liquidus and solidus temperatures culminating in a eutectic reaction with the sigma phase at about 2175°C.

#### 7. Invariant Reactions

There are five invariant reactions in the niobium-osmium binary system as follows:

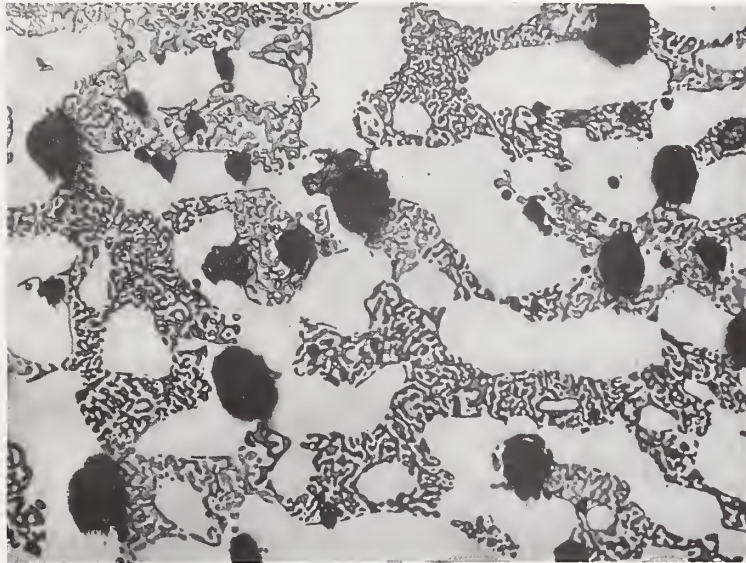
A eutectic reaction occurs at 2175°C;





80X (a)

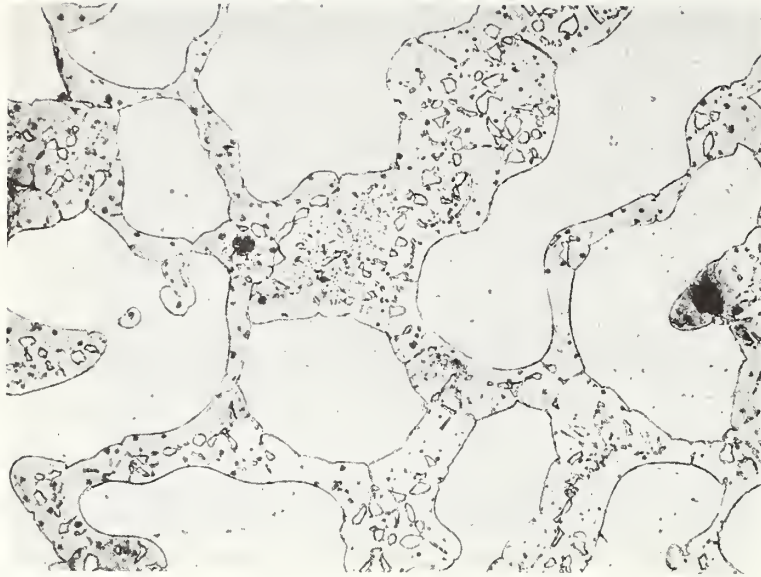
70 at. % Nb, 30 at. % Os. Annealed at 1600°C for one week. Matrix of  $\beta$  phase containing globules of sigma phase in which some precipitation of secondary  $\beta$  has occurred during cooling.



80X (b)

80 at. % Nb, 20 at. % Os. Annealed at 1600°C for one week. Globular clusters of  $\alpha$  Nb in a matrix of  $\beta$  phase.

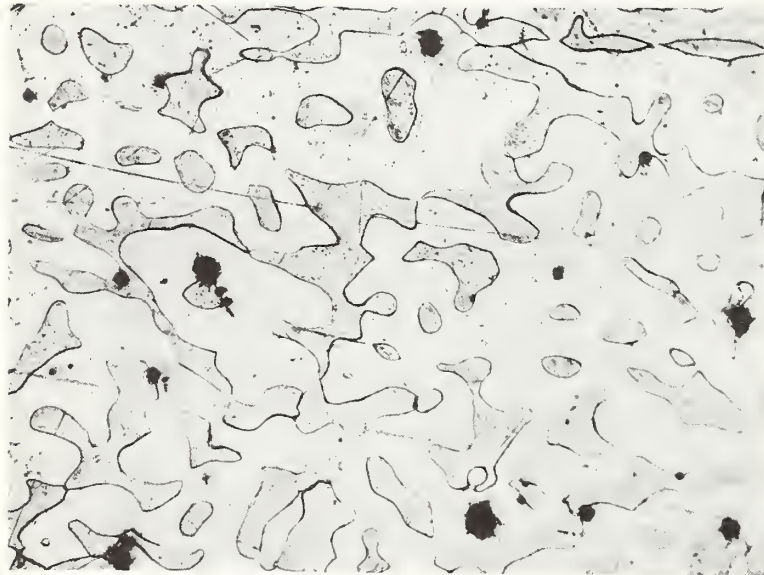
Fig. 16 - Microstructures of niobium-osmium alloys.



160X

(a)

75 at. % Nb, 25 at. % Os. Melted primary sigma phase with interdendritic eutectic of sigma plus  $\alpha$  Nb phases.



160X

(b)

75 at. % Nb, 25 at. % Os. Annealed at 2000°C for twelve hours.  $\alpha$  Nb globules in a matrix of sigma phase.

Fig. 17 - Microstructures of niobium-osmium alloys.

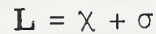
A peritectic reaction occurs at 1975° C;



Congruent melting of the sigma phase occurs at 2200° C;



A eutectic reaction occurs at 2120° C;



A peritectic reaction occurs at 2270° C;



The existence of most of these invariant reactions was established by the solidus measurements and by metallographic examination of the solidus specimens themselves. The peritectoid reaction temperature was established by annealing the alloy Nb<sub>75</sub>Os<sub>25</sub> at various temperatures and noting any microstructural changes (See Fig. 16b and 17b).

## H. Discussion

The niobium-osmium constitution diagram (Fig. 14) is dominated by the presence of the three intermediate phases  $\chi$ ,  $\sigma$  and  $\beta$ . These phases share some common crystallographic features. Each structure seems to contain atoms of differing size arranged in a dense packing such that only tetrahedral interstices are formed and giving rise to some characteristic atomic polyhedra (Kasper polyhedra) with relatively high coordination numbers<sup>(10)</sup>. The structure of the  $\chi$  phase contains Kasper polyhedra having apparent coordination numbers (CN) of 12, 14 and 16. The structure of the sigma phase contains Kasper polyhedra with the coordination numbers 12, 14 and 15 and the structure of the  $\beta$  phase contains Kasper polyhedra based on the coordination numbers 12 and 14. These polyhedra are sometimes distorted, apparently in response to the packing requirements, so that the

actual coordination numbers, in some cases, may not be clearly defined. Nevertheless, these structures contain only tetrahedral interstices in contrast to the common face-centered cubic or hexagonal close-packed structures in which there are both tetrahedral and octahedral interstices<sup>(11)</sup>. Observed variations of the interatomic distances in the  $\sigma$  and  $\beta$  phase structures suggest that a primary factor in their formation is the availability of atomic sites of high coordination<sup>(12)</sup>.

Atomic ordering is commonly observed in these structures and, as a rule, one finds elements with the largest atomic size in the sites of highest coordination number (15 or 16) whereas the smaller atoms seem to prefer atomic sites with the lowest coordination number (12). Atomic sites with intermediate coordination numbers (13 or 14) contain varying mixtures of both large and small atoms and are often associated with the significant composition variations occurring in these phases.

The extent of atomic ordering in the various crystallographic sites has been determined for each of the niobium-osmium intermediate phases and this data is summarized in Table 15. Obviously the extent of filling in each site is determined partly by the over-all composition of the phase but there is also a clear indication that the larger niobium atoms prefer the atomic sites with the largest coordination numbers (CN) while the smaller osmium atoms prefer the sites of lowest coordination.

The niobium-osmium binary system appears to be unique in possessing all three of these structures ( $\chi$ ,  $\sigma$  and  $\beta$ ). At the present time, no other binary system is known to contain more than two of them.

Table 15

Comparison of Site Occupancies for  
the  $\chi$ ,  $\sigma$  and  $\beta$  Phases

	CN 12	CN 14	CN 15	CN 16
$\chi^*$ Nb <sub>36</sub> Os <sub>64</sub>	0%Nb 100%Os	46%Nb 54%Os		100%Nb 0%Os
$\sigma^\dagger$ Nb <sub>60</sub> Os <sub>40</sub>	0%Nb 100%Os		88%Nb 12%Os	100%Nb 0%Os
$\beta^\ddagger$ Nb <sub>75</sub> Os <sub>25</sub>	7%Nb 93%Os	98%Nb 2%Os		

\* From the present study (See Table 13).

+ From reference 7.

‡ From reference 8.

A plot of atomic volume versus composition for the niobium-osmium phases is given in Fig. 39. All three of the intermediate phases closely follow a linear relationship in this plot but negative deviations are observed for both terminal solid solutions.

## REFERENCES

1. Knapton, A. G., An X-ray Survey of Certain Transition-Metal Systems for Sigma Phases, Journ. Inst. Metals 87, pp. 28-32 (1958-1959).
2. Knapton, A. G., Niobium and Tantalum Alloys, II. Constitution, Structure and Physical Properties, J. Less-Common Metals 2, p. 113-124 (1960).
3. Dwight, A. E., "Columbium Metallurgy", AIME Metallurgical Society Conferences, Interscience Publishers, Inc., New York, 10, pp. 383-406 (1961).
4. Taylor, A., Doyle, N. J. and Kagle, B. J., The Constitution Diagram of the System Molybdenum-Osmium, J. Less-Common Metals 4, p. 436 (1962).
5. Giessen, B. C., Koch, R. and Grant, N. J., The Niobium - Iridium Constitution Diagram, Trans. AIME 230, p. 1268 (1964).
6. Waterstrat, R. M. The Vanadium-Platinum Constitution Diagram, Metallurgical Trans. 4, pp. 455-466 (1973).
7. Spooner, F. J. and Wilson, C. G., Ordering in Binary  $\sigma$  Phases, Acta Cryst. 17, pp. 1533-1538 (1964).
8. Van Reuth, E. C. and Waterstrat, R. M., Atomic Ordering in Binary Al<sub>5</sub>-Type Phases, Acta Cryst. B24, pp. 186-196 (1968).
9. Geller, S., Matthias, B. T. and Goldstein, R., Some New Intermetallic Compounds with the " $\beta$ -Wolfram" Structure, Journ. Amer. Chem. Soc. 77, pp. 1502-1504 (1955).

10. Kasper, J. S., "Atomic and Magnetic Ordering in Transition Metal Structures" in Theory of Alloy Phases, American Society for Metals, Cleveland, Ohio 48A, pp. 264-278 (1956).
11. Laves, F., "Factors Governing Crystal Structure" in Intermetallic Compounds edited by J. H. Westbrook, John Wiley & Sons, New York, p. 133 (1967).
12. Pearson, W. B., The Crystal Chemistry and Physics of Metals and Alloys, Wiley-Interscience Division, John Wiley & Sons, New York, pp. 55-57 (1972), p. 663 ff.

## VI. NIOBIUM-PALLADIUM CONSTITUTION DIAGRAM

(Work done at the Massachusetts Institute of Technology by David Parker and Bill C. Giessen and at the National Bureau of Standards by Richard M. Waterstrat)

### A. Previous Studies

The earliest published information on the constitution of niobium-palladium alloys is apparently found in a paper by Greenfield and Beck<sup>(1)</sup> who studied seven alloys which were all annealed at 1000°C. They reported the existence of a sigma phase and did not observe any other intermediate phases. A later survey of this system by Knapton<sup>(2)</sup> reported an appreciable solubility of palladium in body-centered cubic niobium (at least 25 at. % Pd) and the observation of face-centered cubic x-ray powder patterns for palladium-based alloys containing up to 50% Nb. Knapton was unable to confirm the presence of a sigma phase in alloys containing 30 to 50 at. % Pd. No sigma structure was detected after arc-melting or after annealing at 1000 to 1200°C for 5 to 7 days.

In 1961 an equilibrium diagram for the Nb-Pd system was published by Savitskii, Baron and Khotinskaya<sup>(3)</sup>. They reported a sigma phase at 60 wt. % Nb which they chose to designate as Nb<sub>2</sub>Pd. They also reported a compound NbPd<sub>3</sub> whose structure was not determined. The sigma phase was reported as forming by a peritectic reaction at 1650°C. NbPd<sub>3</sub> was described as being formed at 1700°C from the melt. Extensive mutual solid solubility was reported for both of the terminal solid solutions.

In 1964 the structures of several Nb-Pd compounds were identified<sup>(4, 5)</sup> and the phases existing in this system were

listed as  $\sigma$ ,  $\alpha\text{NbPd}$ ,  $\text{NbPd}_2$ ,  $\alpha\text{NbPd}_3$  and  $\beta\text{NbPd}_3$ . However, a somewhat later study<sup>(6)</sup> reported  $\text{Nb}_3\text{-Pd}_2$  forming at low temperatures and  $\text{Nb}_3\text{Pd}_2$  (a  $\sigma$  phase) forming at high temperatures. The compounds  $\text{NbPd}_2$  and  $\text{NbPd}_3$  were also reported. A subsequent reinvestigation of the Nb-Pd system<sup>(7)</sup> yielded a phase diagram which differs significantly from the one reported by Savitskii et al<sup>(3)</sup> and identifies the compounds  $\text{Nb}_2\text{Pd}$ ,  $\text{Nb}_2\text{Pd}_3$ ,  $\text{NbPd}_2$  and  $\text{NbPd}_3$ .

## B. Materials

The niobium metal used for most of this study was in the form of -200-mesh powder having a nominal purity of 99.8%. Some alloys were made using niobium rondelles of 99.6% purity supplied by the Electro Metallurgical Co. but the use of this material was generally confined to some of the Pd-rich samples. The Nb powder was obtained from Leico Industries Inc., New York, and an analysis of this material after arc-melting showed: Al, <300 ppm; Ca, <10 ppm; Fe, <1000 ppm; Mg, <100 ppm; Si, <1000 ppm. Cr, Cu and Ta could not be determined due to niobium interferences but the supplier has indicated that Ta is the major impurity. No other elements were detected spectrographically. Vacuum fusion analysis showed: H, 15 ppm; O, 3866 ppm; C, 53 ppm; and N, 95 ppm.

The palladium metal used in this study was in the form of powder or wire, both having a nominal purity of 99.9+%. The powder was obtained from Engelhard Industries Inc., Newark, N. J. and the wire from the International Nickel Co., Inc. Neither of these materials was submitted to a chemical analysis.

### C. Alloy Preparation

Weighed amounts of the Nb and Pd powders were thoroughly mixed and then compressed in a 1/2-inch diameter cylindrical steel mold. The compressed powder cylinders were sintered in a high-vacuum furnace prior to arc-melting. Weight losses after sintering and after arc-melting three or four times were, in all cases, less than 1%. The arc-melted samples of 5 to 10 grams each were broken or sectioned to check for inhomogeneities but in most cases the samples appeared to be well melted. A few Nb-rich alloys were prepared using Nb rondelles and in some of these samples we observed unmelted Nb. Such alloys were discarded and new alloys were made using powder mixtures to insure homogeneity. Ultimately all of the samples were well melted and suitable for preliminary homogenization treatments. In view of the small weight losses, it was assumed that the actual alloy compositions did not deviate significantly from the nominal compositions.

### D. Temperature Measurement

Temperatures up to 1500°C were measured with a platinum versus platinum-10% rhodium thermocouple. Calibration of furnace temperatures was accomplished by plotting furnace current versus temperature using a standard platinum-6% rhodium versus platinum-30% rhodium thermocouple. This thermocouple had been calibrated at the National Bureau of Standards. Calibration above 1500°C was accomplished using secondary standards

such as the melting points of gold, platinum, rhodium, iridium and niobium. All temperatures are measured on the International Practical Temperature Scale of 1968 (IPTS 68). Temperatures in the vacuum furnace were also measured with a Leeds and Northrup optical pyrometer.

#### E. Thermal Treatments

All alloys were homogenized by annealing at temperatures near the melting point of each alloy for several hours. The homogenization treatments were done using the normal precautions taken during an equilibration treatment and the samples were, therefore, considered as being equilibrated at the homogenization temperature. Equilibration annealing of all samples was done at progressively lower temperatures for each sample.

The annealing treatments above 1100°C were performed in a high-vacuum furnace having a tantalum heating element and tantalum heat shields. A pressure of between  $5 \times 10^{-6}$  and  $2 \times 10^{-5}$  mm Hg was usually obtained during annealing. Samples were rapidly cooled after annealing by turning off the furnace power. The cooling rate was not sufficient to retain all of the high-temperature structures formed during annealing but information obtained from the partially decomposed samples was sufficient to permit an understanding of the high-temperature behavior. A summary of typical annealing treatments is shown in Table 16.

Samples annealed at or below 1100°C were sealed in quartz tubes under a partial pressure of pure argon and were water quenched after annealing.

Table 16

Typical Equilibration Treatments for  
Niobium-Palladium Alloys

Temperature (°C)	Time	Alloys (Atomic %Pd)
1900	2 hrs	10, 20
1700	3 hrs	10, 20, 25
1520	4 hrs	25, 50, 52.5, 55, 57.5, 60, 64, 70, 72.5, 78, 79, 80, 81
1400	12 hrs	10, 20, 25, 28, 30, 32, 34, 36, 38, 40, 47.5, 50, 52.5, 55, 57.5, 60, 62.5, 65, 66.6, 67.5, 70, 72.5, 75, 77, 80
1300	2 days	10, 20, 25, 28, 30, 32, 34, 36, 38, 40, 47.5, 52.5, 55, 57.5, 60, 62.5, 65, 66.6, 67.5, 70, 72.5, 77, 80
1200	1 wk	10, 20, 25, 28, 30, 32, 40, 47.5, 52.5, 57.5, 62.5, 66.6, 67, 72.5, 80
1100	2 wks	25, 28, 30, 32, 34, 36, 38, 40, 52.5, 60, 70, 90
1000	3 wks	25, 28, 30, 32, 34, 36, 38, 40, 57.5, 66.6, 72.5, 77
900	1 month	25, 28, 30, 32, 34, 36, 38
800	2 months	25, 36, 38

## F. Methods for Determination of Phase Boundaries

### 1. Solidus Temperatures

The procedures used in determining the solidus temperatures have been described in a previous paper<sup>(8)</sup>. High-purity alumina crucibles were found to be satisfactory for all alloys containing more than 20 at. % Pd but thoria crucibles were used for the Nb-rich alloys.

### 2. Liquidus Temperatures

In general, we did not attempt to determine the liquidus temperatures but they could be estimated with satisfactory accuracy for alloy compositions lying in the vicinity of a congruent melting maximum or a eutectic minimum. The estimated liquidus boundaries are shown by dashed lines in Fig. 18.

### 3. Invariant Reactions

The existence of invariant reactions and the temperatures at which these reactions occur were established mainly by comparing metallographic and x-ray diffraction data from alloys annealed above and below the transformation temperatures. The phases existing above the transformation temperatures could not always be retained to room temperature by rapid quenching but metallographic studies were successful in revealing the structures characteristic of samples annealed either above or below the transformation temperature. The actual temperature of the transformation is established by successive annealing treatments which bracket this temperature with an accuracy comparable to that of the temperature measurement itself.

#### 4. Other Phase Boundaries

In previous studies we have relied extensively on the analysis of individual phase regions in two-phase alloys using the electron-beam microprobe. Unfortunately, the alloys in this system were frequently unsuited to this method due to the presence of unresolvable fine structures in the alloy samples. These structures originate in the eutectoid decomposition of phases occurring at high temperatures or by precipitation from solid solutions. Two separate eutectoid transformations occur in this system, and we were forced to rely on metallographic studies to locate these phase boundaries. The metallographic studies require more effort and time than the electron probe measurements, but the results are sufficiently reliable to establish the location of the phase boundaries to the desired accuracy.

#### G. Experimental Results

##### 1. General

The proposed constitution diagram for the niobium-palladium system is shown in Fig. 18. The phase boundaries were established mainly by metallographic and x-ray diffraction studies. The alloy samples frequently contained phases which had decomposed from prior high-temperature structures. In all cases, however, it was possible to obtain a consistent and rational interpretation of these structures.

##### 2. Niobium Terminal Solid Solution - $\alpha$

The solubility of palladium in body-centered cubic niobium extends to about 37 at. % Pd at 1520°C. However, there is

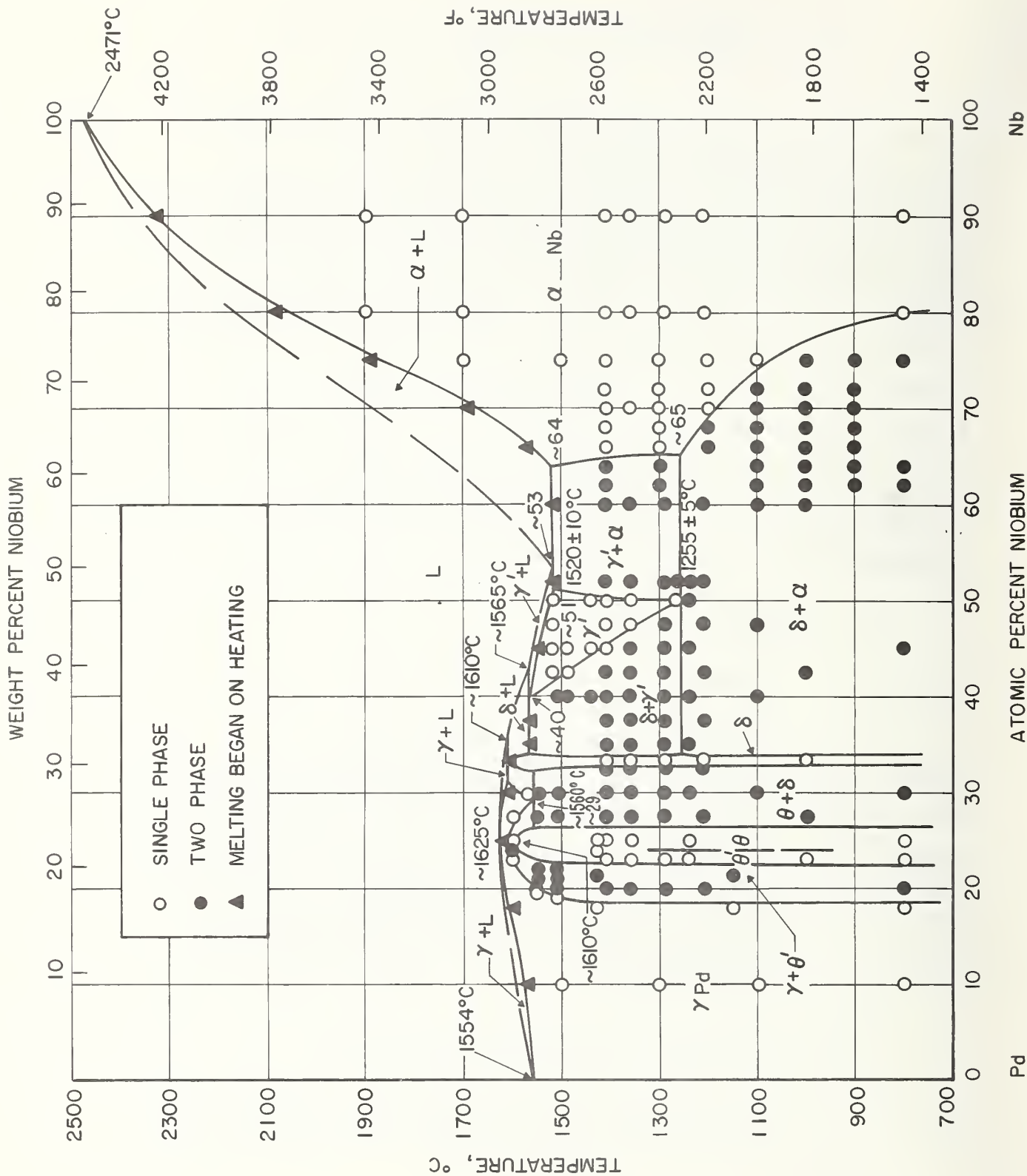
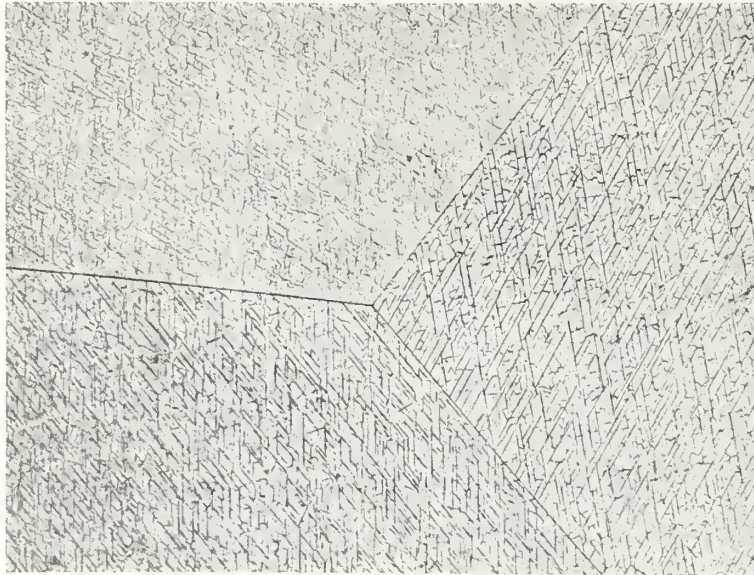


Fig. 18 - The niobium-palladium constitution diagram

a significant reduction in solubility at lower temperatures so that at 800°C the solubility of palladium extends to only about 20 at. % Pd (See Fig. 19a and 19b). Thus, when alloys containing 25 to 37 at. % Pd were annealed above 1200°C and cooled rapidly, the cooling rates employed in this study were apparently insufficient to prevent a significant precipitation of the intermediate phase  $\delta$ -NbPd<sub>2</sub>. This is shown in Fig. 20a. One can still see the outline of the relatively large primary grains of the  $\alpha$ -phase solid solution but there is evidence of a precipitate at the grain boundaries and also within the grains. When alloys containing Pd in excess of the maximum solubility at high temperatures are quenched and examined metallographically, one observes some additional second phase (sometimes showing evidence of decomposition) in addition to the phase which has obviously precipitated (See Fig. 20b, 21a, 21b, 22a). Thus it is possible to estimate the location of the solvus boundary at high temperatures by examination of the alloys which exhibit partial decomposition.

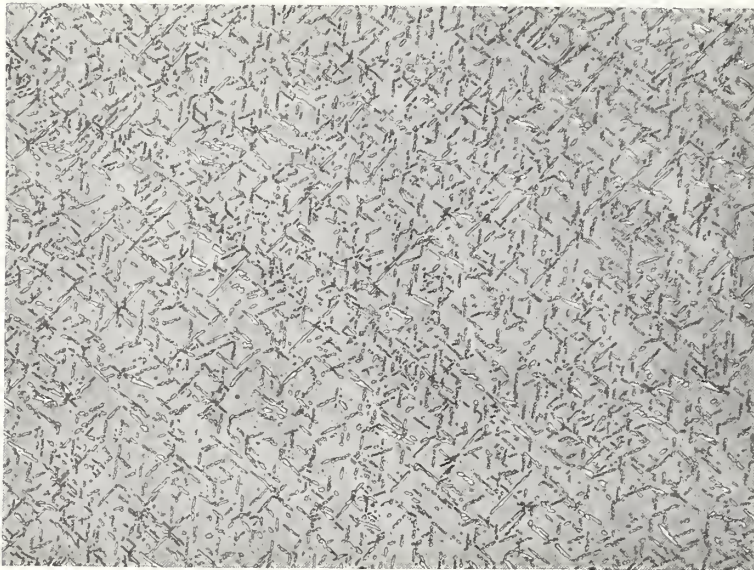
Alloys in this composition range exhibit some interesting microstructures when precipitation occurs at relatively low temperatures, as shown in Fig. 19a and 20b. It is possible that some of these structures are associated with the formation of a metastable phase. Maldonado and Schubert<sup>(6)</sup>, for example, have reported the existence of an orthorhombically deformed structure based on the body-centered cubic structure (NbRu-Unterstruktur) after annealing the alloy Nb<sub>75</sub>Pd<sub>25</sub> at 650°C for 500 hours. This phase was apparently also formed in their alloy Nb<sub>66</sub>Pd<sub>34</sub> after annealing at 700°C for 48 hours and is designated by these authors as Nb<sub>3</sub>-Pd<sub>2</sub>(r) implying that it is a room-temperature phase.



160X

(a)

75 at. % Nb, 25 at. % Pd equilibrated at 1100°C for two weeks. Large grains of  $\alpha$  Nb containing a fine network of striations which are possibly associated with a metastable condition.

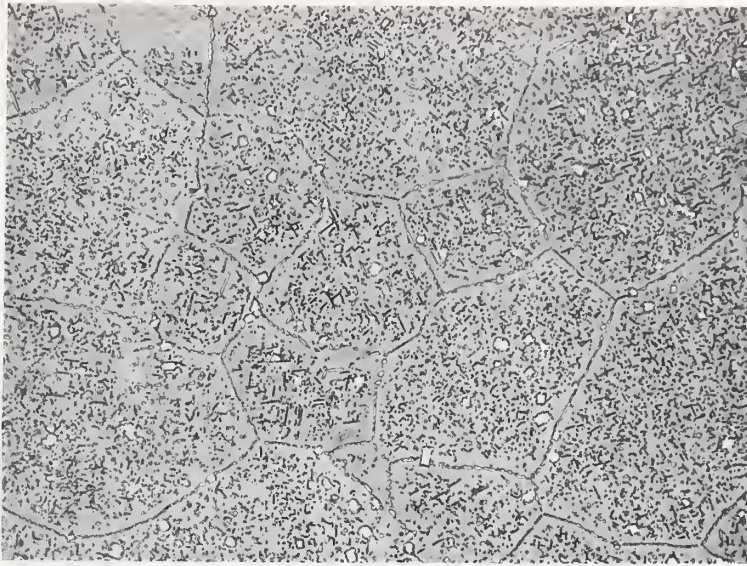


160X

(b)

75 at. % Nb, 25 at. % Pd equilibrated at 1000°C for three weeks. Oriented precipitation of  $\delta$  phase in a matrix of  $\alpha$  Nb solid solution.

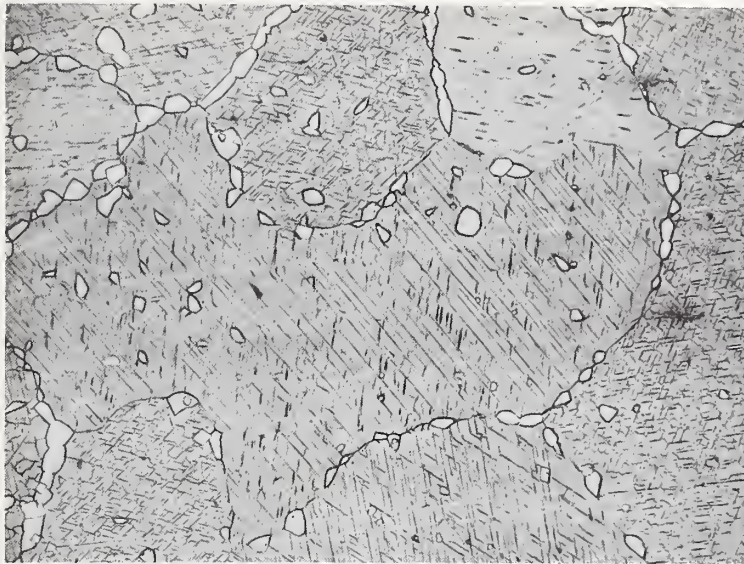
Fig.19 - Microstructures of niobium-palladium alloys.



160X

(a)

72 at. % Nb, 28 at. % Pd equilibrated at 1300°C for two days and rapidly cooled. Precipitation of  $\delta$  phase occurs due to an insufficient rate of cooling.



160X

(b)

70 at. % Nb, 30 at. % Pd equilibrated at 1100°C for two weeks and quenched. Grain boundaries contain equilibrated particles of  $\delta$  phase. The interior of each grain contains characteristic striations formed as a result of an insufficient quenching rate.

Fig.20 - Microstructures of niobium-palladium alloys.



160X (a)

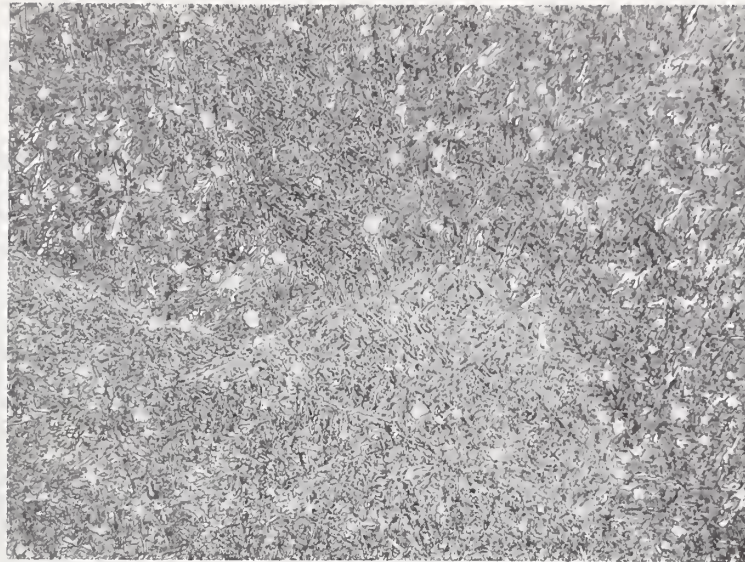
66 at. % Nb, 34 at. % Pd equilibrated at 1300°C for two days and rapidly cooled. Extensive precipitation of  $\delta$  phase occurs despite the rapid cooling.



160X (b)

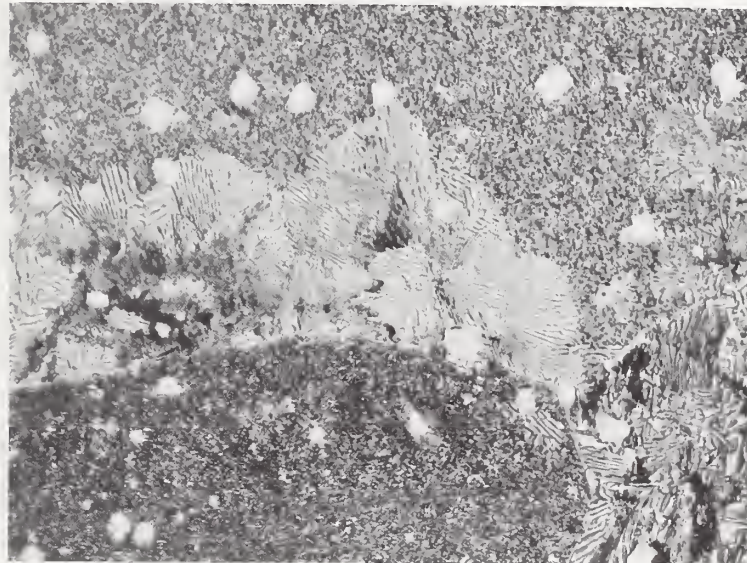
65 at. % Nb, 35 at. % Pd equilibrated at 1100°C for two weeks and quenched. Matrix is  $\alpha$  Nb and contains globular particles of the  $\delta$  phase.

Fig. 21 - Microstructures of niobium-palladium alloys.



160X (a)

64 at. % Nb, 36 at. % Pd equilibrated at 1300°C for two days and rapidly cooled. Prior structure consisted of large grains of  $\alpha$  Nb with a small percentage of  $\delta$  phase. Extensive precipitation of  $\delta$  phase occurs during rapid cooling.



400X (b)

68 at. % Nb, 32 at. % Pd equilibrated for one month at 900°C. Cellular precipitate of  $\delta$  phase consuming a fine point precipitate.

Fig.22 - Microstructures of niobium-palladium alloys.

However, it appears that one cannot yet rule out the possibility that this is a metastable phase which is perhaps formed as a result of cold-working the alloy powders used in the x-ray diffraction studies and then inadequately annealing these powders. We did not observe this structure in alloys which were annealed at higher temperatures. In the sample annealed at 700°C a cellular precipitate was observed which apparently consumes a prior fine structure during its growth (Fig. 22b).

The occurrence of these precipitate structures in the  $\alpha$  solid solution suggests that interesting mechanical properties could perhaps be obtained by a suitable heat-treatment of alloys in this composition range.

### 3. Intermediate Phase - $\gamma'$

In the equiatomic region one observes a high-temperature phase,  $\gamma'$ , which decomposes via a eutectoid reaction at 1255°C. Alloys quenched from above this temperature contained the finely-decomposed structure seen in Fig. 23a. We were, thus, unable to retain the high-temperature phase by rapid quenching. Alloys annealed below this temperature contained spheroidized structures produced by completion of the eutectoid reaction (Fig. 23b). By analogy to the V-Pd system<sup>(9)</sup> it is suggested that the  $\gamma'$  phase is probably an extension of the face-centered cubic  $\gamma$  solid solution. This could perhaps be checked by high-temperature x-ray diffraction studies. High-temperature x-ray studies on this phase have been done by Bowers<sup>(7)</sup>, who reported a cubic pattern, but due to the lack of data at low angles in this camera he was unable to determine whether it was, in fact, a face-centered cubic pattern.

#### 4. Intermediate Phase - $\delta\text{NbPd}_2$

The intermediate phase,  $\delta\text{NbPd}_2$ , apparently forms via a peritectic reaction at about  $1610^\circ\text{C}$ . This was established by our solidus data and, particularly, by annealing the alloys  $\text{Nb}_{38}\text{Pd}_{62}$ ,  $\text{Nb}_{36}\text{Pd}_{64}$  and  $\text{Nb}_{30}\text{Pd}_{70}$  simultaneously at  $1580^\circ\text{C}$ . The  $1580^\circ\text{C}$  anneal produced evidence of melting in the microstructures of  $\text{Nb}_{36}\text{Pd}_{64}$  and  $\text{Nb}_{38}\text{Pd}_{62}$  but no evidence of melting in  $\text{Nb}_{30}\text{Pd}_{70}$ .

The crystal structure of  $\delta\text{NbPd}_2$  has been determined previously<sup>(4-6, 10, 11)</sup> as being an orthorhombic  $\text{MoPt}_2$ -type structure. This was confirmed in the present study. The lattice parameter was not measured since accurate data are already available<sup>(11)</sup>.

#### 5. Intermediate Phases - $\theta$ and $\theta'$

The intermediate phase,  $\theta\text{NbPd}_3$ , has been reported as possessing an orthorhombic crystal structure based on ordered close-packed atomic planes with a 6-layer stacking sequence<sup>(4, 5)</sup>. It has previously been designated  $\theta\text{NbPd}_3$ <sup>(4, 5)</sup>. Another structure,  $\theta'\text{NbPd}_3$  (previously designated as  $\alpha\text{NbPd}_3$ ), has been reported to be a tetragonal  $\text{Ti-Al}_3$ -type structure<sup>(4, 6)</sup>. These two phases are closely associated in the phase diagram; the  $\theta'$  phase being slightly more Pd rich. It is not known whether these two phases are separated by a narrow two-phase region since we were unable to produce any two-phase alloys in this region. One of these phases may, in fact, be a high-temperature phase since Bowers<sup>(7)</sup> has reported evidence of a transformation at  $950^\circ\text{C}$ . We observed that a  $\theta$  phase ( $\text{NbPd}_3$ ) alloy transformed to a  $\theta'$  phase ( $\text{TiAl}_3$ -type structure) after annealing at  $850^\circ\text{C}$ . High-temperature x-ray diffraction studies would help to clarify this situation.

$\theta\text{NbPd}_3$  apparently forms at about  $1610 \pm 10^\circ\text{C}$  via a congruent order-disorder transformation from the face-centered cubic  $\gamma$  solid solution. This construction is supported by metallographic evidence and solidus data as summarized in Fig. 18.

#### 6. Palladium Terminal Solid Solution - $\gamma$

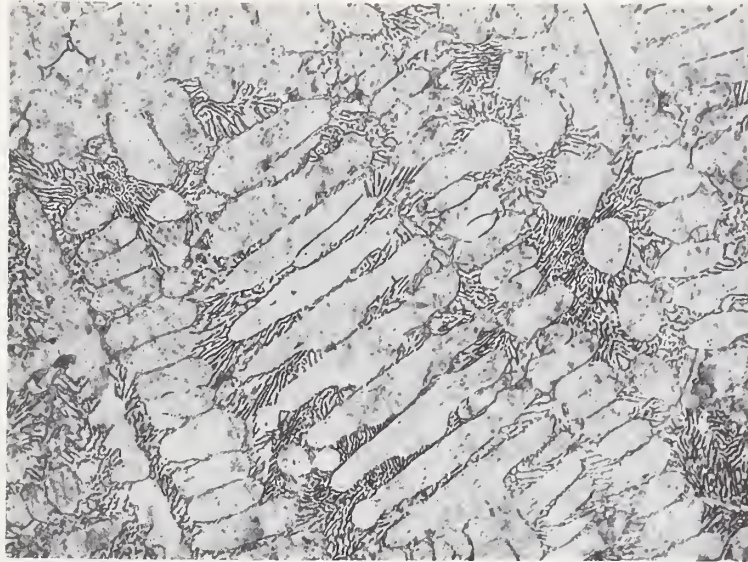
The face-centered cubic palladium solid solution apparently passes through a congruent melting maximum at  $1630^\circ\text{C}$  and 25 at. % Nb and then extends to about 31 at. % Nb at high temperatures. It decomposes via a eutectoid reaction at about  $1570^\circ\text{C}$  and 29 at. % Nb (Fig. 24a). However, at temperatures below  $1500^\circ\text{C}$  it appears that the solubility of Nb extends only to about 18 at. % Nb.

Alloys annealed in the two-phase ( $\theta' + \gamma$ ) region show evidence of a coherent precipitation of  $\theta'$  in a matrix of the  $\gamma$  phase (Fig. 24b). One might expect to produce some interesting mechanical properties in alloys containing about 20 at. % Nb.

Accurate lattice parameters for  $\theta$  and  $\theta'$  phases have been reported previously and we have, therefore, accepted these values<sup>(5, 12)</sup>.

#### 7. Eutectic: $L \rightleftharpoons \alpha + \gamma'$

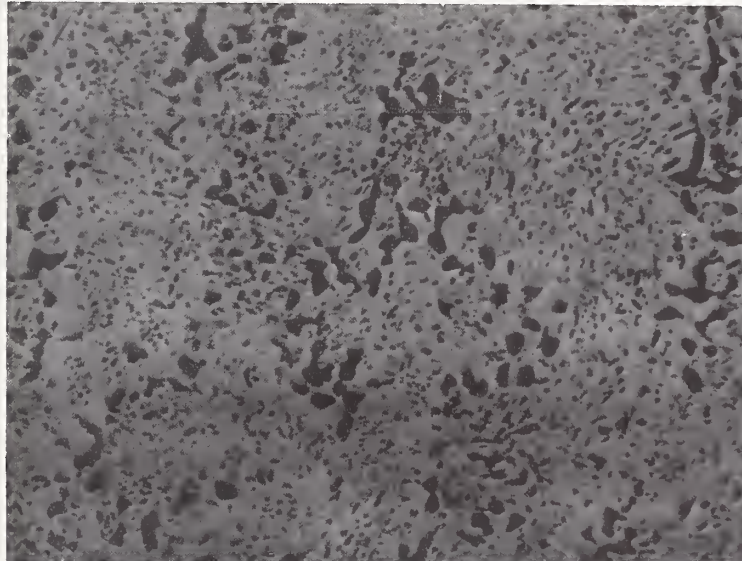
This eutectic reaction was located at  $1520 \pm 10^\circ\text{C}$  by solidus measurements. A typical eutectic microstructure is seen in Fig. 23a.



160X

(a)

52 at. % Nb, 48 at. % Pd in the "as-cast" condition. Rapidly cooled dendrites (originally  $\gamma^1$ ) containing a finely decomposed structure of  $\alpha$  Nb +  $\delta$  phase. The interdendritic regions contain a eutectic which was originally  $\alpha$  Nb +  $\gamma^1$ . The  $\gamma^1$ , however, has decomposed eutectoidally both in the primary dendrites and in the eutectic regions.

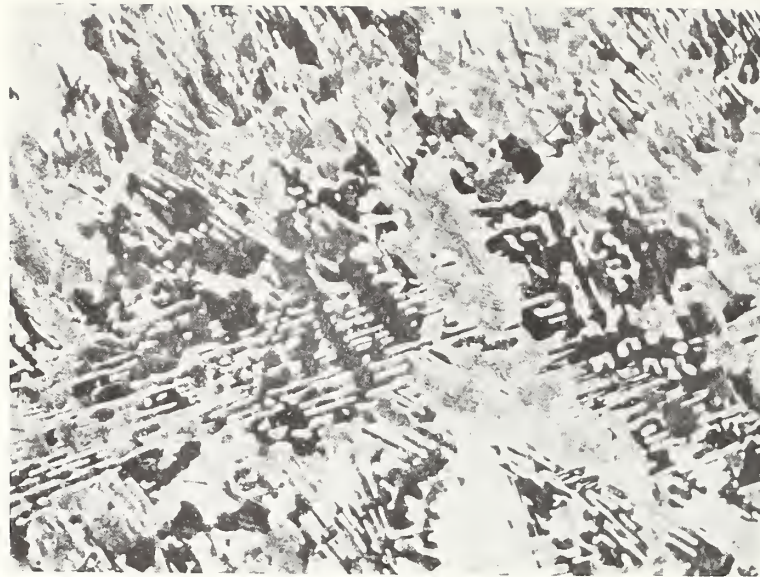


1000X

(b)

42.5 at. % Nb, 57.5 at. % Pd. Annealed at 1000°C for three weeks. Spheroidized structure produced by the eutectoid decomposition of  $\gamma^1$  phase.

Fig.23- Microstructures of niobium-palladium alloys.



400X

(a)

30 at. % Nb, 70 at. % Pd annealed at 1580 °C for two hours and rapidly cooled. Relatively coarse eutectoid structure of  $\theta + \delta$  phases produced by decomposition of the high-temperature  $\gamma$  Pd solid solution.



500X

(b)

20 at. % Nb, 80 at. % Pd. Annealed at 1357 °C for two days. Coherent precipitate of  $\theta$  phase in a matrix of  $\gamma$  Pd.

Fig.24 - Microstructures of niobium-palladium alloys.

8. Peritectic:  $L + \delta \rightleftharpoons \gamma'$

This reaction was located at  $1570 \pm 10^\circ \text{C}$  primarily on the basis of solidus measurements and metallographic studies as summarized in Fig. 18.

9. Peritectic:  $L + \gamma' \rightleftharpoons \delta$

This reaction was established at  $1610 \pm 10^\circ \text{C}$  mainly by careful solidus measurements.

10. Eutectoid:  $\gamma \rightleftharpoons \delta + \theta$

This reaction was located at about  $1575 \pm 10^\circ \text{C}$  based on metallographic studies of samples cooled rapidly from various temperatures. A typical eutectoid microstructure is seen in Fig. 24a.

11. Eutectoid:  $\gamma' \rightleftharpoons \alpha + \delta$

This reaction was observed to occur at  $1255 \pm 5^\circ \text{C}$  based on metallographic studies quenched from above and below the transformation temperature (Fig. 23a and 23b).

## H. Discussion

### 1. Absence of Sigma Phase

The existence of a binary Nb-Pd sigma phase has been reported by various investigators<sup>(1, 3, 4, 6)</sup> but it is somewhat uncertain whether all of these investigators actually

observed a sigma phase or whether they simply listed sigma phase among the phases forming in this system based on the earlier paper of Greenfield and Beck<sup>(1)</sup>.

Knapton<sup>(2)</sup> apparently made a deliberate attempt to confirm the observation of sigma phase since he studied alloys in the appropriate composition range (30 to 50 at. % Pd) and annealed them in a suitable temperature range (1000 to 1200°C) to correspond with the observations of Greenfield and Beck<sup>(1)</sup>. However, there was no evidence of sigma formation. We made a similar attempt to reproduce the conditions reported by Greenfield and Beck by preparing an alloy Nb<sub>60</sub>Pd<sub>40</sub> and then using the exact annealing treatment reported by Greenfield and Beck (72 hrs. at 1000°C). The alloy was two-phase ( $\alpha$ Nb +  $\delta$ NbPd<sub>2</sub>) and there was no evidence of sigma phase. Thus we have confirmed Knapton's observations<sup>(2)</sup> in contradiction to the report of Greenfield and Beck<sup>(1)</sup>.

It is possible that small amounts of impurities could stabilize the sigma phase and, in this connection, we note that the Nb metal used by Greenfield and Beck contained a rather large amount of carbon (0.5% by weight). It also contained tantalum (0.2%), iron (0.01%), silicon (0.01%) and titanium (0.03%). There were no figures given for the gaseous impurities oxygen, nitrogen and hydrogen. The niobium used by Knapton<sup>(2)</sup> was apparently obtained from Johnson, Matthey and Co., Ltd. but no details are given regarding the purity of this material. Our own niobium had a much lower carbon content (53 ppm) than the material used by Greenfield and Beck. At any rate, it appears that sigma phase did not form in any of our alloys after annealing at progressively lower temperatures in 100° increments from 1400°C to 800°C.

This is particularly surprising since in the Ta-Pd system the sigma phase is stable up to approximately 2550°C<sup>(13)</sup>. The V-Pd system<sup>(9)</sup> contains an A15-type phase in this range of Pd content but no A15-type phase was detected in our Nb-Pd alloys even though we annealed the alloy Nb<sub>3</sub>Pd and others at various temperatures down to 800°C. It, therefore, appears that the Nb-Pd system is unique among these three systems in not forming either a sigma or an A15-type phase. Instead it appears that there is a greater solubility of Pd in the body-centered cubic αNb solid solution than is the case with Pd in the αTa solid solution. This observation may be of some practical importance in developing useful Nb or Pd alloys by suppressing the formation of the brittle compounds.

## 2. Alloying Behavior

Exploration of ternary systems such as Ta-Nb-Pd may suggest some reason for the remarkable behavior of Nb in suppressing these phases. We have prepared several alloys in the Ta-Nb-Pd system and annealed them for three weeks at 1100°C. We observed the sigma phase as a major constituent of ternary alloys with Ta contents ranging from 15 to 20 at.%. The alloy Ta<sub>15</sub>Nb<sub>55</sub>Pd<sub>30</sub> was essentially all sigma despite its low Ta content. We also prepared several alloys in the V-Nb-Pd system and observed sigma phase as a major constituent for V contents ranging from 15 to 20 at.%.

Thus it appears that small amounts (< 15 at.%) of either V or Ta, when added to Nb-Pd alloys, will stabilize the brittle sigma phase. Previous reports of a sigma phase forming in the Nb-Pd binary system may, therefore, be in error; probably due to the effects of a slight contamination of the experimental alloys. Crystallographic data for Nb-Pd alloys are summarized in Tables 17 and 18.

Table 17

## Crystallographic Data for Niobium-Palladium Intermediate Phases

Intermediate Phase	Crystal System	Space Group	Structure Type	No. Atoms		Composition Limits At. %Pd
				Per Unit Cell		
$\gamma'$ NbPd	Unknown	-	Unknown	-		49 to 58 1520°C
$\delta$ NbPd <sub>2</sub>	Orthorhombic	D <sub>2h</sub> <sup>5</sup> - Immm	MoPt <sub>2</sub>	6		~67 1400°C
$\epsilon$ NbPd <sub>3</sub>	Orthorhombic	D <sub>2h</sub> <sup>13</sup> - Pmmn	$\beta$ NbPd <sub>3</sub>	24		~75 1300°C
$\theta'$ NbPd <sub>3</sub>	Tetragonal	D <sub>4h</sub> <sup>17</sup> - I4/mmm	DO <sub>22</sub> , TiAl <sub>3</sub>	8		~75 1300°C 850°C

Table 18

Lattice Parameters of Intermediate Phases and Terminal  
Solid Solutions for Niobium-Palladium

At. %Pd	Phase	Lattice Parameters			c/a	Ref.
		a	b	c		
10	$\alpha$ Nb	3.274				
20	$\alpha$ Nb	3.255				
25	$\alpha$ Nb	3.242				
67	$\delta$	2.839	8.376	3.886		11
75	$\theta$	5.486	4.845	13.602		5
75	$\theta'$	3.895		7.913	2.032	12
82	$\gamma$ Pd	3.905				
90	$\gamma$ Pd	3.901				

## REFERENCES

1. Greenfield, P. and Beck, P.A., Intermediate Phases in Binary Systems of Certain Transition Elements, Trans. AIME 206, pp. 265-276 (1956).
2. Knapton, A. G., Niobium and Tantalum Alloys. II Constitution, Structure and Physical Properties, J. Less-Common Metals, 2, pp. 113-124 (1960).
3. Savitskii, E. M., Baron, V. V. and Khotinskaya, A. N., Equilibrium Diagram of the Niobium-Palladium System, Russian Journal of Inorganic Chemistry, 6, pp. 1316-1317 (1961).
4. Giessen, W. C., Parker, D. and Grant, N. J., The Intermediate Phases  $Ab$ ,  $Ab_2$  and  $Ab_3$  in the Nb-Pd and Nb-Pt Systems. Journ. Metals (abstract) pp. 92-93 Jan. (1964).
5. Giessen, B. C. and Grant, N. J., New Intermediate Phases in Systems of Nb or Ta with Rh, Ir, Pd or Pt, Acta Cryst., 17, pp. 615-616 (1964).
6. Maldonado, A. and Schubert, K. Structure Investigation in the  $T^5$ - $T^{10}$  Homologous and Quasihomologous Alloy Systems, Z. Met. 55, pp. 619-626 (1964).
7. Bowers, I., personal communication to B. C. Giessen (1968).
8. Waterstrat, R. M., The Vanadium-Platinum Constitution Diagram, Met. Trans. 4, pp. 455-466 (1973).
9. Köster, W. and Haehl, W. D., The Binary System Palladium-Vanadium, Z. Met. 49, pp. 647-649 (1958).
10. Schubert, K., Frank, K., Gohle, R., Maldonado, A., Meissner, H. G., Raman, A., and Rossteutscher, W., Some Structure Data for Metallic Phases, Naturwiss. 50, p. 41 (1963).

11. Giessen, B. C. and Grant, N. J., The Crystal Structure of  $\text{VNi}_2$ ,  $\text{VPd}_2$ ,  $\text{VPt}_2$  and Related  $\text{AB}_2$  Phases. J. Less-Common Metals 8, pp. 114-119 (1965).
12. Dwight, A. E., "Columbium Metallurgy", AIME Metallurgical Society Conferences 10, pp. 383-406 (1961). Interscience Publishers, Inc., New York.
13. Waterstrat, R. M., Koch, R. and Giessen, B. C., The Tantalum-Palladium Constitution Diagram. To be published (1973).

## VII. NIOBIUM-PLATINUM CONSTITUTION DIAGRAM

(Work done at the Massachusetts Institute of Technology by Bill C. Giessen and at the National Bureau of Standards by Richard M. Waterstrat and Richard C. Manuszewski)

### A. Previous Studies

Identification of intermediate phases in the niobium-platinum system was begun by Greenfield and Beck<sup>(1)</sup> who identified a sigma phase and a phase having an A15 ( $\beta$ -W)-type structure. Knapton<sup>(2)</sup> later reported that the liquidus in this system passes through a maximum near the composition NbPt<sub>3</sub>. In 1961 a phase diagram for the platinum-niobium system was presented by Kimura and Ito<sup>(3)</sup> who confirmed the presence of the sigma and  $\beta$ -W type phases and also reported an intermetallic compound having the approximate composition NbPt<sub>3</sub> but the crystal structure of this compound was not determined. There was some evidence of a compound at the equiatomic (NbPt) composition.

In 1964 Giessen et al<sup>(4, 5)</sup> reported that the equiatomic compound, NbPt, possesses a B19 or AuCd-type structure and that another phase occurs near this composition which is only stable at high temperatures (1680-1770°C). They also reported<sup>(4-6)</sup> a compound, NbPt<sub>2</sub>, having an orthorhombic structure isomorphous with TaPd<sub>2</sub>(MoPt<sub>2</sub>-type) and two compounds at the approximate composition NbPt<sub>3</sub>.  $\alpha$ NbPt<sub>3</sub> was reported as having an orthorhombic DO<sub>a</sub> or TiCu<sub>3</sub>-type structure and  $\beta$ NbPt<sub>3</sub> was identified as a monoclinic phase with a 12-layer stacking sequence isomorphous with  $\beta$ TaPt<sub>3</sub><sup>(4-6)</sup>. It has been suggested<sup>(5)</sup> that  $\alpha$ NbPt<sub>3</sub> is probably stabilized with respect to  $\beta$ NbPt<sub>3</sub> by very small amounts of inter-

stitial impurities. However, Maldonado and Schubert<sup>(7)</sup> indicate that  $\beta\text{NbPt}_3$  may have a somewhat higher platinum content ( $\text{NbPt}_{3+}$ ) than  $\alpha\text{NbPt}_3$ . All of these phases, previously reported, have been confirmed by Maldonado and Schubert.<sup>(7)</sup>

## B. Materials

The niobium metal used in this study was in the form of pellets or rondelles which were obtained from both the Electro Metallurgical Co. and from the Gallard Schlesinger Chemical Manufacturing Corp., New York. The nominal minimum purity of this material was 99.6% with the principal impurity being tantalum. A spectrographic analysis showed: Ag, < 10 ppm; Al, < 300 ppm; Ca, < 100 ppm; Fe, < 1000 ppm; Mg, < 100 ppm; Mn, < 10 ppm; Mn, < 10 ppm; Ni, < 10 ppm; Si, < 300 ppm. Cr, Cu and Ta could not be determined due to niobium interferences but all other impurities were less than 10 ppm.

The platinum metal used in this study was in the form of 1/32-inch thick sheet from an unknown source. It had a nominal purity of 99.9% and spectrographic analysis revealed: Fe, < 10 ppm; Cu, < 100 ppm; Mg, < 100 ppm; Si, < 100 ppm; Pd, < 1000 ppm; Ru, < 100 ppm; all other impurities, < 10 ppm.

## C. Alloy Preparation

Carefully weighed quantities of Nb and Pt were arc-melted at least four times using a sufficient arc current to insure that the alloy button was thoroughly melted. Weight losses during melting were in all cases less than 1% except for the alloy,  $\text{Nb}_{95}\text{Pt}_5$ , which had a weight loss of 1.5%. The actual alloy compositions were

therefore assumed to be reasonably close to the intended nominal compositions. Each alloy sample contained 20 grams of material and was sectioned or broken for visual inspection prior to homogenization treatments. In all cases the samples were well melted and no problems were encountered in producing them.

#### D. Temperature Measurement

Temperatures up to 1500°C were measured with a platinum versus platinum-10% rhodium thermocouple. Calibration of furnace temperatures was accomplished by plotting furnace current versus temperature using a standard platinum-6% rhodium versus platinum-30% rhodium thermocouple. This thermocouple had been calibrated at the National Bureau of Standards. Calibration above 1500°C was accomplished using secondary standards such as the melting points of gold, platinum, rhodium, iridium and niobium. All temperatures are measured on the International Practical Temperature Scale of 1968 (IPTS 68). Temperatures in the vacuum furnace were also measured with a Leeds and Northrup optical pyrometer.

#### E. Thermal Treatments

All alloys were first homogenized by annealing them at temperatures slightly below their melting points for several hours. The samples could be considered as being equilibrated at these temperatures and were rapidly cooled by turning off the furnace power. Further, equilibration treatments were then conducted at progressively lower temperatures.

The annealing treatments above 1100°C were done in a high vacuum ( $\sim 5 \times 10^{-6}$  mm Hg) using a Ta-strip heating element and Ta heat shields. There was no evidence of unusual weight losses or contamination of the samples. Nb foil was sometimes used to wrap or hold the samples but in most cases Ta foil seemed adequate for this purpose. Alloys annealed at or below 1100°C were sealed in quartz tubes under a partial pressure of argon. These tubes were water-quenched following their annealing treatments. A summary of typical annealing treatments is shown in Table 19.

## F. Methods for Determination of Phase Boundaries

### 1. Solidus Temperatures

The procedures used in determining the solidus temperatures have been described in a previous paper<sup>(10)</sup>. High-purity alumina crucibles were found to be satisfactory for all alloys containing more than 20 at. % Pt but thoria crucibles were used for the Nb-rich alloys.

### 2. Liquidus Temperatures

In general, we did not attempt to determine the liquidus temperatures but they could be estimated with satisfactory accuracy for alloy compositions lying in the vicinity of a congruent melting maximum or a eutectic minimum. The estimated liquidus boundaries are shown by dashed lines in Fig. 25.

### 3. Invariant Reactions

The existence of invariant reactions was established by solidus measurements and metallographic studies on

Table 19

Typical Equilibration Treatments for  
Niobium-Platinum Alloys

Temperature (°C)	Time	Alloys (Atomic % Pt)
1900	3 hrs	16, 18, 20
1700	6 hrs	5, 10, 16, 18, 22, 26, 30, 50, 52.5, 55, 57.5, 60, 62.5, 66.6
1600	12 hrs	45, 50, 51, 52.5, 55, 57.5, 60, 62.5, 67.5, 70
1500	1 day	5, 10, 18, 22, 26, 30, 32, 34, 36, 38, 45, 50, 52.5, 55, 57.5, 60, 62.5, 72, 73, 77.5, 80, 82.5, 85, 90, 95
1300	1 wk	45, 50, 52.5, 55, 57.5, 60, 62.5, 73, 77.5
1150	3 wks	5, 10, 16, 18, 20, 22, 26, 30, 32, 34, 36, 38, 50, 70, 77.5, 80, 82.5, 85, 90, 95
1000	1 month	50

rapidly-cooled samples. We obtained no evidence supporting the existence of any solid-state reactions in this system other than precipitation from the saturated terminal solid solutions.

#### 4. Other Phase Boundaries

Phase boundaries were generally determined by metallographic and x-ray diffraction studies but in many cases we were also able to make use of the electron-beam microprobe to obtain individual chemical analyses of the phases coexisting in two-phase alloys equilibrated at various temperatures. This was of great help in locating the phase boundaries except for samples in which precipitation had occurred in one of the coexisting phases. In such cases, the use of metallography was our only recourse. It is estimated that the phase boundaries shown in Fig.25 are accurate  $\pm 1$  at. %.

### G. Experimental Results

#### 1. General

The proposed constitution diagram is shown in Fig.25. A discussion of the individual phase regions follows. All alloys were examined either by x-ray diffraction or metallographically or both. In addition, x-ray microprobe data were used to establish the location of certain phase boundaries. The accuracy of these boundaries is believed to be about  $\pm 1$  at. % in composition.

#### 2. Niobium Terminal Solid Solution - $\alpha$

Platinum is soluble in the body-centered cubic niobium solid solution to the extent of about 14 at. % Pt at 2040° C



but the solubility diminishes to about 5 at. % Pt at lower temperatures and precipitation of a second phase is frequently seen in alloys cooled slowly enough to permit such effects (Fig.26a). The  $\alpha$ -phase lattice parameters are affected by Pt in solid solution which gradually decreases the lattice constant of pure Nb.

### 3. Intermediate Phase - $\beta$

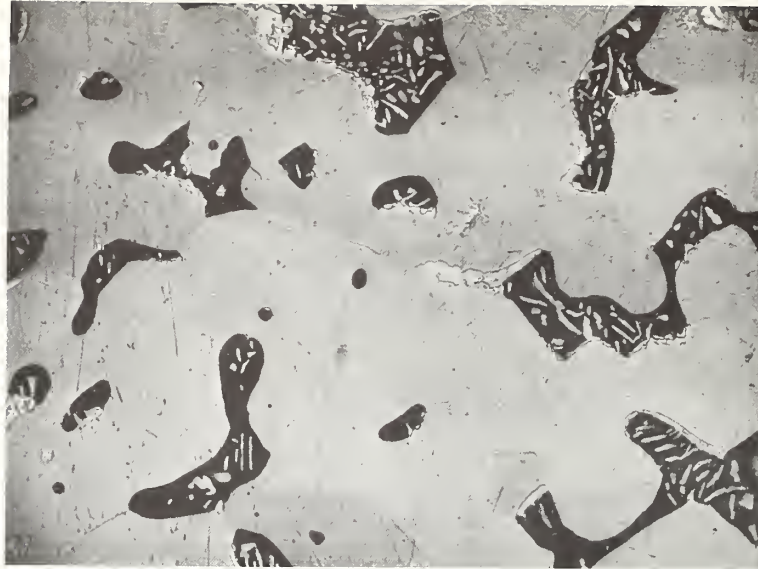
This phase was apparently first discovered by Geller, Matthias and Goldstein<sup>(8)</sup> who also reported on the degree of atomic ordering. Their discovery was confirmed by Greenfield and Beck<sup>(1)</sup> and later by other workers<sup>(3, 4, 7)</sup>. The structure is a cubic A15 ( $\beta$ -W) type and the phase extends from about 19 at. % Pt at 2040°C to about 28 at. % Pt at 1800°C. It apparently forms by a peritectic reaction at 2040°C.

### 4. Intermediate Phase - $\sigma$

This phase was first reported by Greenfield and Beck<sup>(1)</sup> who identified its tetragonal crystal structure as that of a new sigma phase. It exists over a composition range extending from about 31 to 38 at. % Pt at high temperatures but its range diminishes at lower temperatures (See Fig.26b). Its presence in the Nb-Pt system has been confirmed by various investigators<sup>(3, 4, 7)</sup>. It apparently forms by a peritectic reaction at 1800°C.

### 5. Intermediate Phase - $\zeta$

This phase was first identified by Giessen et al<sup>(4, 5)</sup> as having an orthorhombic AuCd-type structure. It is apparently stable from its solidus point at about 1750°C down to below 1000°C. It coexists with the sigma and  $\delta$  phases (Fig.27a and 27b).



400X

(a)

82 at. % Nb, 18 at. % Pt. Annealed at 1150 C for three weeks. Beta phase matrix containing  $\alpha$  Nb globules in which further precipitation of beta has occurred.

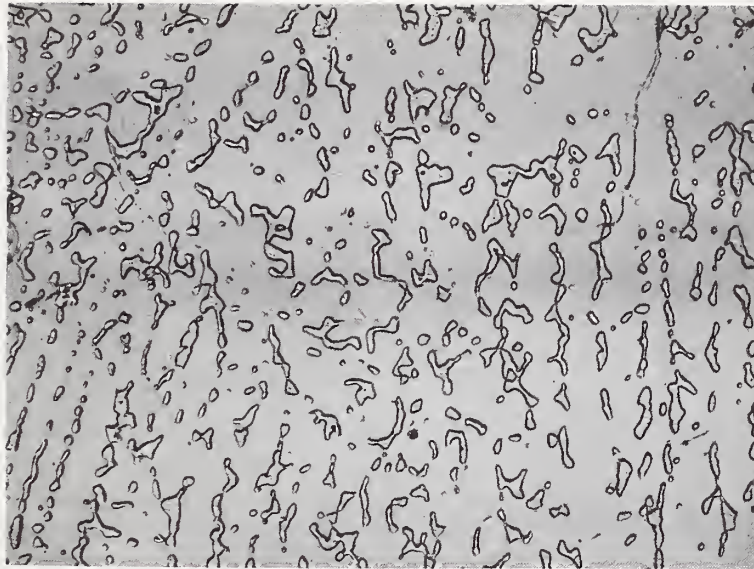


160X

(b)

70 at. % Nb, 30 at. % Pt. Annealed at 1500 C for one day. Beta phase in a matrix of sigma phase.

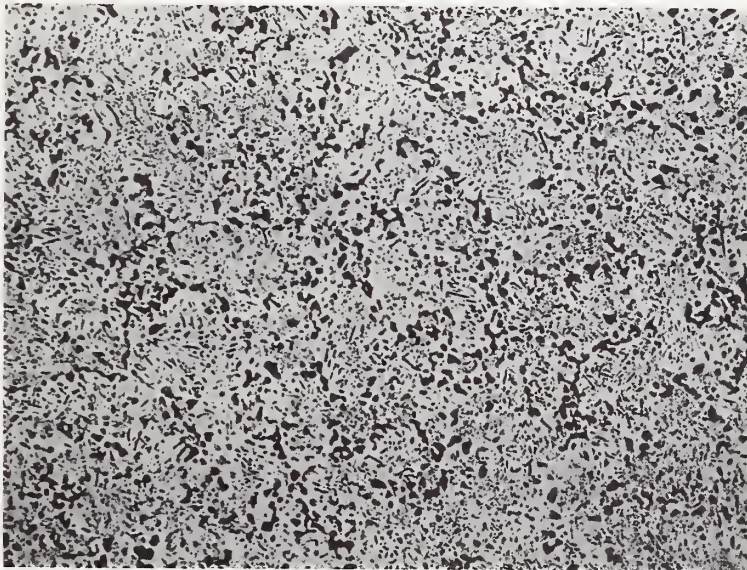
Fig. 26 - Microstructures of niobium-platinum alloys.



160X

(a)

62 at. % Nb, 38 at. % Pt. Annealed at 1500 C for one day.  $\zeta$  phase globules in a matrix of sigma phase.



400X

(b)

42.5 at. % Nb, 57.5 at. % Pt. Annealed at 1000 C for one month.  $\delta$  phase globules in a matrix of  $\zeta$  phase.

Fig.27 - Microstructures of niobium-platinum alloys.

An analogous phase having this same crystal structure occurs in the V-Pt binary system<sup>(10)</sup> where it is also observed at the equi-atomic composition but is stable only up to about 1500°C.

#### 6. Intermediate Phase - $\gamma'$

The existence of this high-temperature phase has been deduced<sup>(4)</sup> from solidus measurements and metallographic studies. It apparently forms by a peritectic reaction at 1790°C and decomposes below 1680°C to produce the fine structure shown in Fig. 28a. By analogy to the V-Pt system<sup>(9)</sup> we would expect this phase to be essentially an extension of the face-centered cubic  $\gamma$  solid solution and have therefore labelled it  $\gamma'$ . Confirmation of its crystal structure, however, must await a high-temperature x-ray diffraction study.

#### 7. Intermediate Phase - $\delta$

This phase forms over a narrow composition range around the composition NbPt<sub>2</sub>. It possesses an orthorhombic crystal structure of the MoPt<sub>2</sub>-type<sup>(4, 7, 9)</sup>. It probably forms by a peritectic reaction at about 1990°C. Accurate lattice parameter values have been reported previously and were accepted in this study<sup>(5, 9)</sup>.

#### 8. Intermediate Phases - $\theta$ and $\theta'$

Two different crystal structures have been observed at the composition NbPt<sub>3</sub>. The  $\theta'$  phase (formerly designated  $\alpha$ NbPt<sub>3</sub>)<sup>(4, 5, 7)</sup> has an orthorhombic DO<sub>a</sub> or TiCu<sub>3</sub>-type structure. The  $\theta$  phase (formerly designated  $\beta$ NbPt<sub>3</sub>)<sup>(4, 5)</sup> has a monoclinic structure with a 12-layer stacking sequence and is isomorphous with  $\beta$ -TaPt<sub>3</sub><sup>(4-7)</sup>. Maldonado and Schubert<sup>(7)</sup> have stated that the TiCu<sub>3</sub>-type structure is

stable below 1000°C and they designate the TaPt<sub>3</sub>-type structure as having a Pt-content which is somewhat higher than the stoichiometric (Ab<sub>3</sub>) composition. High-temperature x-ray diffractometry may help to clarify the structural behavior. The  $\theta$  phase melts congruently at about 2030°C. Accurate lattice parameters for the  $\theta$  and  $\theta'$  phases have been reported previously and were accepted in this study<sup>(5, 7)</sup>.  $\theta$  phase coexists with  $\delta$  phase (Fig.28b) and  $\gamma$ Pt (Fig.29a).

9. Platinum Terminal Solid Solution -  $\gamma$

Face-centered cubic platinum can dissolve up to 20 at. % Nb at 2000°C with some small reduction in solubility occurring at lower temperatures. Additions of Nb produce a sharp rise in the solidus and liquidus of the Pt solid solution and a gradual increase in its lattice parameter. This may perhaps be accompanied by some interesting mechanical properties.

10. Peritectic:  $\alpha + L \rightleftharpoons \beta$

The existence of this peritectic reaction was established by solidus measurement and by observation of a typical peritectic microstructure. The reaction temperature is  $2040 \pm 10^\circ\text{C}$ .

11. Peritectic:  $\beta + L \rightleftharpoons \sigma$

This peritectic reaction was located at  $1800 \pm 10^\circ\text{C}$  mainly by solidus measurements in this composition region.

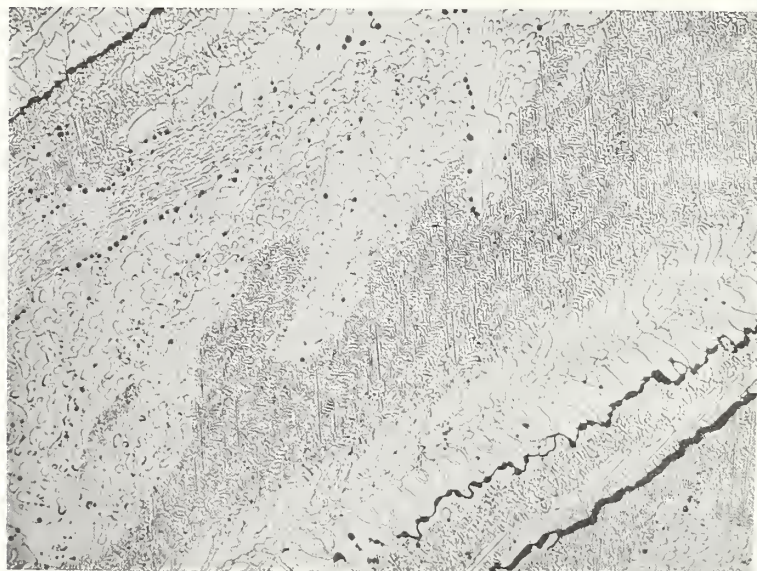
12. Eutectic:  $L \rightleftharpoons \sigma + \zeta$

The eutectic reaction at  $1700 \pm 10^\circ\text{C}$  was determined by solidus measurement and by observation of typical eutectic microstructures (Fig. 29b).



400X (a)

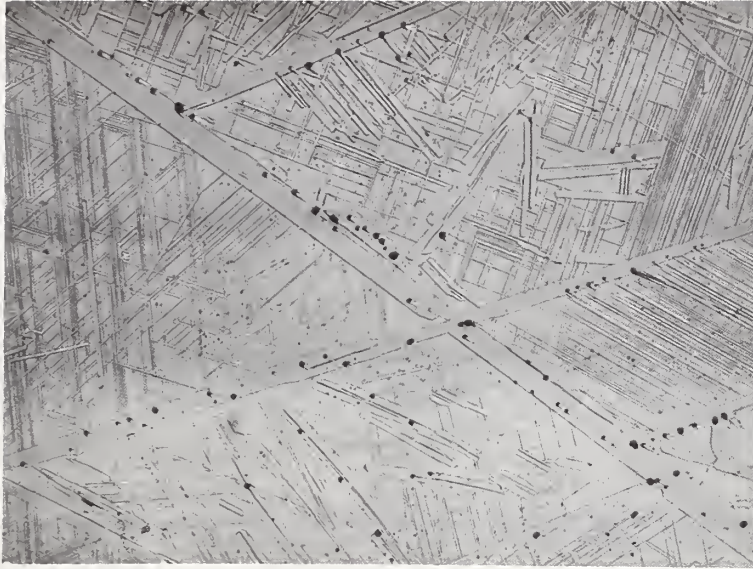
45 at. % Nb, 55 at. % Pt. Annealed at 1600°C for twelve hours.  $\zeta$  phase plus  $\delta$  phase fine structure probably produced by decomposition of prior  $\gamma'$  phase.



160X (b)

30 at. % Nb, 70 at. % Pt. Annealed at 1800°C for four hours.  $\theta$  phase globules in a matrix of  $\delta$  phase.

Fig.28 - Microstructures of niobium-platinum alloys.



160X

(a)

20 at. % Nb, 80 at. % Pt. Annealed at 1500°C for one day. Coherent precipitate of  $\theta$  phase in  $\gamma$  Pt.



400X

(b)

55 at. % Nb, 45 at. % Pt. "As-cast" fine eutectic of sigma plus  $\zeta$  phases.

Fig.29 - Microstructures of niobium-platinum alloys.

13. Peritectic:  $L + \gamma' \rightleftharpoons \zeta$

This reaction occurs at about  $1750 \pm 10^\circ\text{C}$  on the basis of solidus measurements.

14. Peritectic:  $L + \delta \rightleftharpoons \gamma'$

Solidus data suggest that this reaction occurs at about  $1790 \pm 10^\circ\text{C}$ .

15. Peritectic:  $L + \theta \rightleftharpoons \delta$

Solidus measurements in this region suggest a peritectic reaction occurs at about  $1990 \pm 10^\circ\text{C}$ .

16. Congruent melting maximum:  $L \rightleftharpoons \theta$

It is estimated on the basis of solidus measurements that the  $\theta$  phase melts congruently at  $2030 \pm 10^\circ\text{C}$ .

17. Peritectic:  $\theta + L \rightleftharpoons \gamma$

This peritectic reaction apparently occurs at about  $2000 \pm 10^\circ\text{C}$  on the basis of solidus measurements.

## H. Discussion

The proposed constitution diagram of the Nb-Pt system shares some similarities with the V-Pt<sup>(10)</sup> and the Ta-Pt<sup>(7)</sup> systems. The crystal structures of the  $\beta$ ,  $\sigma$ ,  $\zeta$ ,  $\delta$  and  $\theta$  phases are all reproduced in at least two and sometimes in all three of these systems (See Tables 20 and 21). There is a notable tendency toward an increased stability of the  $\beta$  phase as one proceeds from the Ta-Pt

to the Nb-Pt to the V-Pt systems. This is accompanied by a decreasing stability for the sigma phase. Each of these three systems also exhibits ordered close-packed structures at the  $AB_2$  and  $AB_3$  stoichiometries where, in these cases, "B" is platinum. It would, therefore, appear that similar electronic conditions exist in these three related systems which may be attributed to periodic table relationships of the constituent elements. Further study of physical properties in these three systems may yield some insight into the reasons for the similarities.

Table 20

## Crystallographic Data for Niobium-Platinum Intermediate Phases

Intermediate Phase	Crystal System	Space Group	Structure Type	No. Atoms Per Unit Cell	Composition Limits At. % Pt
$\beta\text{Nb}_3\text{Pt}$	Cubic	$O_h^3 - Pm\bar{3}n$	A15, $\text{Cr}_3\text{O}$	8	19 to 28 1800°C
$\sigma\text{Nb}_2\text{Pt}$	Tetragonal	$D_{4h}^{14} - P4/mnm$	$D_{8b}$ , $\beta\text{U}$	30	31 to 38 1700°C
$\zeta\text{NbPt}$	Orthorhombic	$D_{2h}^5 - Pmma$	B19, AuCd	4	50 to 53 1700°C
$\gamma'\text{NbPt}$	Unknown	-	Unknown	-	~57 1750°C
$\delta\text{NbPt}_2$	Orthorhombic	$D_{2h}^{28} - Immm$	$\text{MoPt}_2$	6	~67 1600°C
$\theta\text{NbPt}_3$	Monoclinic	$C_{2h}^2 - P2_1/m$	$\beta\text{TaPt}_3$	48	~76 1600°C
$\theta'\text{NbPt}_3$	Orthorhombic	$D_{2h}^{13} - Pmnm$	$\text{DO}_{a'}$ , $\beta\text{TiCu}_3$	8	~75 1600°C

Table 21

Lattice Parameters of Intermediate Phases and Terminal  
Solid Solutions for Niobium-Platinum

At. %Pt	Phase	Lattice Parameter(s), Å			c/a	Ref.
		a	b	c		
5	$\alpha$ Nb	3.277				5
10	$\alpha$ Nb	3.260				5
20	$\beta$	5.182				5
28	$\beta$	5.139				5
32	$\sigma$	9.940		5.145	0.518	5
38	$\sigma$	9.902		5.132	0.518	5
50	$\zeta$	2.780	4.983	4.611		5
67	$\delta$	2.801	8.459	3.951		5
75	$\theta$	5.537	4.870	2.733	$\alpha = 90^\circ 32'$	5
75	$\theta'$	5.534	4.873	4.564		5
82	$\gamma$ Pt	3.940				
85	$\gamma$ Pt	3.935				
90	$\gamma$ Pt	3.927				
95	$\gamma$ Pt	3.924				

## REFERENCES

1. Greenfield, P. and Beck, P. A., Intermediate Phases in Binary Systems of Certain Transition Elements, Trans. AIME 206, p. 265 (1956).
2. Knapton, A. G., Niobium and Tantalum Alloys. II, Constitution, Structure and Physical Properties, J. Less-Common Metals 2, pp. 113-124 (1960).
3. Kimura, H. and Ito, A., The Platinum-Niobium System, Trans. Nat'l. Res. Inst. for Metals 3, pp. 27-34 (1961).
4. Giessen, B. C., Parker, D. and Grant, N. J., The Intermediate Phases  $Ab$ ,  $Ab_2$  and  $AB_3$  in the Nb-Pd and Nb-Pt Systems, Journ. Metals (abstract), pp. 92-93 (1964).
5. Giessen, B. C. and Grant, N. J., New Intermediate Phases in Systems of Nb or Ta with Rh, Ir, Pd or Pt, Acta Cryst. 17, pp. 615-616 (1964).
6. Giessen, B. C., Kane, R. H. and Grant, N. J., On the Constitution Diagram Ta-Pt Between 50-100 At. Pct. Pt, Trans. Met. Soc. AIME 233, pp. 855-864 (1965).
7. Maldonado, A. and Schubert, K. Structure Investigation in the  $T^5$ - $T^{10}$  Homologous and Quasihomologous Alloy Systems. Z. Met. 55, pp. 619-626 (1964).
8. Geller, S.; Matthias, B. T.; and Goldstein, R., Some New Intermetallic Compounds with " $\beta$ -Wolfram" Structure, Journ. Amer. Chem. Soc. 77, p. 210 (1955).
9. Giessen, B. C. and Grant, N. J., The Crystal Structure of  $VNi_2$ ,  $VPd_2$ ,  $VPt_2$  and Related  $AB_2$  Phases. J. Less-Common Metals 8, pp. 114-119 (1965).
10. Waterstrat, R. M., The Vanadium-Platinum Constitution Diagram, Met. Trans. 4, pp. 455-466 (1973).

## VIII. TANTALUM-PALLADIUM CONSTITUTION DIAGRAM

(Work done at the National Bureau of Standards by Richard M. Waterstrat and at the Massachusetts Institute of Technology by Rosmarie Koch and Bill C. Giessen)

### A. Previous Studies

The earliest work on the tantalum-palladium system is apparently that of Greenfield and Beck<sup>(1)</sup> who prepared only three alloys, annealed them at 1000°C and concluded that no intermediate phases exist at this temperature. Later work by Darby et al<sup>(2)</sup>, however, established the existence of several intermediate phases. A sigma phase was discovered and a phase having a  $\text{TiAl}_3$ -type structure was reported; the latter near the composition  $\text{TaPd}_3$ . A body-centered tetragonal Bll-type structure was found at the equiatomic composition and an unidentified phase (X) was observed at the composition  $\text{TaPd}_2$ . Several of these phases were identified in a subsequent study by Kane, Giessen and Grant<sup>(3)</sup>. The equiatomic phase was confirmed as having a Bll or  $\gamma\text{TiCu}$ -type structure and the X-phase ( $\text{TaPd}_2$ ) was identified as having a Mo-Pt<sub>2</sub>-type structure<sup>(3, 4)</sup> isomorphous with  $\text{NbPt}_2$ . The presence of a sigma phase and a  $\text{TiAl}_3$ -type structure was also confirmed<sup>(3)</sup>. A further confirmation of all these phases was provided by Maldonado and Schubert<sup>(5)</sup>. Finally, a phase diagram for the palladium-tantalum system was presented by Savitskii et al<sup>(6)</sup> but it is based on a rather small amount of experimental data and the phase boundaries are apparently not precisely defined. Nevertheless, intermetallic compounds were observed at the compositions mentioned previously and their presence is thus again confirmed.

However, it appears that more work is needed to delineate the various phase regions in this diagram and to insure

the reliability of the final result. We have, therefore, undertaken a complete reinvestigation of the tantalum-palladium system with a view toward obtaining a more reliable phase diagram.

## B. Materials

The tantalum metal used in this study was either in the form of rod having a purity of 99.95% or in the form of powder having a purity of 99.99%. The rod was obtained from National Research Corp. and the powder was obtained from Leico Industries Inc. The impurities in these materials consisted of O, C, N, Si, Nb, Mo and W but none of these impurities were present in excess of 100 ppm.

The palladium metal used in this study was in the form of powder or wire, both having a nominal purity of 99.9+%. The powder was obtained from Engelhard Industries Inc. and the wire from the International Nickel Co. Inc. Neither of these materials was submitted to chemical analysis.

## C. Alloy Preparation

Alloys rich in Pd could be easily prepared using Ta rod and Pd wire as starting materials but when these materials were used for Ta-rich alloys there were significant metal losses during melting and in many cases we observed large pieces of unmelted Ta in the alloy after it had been broken or sectioned. Eventually we changed our procedures for the Ta-rich alloys and used powder metallurgical methods to prepare these alloys for arc-melting. Weighed amounts of Ta and Pd powders were thoroughly mixed and

then compressed in a 1/2-inch diameter cylindrical steel mold. This was followed by a short sintering at about 1200°C in a high vacuum and then by arc-melting of the pre-sintered compacts. The Ta-rich powder alloys were each of about 10 grams and appeared to be well-melted. The Pd-rich alloys contained about 5 grams of material. Weight losses were in all cases less than 1% during melting.

#### D. Temperature Measurement

Temperatures up to 1500°C were measured with a platinum versus platinum-10% rhodium thermocouple. Calibration of furnace temperatures was accomplished by plotting furnace current versus temperature using a standard platinum-6% rhodium versus platinum-30% rhodium thermocouple. This thermocouple had been calibrated at the National Bureau of Standards. Calibration above 1500°C was accomplished using secondary standards such as the melting points of gold, platinum, rhodium, iridium and niobium. All temperatures are measured on the International Practical Temperature Scale of 1968 (IPTS 68). Temperatures in the vacuum furnace were also measured with a Leeds and Northrup optical pyrometer.

#### E. Thermal Treatments

All alloys were homogenized by annealing at temperatures near the melting point of each alloy for several hours. The homogenization treatments were done using the normal precautions taken during an equilibration treatment and the samples were, therefore, considered as being equilibrated at the homogenization temperature. Equilibration annealing of all samples was done at progressively lower temperatures for each sample.

The annealing treatments above 1100°C were performed in a high-vacuum furnace having a tantalum heating element and tantalum heat shields. A pressure of between  $5 \times 10^{-6}$  and  $2 \times 10^{-5}$  mm Hg was usually obtained during annealing. Samples were rapidly cooled after annealing by turning off the furnace power. The cooling rate was not sufficient to retain all of the high-temperature structures formed during annealing but information obtained from the partially decomposed samples was sufficient to permit an understanding of the high-temperature behavior. A summary of typical annealing treatments is shown in Table 22.

Samples annealed at or below 1100°C were sealed in quartz tubes under a partial pressure of pure argon and were water quenched after annealing.

Table 22

Typical Equilibration Treatments for Tantalum-Palladium Alloys

Temperature (°C)	Time	Alloys (Atomic % Pd)
2300	3 hrs	20, 25
2000	6 hrs	13, 20, 25
1680	1 day	13, 20, 25, 30, 40, 48, 50, 53, 55, 57, 60, 65, 66.6, 67, 70, 74, 75, 76, 77.5, 80, 82, 84, 90
1350	1 wk	13, 20, 25, 30, 40, 47.5, 49, 50, 51, 52, 55, 56, 57, 60, 65, 66.6, 67, 70, 74, 75
1150	1 month	13, 25, 30, 47.5, 49, 50, 51, 52, 55, 65, 67, 74, 76, 80, 82, 84, 90
1000	1 month	25, 40, 50, 51, 55, 60, 66.6, 67 70, 75, 80, 82, 84, 90

## F. Methods for Determination of Phase Boundaries

### 1. Solidus Temperatures

The procedures used in determining the solidus temperatures have been described in a previous paper<sup>(7)</sup>. High-purity alumina crucibles were found to be satisfactory for all alloys containing more than 30 at. % Pd but thoria crucibles were used for the Nb-rich alloys.

### 2. Liquidus Temperatures

In general, we did not attempt to determine the liquidus temperatures but they could be estimated with satisfactory accuracy for alloy compositions lying in the vicinity of a congruent melting maximum or a eutectic minimum. The estimated liquidus boundaries are shown by dashed lines in Fig.30.

### 3. Invariant Reactions

The existence of invariant reactions and the temperatures at which these reactions occur were established mainly by comparing metallographic and x-ray diffraction data from alloys annealed above and below the transformation temperatures. The phases existing above the transformation temperatures could not always be retained to room temperature by rapid quenching but metallographic studies were successful in revealing the structures characteristic of samples annealed either above or below the transformation temperature. The actual temperature of the transformation is established by successive annealing treatments which bracket this temperature with an accuracy comparable to that of the temperature measurement itself.

#### 4. Other Phase Boundaries

In most cases it was possible to supplement our metallographic studies with electron microprobe data. The only limitation on the use of the probe in this system was for alloys containing decomposed  $\gamma'$  phase. The decomposition of  $\gamma'$  produces a fine structure which is unresolvable to the electron beam in the microprobe. In some cases where samples contained unmelted Ta or when the surface of the sample had been depleted of Pd by annealing in a vacuum, it was decided to treat the samples as if they were diffusion couples and analyze the phases along a path perpendicular to the interface between the phases. This assumes that equilibrium conditions prevail along this path and we were unable to test this assumption. The data obtained, however, are consistent with metallographic data in the same composition region.

#### G. Experimental Results

##### 1. General

The proposed constitution diagram for the tantalum-palladium system is shown in Fig. 30. It differs significantly from the diagram reported previously<sup>(6)</sup>. Individual phase regions are discussed below.

##### 2. Tantalum Terminal Solid Solution - $\alpha$

Palladium is soluble in the body-centered cubic tantalum solid solution to the extent of about 19 at. % Pd at 2550°C but there is a decrease in solubility at lower temperatures to about 10 at. % Pd at 1200°C (See Fig. 31a). The solvus boundary was

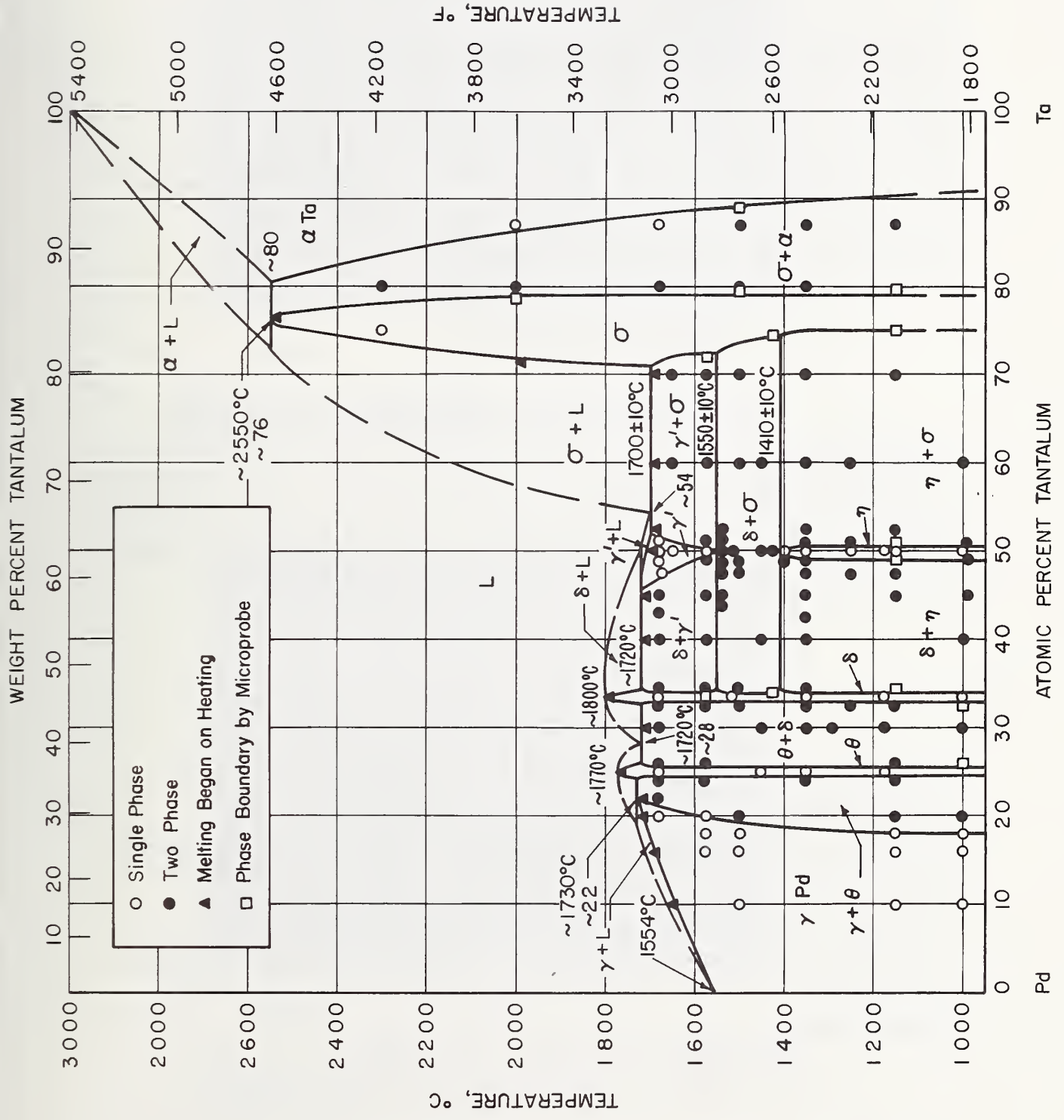


Fig. 30- The tantalum-palladium constitution diagram

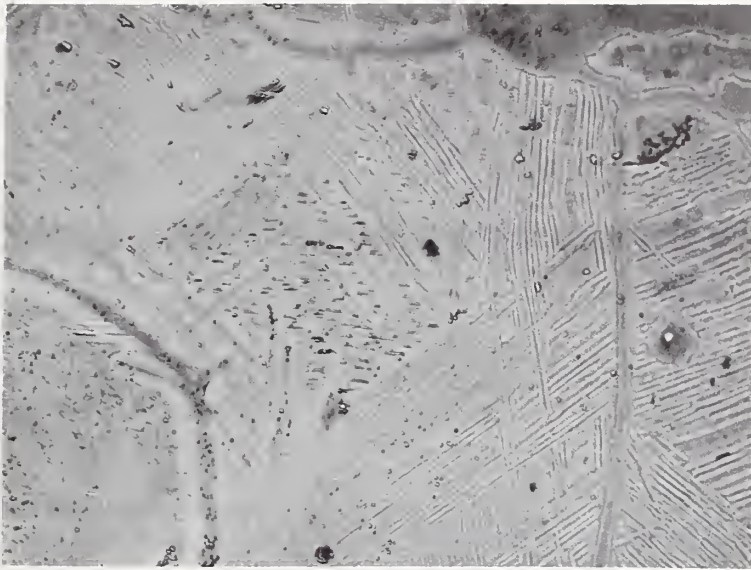
located mainly by quantitative analysis of the  $\alpha$ -phase in two-phase alloys using the electron beam microprobe. The alloys were equilibrated at various temperatures prior to each analysis. In some cases it was possible to traverse a reaction zone between an unmelted piece of pure Ta and a partly melted Pd-rich region. This, in effect, is a diffusion couple which may or may not correspond to equilibrium conditions. In this case, however, the data were consistent with data obtained from conventional metallographic specimens in this composition range. The  $\alpha$ Ta solid solution coexists with the sigma phase (See Fig. 3lb).

### 3. Intermediate Phase - $\sigma$

This phase was originally discovered by Darby et al<sup>(2)</sup> and later confirmed by other authors<sup>(3, 5, 6)</sup>. It possesses a tetragonal crystal structure and it apparently forms by a peritectic reaction at 2550°C. It is rather remarkable that the sigma phase is stable to such an elevated temperature in this system while, in the Nb-Pd system, it does not appear at all, at least above 800°C.

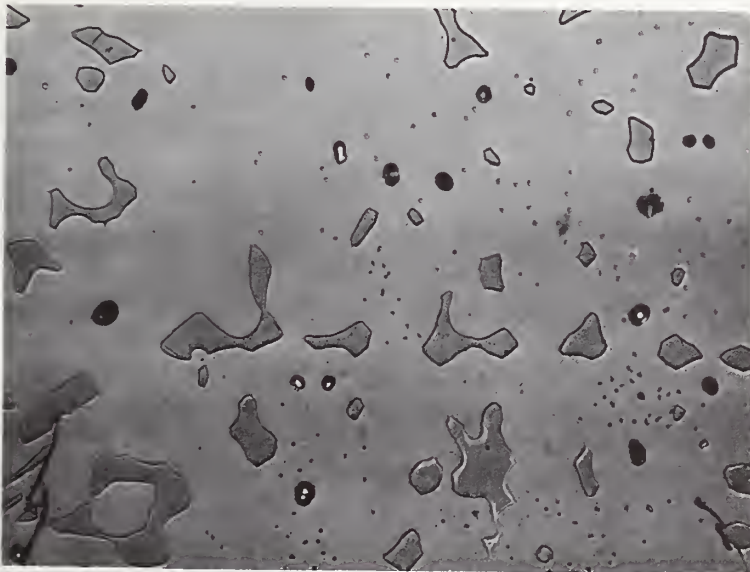
### 4. Intermediate Phase - $\gamma'$

The existence of this phase was established mainly by the observation of finely decomposed microstructures in alloys quenched from above 1550°C. This microstructure (Fig. 32a) is characteristic of a eutectoid decomposition. By analogy to the V-Pd system<sup>(8)</sup> and the V-Pt system<sup>(7)</sup> one might expect either that the  $\gamma'$  phase is essentially an extension of the face-centered cubic  $\gamma$  solid solution or, alternatively, that it possesses a AuCd-type structure. Clarification of this question must await further studies.



400X (a)

87 at. % Ta, 13 at. % Pd. Annealed at 1150°C for one month. Widmanstätten precipitate of sigma phase in  $\alpha$  phase.



400X (b)

80 at. % Ta, 20 at. % Pd. Annealed at 1500°C for one day. Particles of  $\alpha$  phase in a matrix of brittle sigma phase.

Fig.31 - Microstructures of tantalum-palladium alloys.

#### 5. Intermediate Phase - $\eta$

The existence of a body-centered tetragonal B11 or  $\gamma$ TiCu-type structure was discovered by Darby et al<sup>(2)</sup> and confirmed by other investigators<sup>(3, 5, 6)</sup>. It forms by a peritectoid reaction at about 1410°C (See Fig. 32b and 33a) and has a rather narrow composition range near the equiatomic composition. Its lattice parameter has already been accurately measured<sup>(2)</sup> and this value was accepted in the present study. It coexists with  $\delta$  phase (Fig.33a) and sigma phase (Fig. 33b and 34a).

#### 6. Intermediate Phase - $\delta$

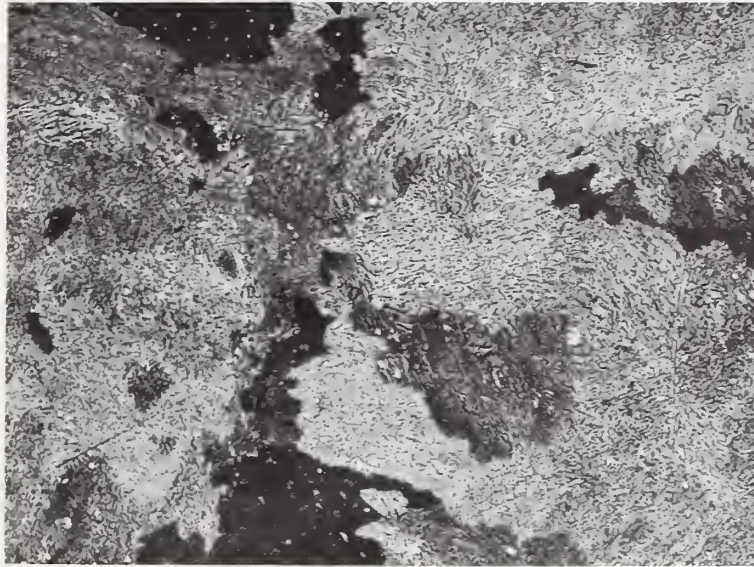
The  $\delta$  phase TaPd<sub>2</sub> exists over a narrow composition range near the stoichiometric composition and possesses an orthorhombic structure of the MoPt<sub>2</sub>-type<sup>(3, 4)</sup>. It melts congruently at about 1800°C. An accurate lattice parameter has already been measured for this phase<sup>(4)</sup> which we have adopted.

#### 7. Intermediate Phase - $\theta$

The  $\theta$  phase, TaPd<sub>3</sub>, has a tetragonal structure of the TiAl<sub>3</sub>-type and exists within a narrow composition range at the ideal stoichiometry. It melts congruently at about 1780°C. The published lattice parameter values<sup>(2)</sup> were adopted in this study.

#### 8. Palladium Terminal Solid Solution - $\gamma$

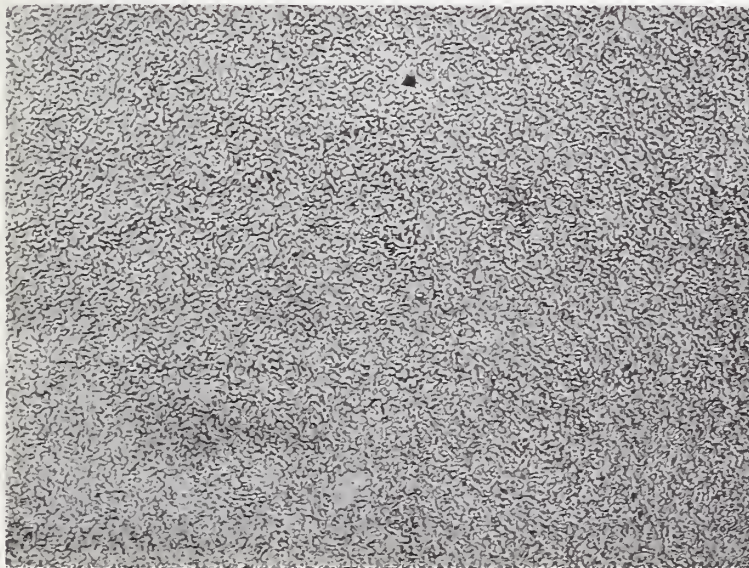
The face-centered cubic palladium solid solution dissolves up to about 22 at. % Ta at 1730°C but the solubility



400X

(a)

50 at. % Ta, 50 at. % Pd. Annealed at 1575°C for six hours. Fine eutectoid structure produced by decomposition of prior  $\gamma^1$  phase.

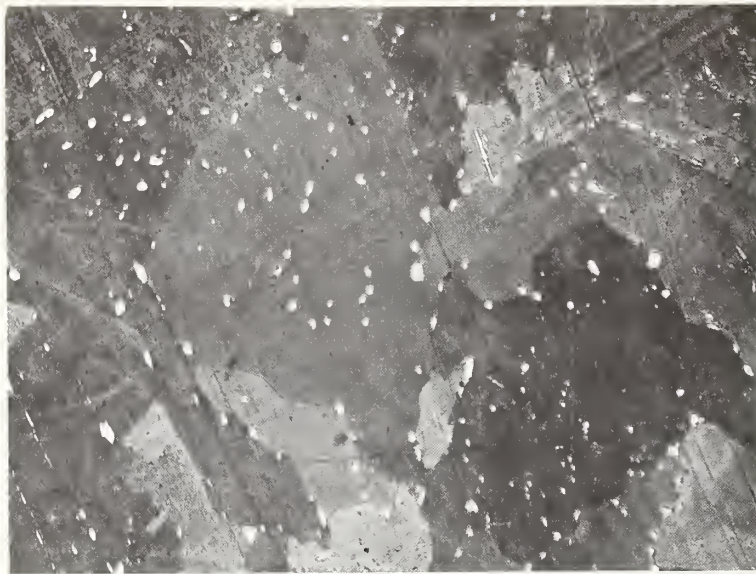


160X

(b)

50 at. % Ta, 50 at. % Pd. Annealed at 1425°C for one day. Islands of sigma phase in a matrix of  $\delta$  phase.

Fig.32 - Microstructures of tantalum-palladium alloys.



400X (a)

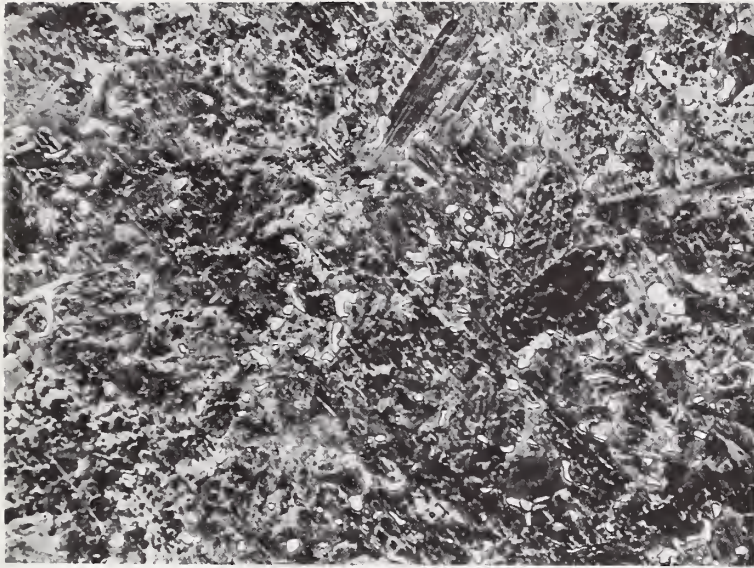
50 at. % Ta, 50 at. % Pd. Annealed at 1150°C for one month. Particles of  $\delta$  phase in a large-grained matrix of  $\eta$  phase.



400X (b)

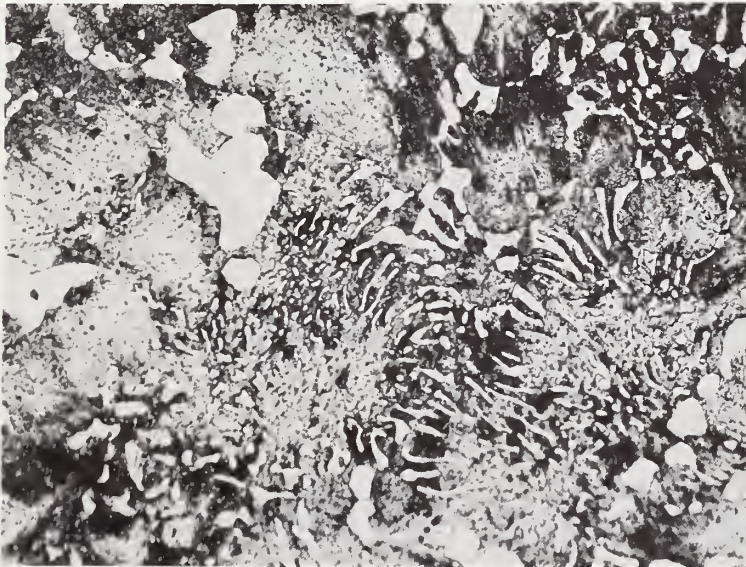
70 at. % Ta, 30 at. % Pd. Annealed at 1150°C for one month. Islands of  $\eta$  phase in a matrix of sigma phase.

Fig. 33- Microstructures of tantalum-palladium alloys.



400X (a)

52.5 at. % Ta, 47.5 at. % Pd. Annealed at 1150° C for one month. Particles of sigma phase in a matrix of η phase.



400X (b)

70 at. % Ta, 40 at. % Pd. Partially melted at 1700°C. Eutectic structure produced by partial melting is composed of light sigma phase and partially decomposed γ phase.

Fig.34 - Microstructures of tantalum-palladium alloys.

diminishes at lower temperatures until at 1000°C it is probably not more than 18 at. % Ta. It is possible that the mechanical properties of alloys in this composition range would be of some interest.

9. Peritectic:  $\alpha + L \rightleftharpoons \sigma$

The existence of a peritectic reaction at 2550°C was established mainly by a solidus measurement on the alloy Ta<sub>3</sub>Pd followed by metallographic study of the solidus sample. Solidus measurements on alloys with higher Pd contents indicated that a very sharp decrease in the solidus boundary occurs with increasing Pd content. Traces of liquid were found, for example, in the alloy Ta<sub>70</sub>Pd<sub>30</sub> after annealing at only 1700°C.

10. Eutectic:  $L \rightleftharpoons \sigma + \gamma'$

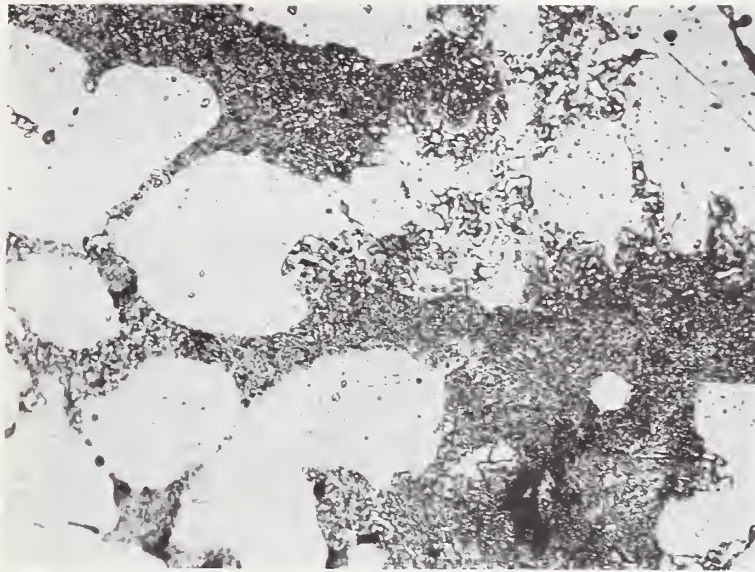
Solidus measurements and metallographic studies (Fig.34b) established a eutectic reaction at about 46 at. % Pd and 1700 ± 10°C.

11. Peritectic:  $L + \delta \rightleftharpoons \gamma'$

This reaction was indicated mainly by solidus measurements as occurring at about 1720 ± 10°C.

12. Eutectic:  $L \rightleftharpoons \delta + \theta$

Solidus measurements and metallographic studies (Fig.35a) located this reaction at about 72 at. % Pd and 1720 ± 10°C.



400X

(a)

30 at. % Ta, 70 at. % Pd. (Melted) Eutectic structure of  $\delta$  plus  $\theta$  phases with primary grains of  $\delta$  phase.

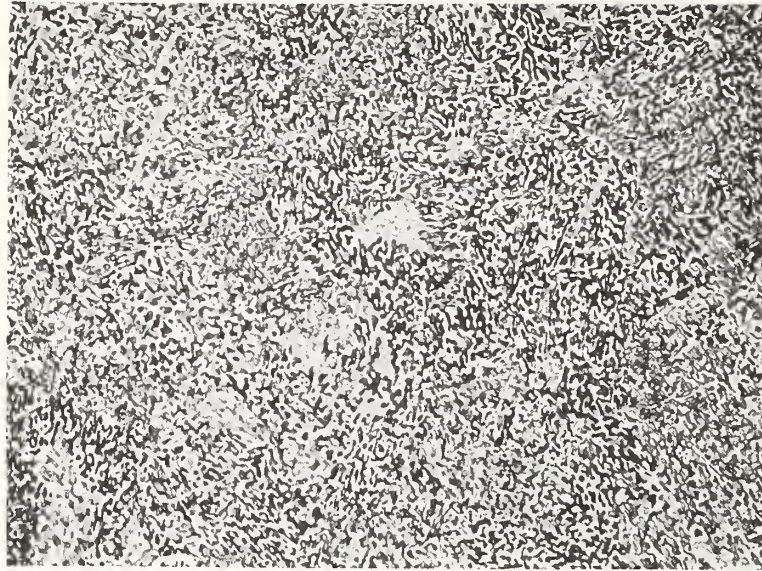


400X

(b)

60 at. % Ta, 40 at. % Pd. Annealed at 1575 C for one day. Sigma phase (light) plus finely decomposed  $\gamma'$  phase (dark).

Fig. 35 - Microstructures of tantalum-palladium alloys.



400X

(a)

50 at. % Ta, 50 at. % Pd. Annealed at 1475°C for one day. Partially spheroidized structure of decomposed  $\gamma'$ .

Fig. 36 - Microstructure of a tantalum-palladium alloy.

13. Peritectic:  $\theta + L \rightleftharpoons \gamma$

Solidus measurements indicated a continuous rise in the melting range of the Pd terminal solid solution with increasing Ta content terminating in a peritectic reaction at about  $1730 \pm 10^\circ\text{C}$ .

14. Eutectoid:  $\gamma' \rightleftharpoons \sigma + \delta$

This eutectoid reaction was established mainly by metallographic studies which showed a typical fine eutectoid structure in alloys quenched from above  $1550^\circ\text{C}$  (Fig. 32a, 34b and 35b).

15. Peritectoid:  $\sigma + \delta \rightleftharpoons \eta$

The existence of this peritectoid reaction was established mainly by metallographic studies of alloys quenched from above and below the transformation temperature (See Fig. 32b and 33a).

## H. Discussion

The Ta-Pd phase diagram possesses some unique features when compared with the systems Nb-Pd and Ta-Pt, for which one might expect to observe analogous behavior. The Ta-Pd system possesses a very stable sigma phase in sharp contrast to the Nb-Pd system where no sigma phase has been observed, at least above  $800^\circ\text{C}$ <sup>(9)</sup>. The Ta-Pd system also contains a B11-type phase at the equiatomic composition in contrast to the Ta-Pt system where no B11-type phase is observed, at least above  $1000^\circ\text{C}$ <sup>(10)</sup>.

However, all three of these systems form intermediate phases with the  $AB_2$  and  $AB_3$  stoichiometry. Measurements of physical properties in these three systems could be helpful in revealing the reasons for the significant differences in their alloying behavior.

Table 23

## Crystallographic Data for Tantalum-Palladium Intermediate Phases

Intermediate Phase	Crystal System	Space Group	Structure Type	No. Atoms Per Unit Cell	Composition Limits At. % Pd
$\sigma$ Ta <sub>3</sub> Pd	Tetragonal	D <sub>4h</sub> <sup>14</sup> - P4/mmm	D8 <sub>p</sub> , $\beta$ U	30	21 to 29 1700°C
$\gamma'$ TaPd	Unknown	-	Unknown	-	49 to 53 1700°C
$\eta$ TaPd	Tetragonal	D <sub>4h</sub> <sup>7</sup> - P4/nmm	B11, $\gamma$ TiCu	4	49 to 50 1100°C
$\delta$ TaPd <sub>2</sub>	Orthorhombic	D <sub>2h</sub> <sup>5</sup> - Immm	MoPt <sub>2</sub>	6	~67 1500°C
$\epsilon$ TaPd <sub>3</sub>	Tetragonal	D <sub>4h</sub> <sup>17</sup> - I4/mmm	DO <sub>22</sub> , TiAl <sub>3</sub>	8	~75 1500°C

Table 24

Lattice Parameters of Intermediate Phases and Terminal  
Solid Solutions for Tantalum-Palladium

At. %Pd	Phase	Lattice Parameter(s), Å			c/a	Ref.
		a	b	c		
12	$\alpha$ Ta	3.285				
25	$\sigma$	9.978		5.208	0.522	2
50	$\eta$	3.279		6.036	1.841	2
67	$\delta$	2.896	8.397	3.790		4
75	$\theta$	3.880		7.978	2.056	2
82	$\gamma$ Pd	3.897				
90	$\gamma$ Pd	3.898				

## REFERENCES

1. Greenfield, P. and Beck, P. A., Intermediate Phases in Binary Systems of Certain Transition Elements, Trans. AIME 206, p. 265 (1956).
2. Darby, J. B., Downey, J. W. and Norton, L. J., Intermediate Phases in the Tantalum-Palladium System, Trans. AIME 227, pp. 1028-1029 (1963).
3. Kane, R., Giessen, B. C. and Grant, N. J., The Intermediate Phases AB, AB<sub>2</sub> and AB<sub>3</sub> in the Ta-Pd and Ta-Pt Systems, Journ. Metals (abstract), p. 687 Sept (1963).
4. Giessen, B. C. and Grant, N. J., New Intermediate Phases in Systems of Nb or Ta with Rh, Ir, Pd or Pt, Acta Cryst. 17, pp. 615-616 (1964).
5. Maldonado, A. and Schubert, K., Structure Investigation in the T<sup>5</sup>-T<sup>10</sup> Homologous and Quasihomologous Alloy Systems, Z. Met. 55, pp. 619-626 (1964).
6. Savitskii, E. M., Polyakova, V. P., Tylkina, M. A. and Burkhanov, G. S. The Palladium-Tantalum System, Russian Journal of Inorganic Chemistry 9, pp. 890-893 (1964).
7. Waterstrat, R. M., The Vanadium -Platinum Constitution Diagram, Met. Trans. 4, pp. 455-466 (1973).
8. Köster, W. and Haehl, W. D., The Binary System Palladium-Vanadium, Z. Met. 49, pp. 647-649 (1958).
9. Parker, D.; Giessen, B. C. and Waterstrat, R. M., The Niobium-Palladium Phase Diagram, unpublished results presented elsewhere in this report (1973).
10. Waterstrat, R. M., unpublished results (1973).

## APPENDIX I: METALLOGRAPHIC PROCEDURES

Alloy specimens used for this study were in the form of small pieces which had been removed from the arc-melted buttons by an abrasive cut-off wheel or, in the case of brittle alloys, by breaking the button with a hammer. Sufficient material was usually available to permit the use of separate pieces for the various heat-treatments and consequently, remounting of specimens was seldom necessary. Samples were, therefore, mounted in bakelite. A compressed ball of copper turnings was placed in the bakelite wrapped around the rear of the specimen to produce a good electrical contact. A small hole was then drilled into the mount from behind the specimen and into the region containing the copper turnings but not deep enough to contact the sample directly. This hole served as an electrical contact area for electro polishing or etching.

Grinding operations were performed manually on a Handimet\* surface grinder lubricated with cold running water. Silicon carbide papers were used in the grit sequence 240, 320, 400 and 600. The samples were then given a preliminary polish on Microcut paper sheets (Grit 600 soft). Final polishing procedures involved the use of 7 micron size diamond compound on a Struers DUR cloth followed by 1/4 micron size diamond compound on a Struers MOL cloth using the recommended lubricants. In most cases, this was sufficient preparation for electro etching but in some cases a final polish of MgO slurry on a Rayvel cloth was used.

---

\* Certain commercial equipment, instruments, or materials are identified in this paper in order to adequately specify the experimental procedure. In no case does such identification imply recommendation or endorsement by the National Bureau of Standards, nor does it imply that the material or equipment identified is necessarily the best available for the purpose.

The alloys used in this study are frequently very resistant to conventional etchants such as hydrochloric or nitric acid and consequently, it was necessary to develop more suitable methods of etching. We have found that in most cases one may obtain satisfactory microstructures on these alloys by electro etching in an aqueous solution of 2% to 10% potassium cyanide using 1 to 2 amperes at an applied AC voltage of up to 30 volts. This method was particularly effective when used with a simultaneous etch-polish technique which tended to reduce any tendency toward pitting. The electrolytic cyanide etch is quite effective in delineating the boundaries of the various phases in these noble-metal alloys and also in revealing grain boundaries or twinning. However, it frequently does not produce a contrasting color within the various phase regions and consequently, it is sometimes difficult to establish the identity of an observed phase. In such cases the use of the electron microprobe was most helpful since we were unable to develop conventional etching procedures which would produce color contrast in alloys having a high noble-metal content.

In a few cases, particularly in alloys having a high rhodium or palladium content, it was not possible to obtain satisfactory results using the cyanide etch. For these alloys we, therefore, used a concentrated hydrochloric acid etchant electrolytically with varying voltages and currents depending on the sample composition.

Tantalum-palladium alloys were frequently etched with a solution containing 1 part HF, 1 part HNO<sub>3</sub>, 2 parts H<sub>2</sub>SO<sub>4</sub> and 5 parts H<sub>2</sub>O. This etchant was particularly effective in revealing the microstructures in this system.

Niobium-rich alloys were etched with a 50% HF solution which was particularly useful in the case of the niobium-palladium alloys.

## APPENDIX II: X-RAY DIFFRACTION PROCEDURES

Debye-Scherrer powder patterns were taken of nearly all equilibrated samples. A Phillips 114.6 mm diameter camera was employed for these pictures using nickel-filtered copper radiation. In some cases, it was necessary to obtain an x-ray pattern directly from the surface of a flat sample or to obtain quantitative information on relative intensities. In such cases, an x-ray diffractometer was used and Mr. Howard Swanson of the National Bureau of Standards was most generous in assisting us to obtain this data.

Most of the lattice parameters given in this report were obtained by carefully measuring the Debye-Scherrer films and then applying the usual extrapolation methods in order to obtain higher accuracy. However, the precision obtainable by the methods which we employed is probably not higher than about one part in 1,000 but this seemed adequate for our purposes and limitations in the available time prevented us from extending these measurements using methods of higher precision. In most cases relative intensities were estimated by visual comparison of the lines on the Debye-Scherrer films.

Powder from the brittle alloys could be obtained simply by crushing the alloy fragments in a glazed mullite mortar and pestle but the more ductile alloys could not be crushed in this manner. Powders of the ductile alloys were, therefore, obtained by grinding a sectioned surface of the alloy fragment. Grinding of these surfaces was accomplished using a dental diamond disc (S. S. White #142 or 182) mounted in a horizontal 1/6 H. P. electric motor rotating at 3500 rpm. During the grinding process the alloy powders became mixed with diamond particles which had been dislodged from the discs. Fortunately the diamond particles could be almost completely removed from the collected powders by sieving through a 400-mesh screen.

The diamond particles remained on the screen while almost all of the alloy powder passed through the screen. Therefore, differential sieving, whereby the balance of the phase content is altered, was apparently not a significant factor in our x-ray data. If any residual diamond particles remained in the alloy powder, it did not seriously interfere with our interpretation of the powder patterns since the diamond lines were very spotty and readily identified as such. Care was taken to replace the discs before excessive wear had occurred since one would otherwise introduce contamination from the substance used in bonding the diamond powder to the metal disc.

Alloy powders obtained in this manner were highly strained and contained much residual cold work. This would produce considerable x-ray line broadening and such patterns would be unsuitable for accurate lattice parameter measurements. It was, therefore, necessary to remove the residual cold work by means of a high-temperature annealing treatment. This was done by placing the powder in a container of either Ta foil, alumina or thoria, depending on the alloy composition, and then heating the powder in our vacuum furnace at a pressure of less than  $10^{-5}$  mm for a few seconds to several minutes depending on alloy composition and annealing temperature. In all cases the annealing temperature used for the powders was identical to that used in the last equilibration treatment for the bulk sample from which the powder had been obtained. After the annealing treatment, the powders were rapidly cooled by turning off the furnace power. Excessive annealing resulted in a partial sintering of the powders and, therefore, the minimum annealing time needed to effectively remove the internal strains is usually employed. Satisfactory x-ray diffraction patterns were obtained using these procedures.

### APPENDIX III: ELECTRON MICROPROBE ANALYSIS

The electron microprobe is an instrument capable of focusing a beam of electrons on a spot approximately one micron (0.00004 inch) in diameter. These electrons excite x-rays, characteristic of the elements irradiated, which can be analyzed to yield a quantitative chemical analysis of the spot irradiated. The probe is equipped with an optical microscope and the electron beam is focused in the desired areas. The wave lengths emitted by the elements in the specimens are separated by diffraction from an analyzing crystal, and their intensities are recorded by radiation counters. By comparing the observed intensity of characteristic radiation from the sample with that of a pure element as a standard, a quantitative analysis can be obtained for the irradiated spots.

The characteristic intensities for a given element in the sample and in the standard are first corrected for pulse coincidence losses and background. From this data one obtains an intensity ratio for the sample relative to the standard. The percentage of a given element necessary to produce such an intensity ratio is calculated by either of the programs COR or MULTI8 on a digital computer. This introduces corrections for x-ray absorption, atomic number differences and secondary x-ray fluorescence. The calculations are checked by analyzing alloys of known composition which have been chemically analyzed.

Phase identity was readily established for each sample by operating the probe as a scanning electron microscope. This permits one to establish which of the two phases has the highest average atomic number as revealed by differences in brightness of the specimen image on an oscilloscope screen. This was particularly helpful in our alloys since the identity of each phase

could not usually be clearly established by chemical etching methods but differences in the atomic numbers were quite large. The determination of phase diagrams using annealed two-phase alloys is particularly efficient when each individual phase can be chemically analyzed. Since the phases are in equilibrium with one another, the phase boundary compositions are given directly by the compositions of the two phases. This permits a great saving in the number of samples needed. Only one sample is required for each equilibration annealing temperature in a given two-phase region. Conventional methods of metallographic examination usually require the preparation of many different alloy compositions in order to obtain an identical amount of information by bracketing the phase boundary. The use of the electron microprobe also provides valuable information on the equilibrium status of the alloys and the effectiveness of quenches, since it very quickly reveals composition gradients or precipitation of a third phase.

We were particularly careful in searching for fine precipitated particles in our samples since a representative microprobe analysis will not be obtained when such precipitates occupy an area smaller than the diameter of the electron beam. In several cases, fine precipitates were suggested as being responsible for erratic results during microprobe analysis. The presence of these precipitates was later verified by optical microscopy. It is not possible to obtain an accurate quantitative analysis from phase regions containing such fine precipitates.

#### APPENDIX IV: ATOMIC VOLUME RELATIONSHIPS

It is sometimes desirable to compare the unit cell dimensions for each of the various phases which occur in a given alloy system. In order to make such a comparison it is necessary to bring the unit cell dimensions to a common basis. This is done by plotting the lattice parameter data in the form of atomic volumes (volume of the unit cell divided by the number of atoms per unit cell) as a function of composition. If one draws a straight line between the atomic volumes of each elemental component, then it is possible to determine whether any net expansion or contraction has occurred in the various intermediate phases, i. e., whether there is a positive or negative departure from a "volume Vegard's Law" relationship.

Plots of atomic volume versus composition have, therefore, been constructed for the phases occurring in each of the six binary systems explored in this investigation. These plots are shown in Figs. 37-42.

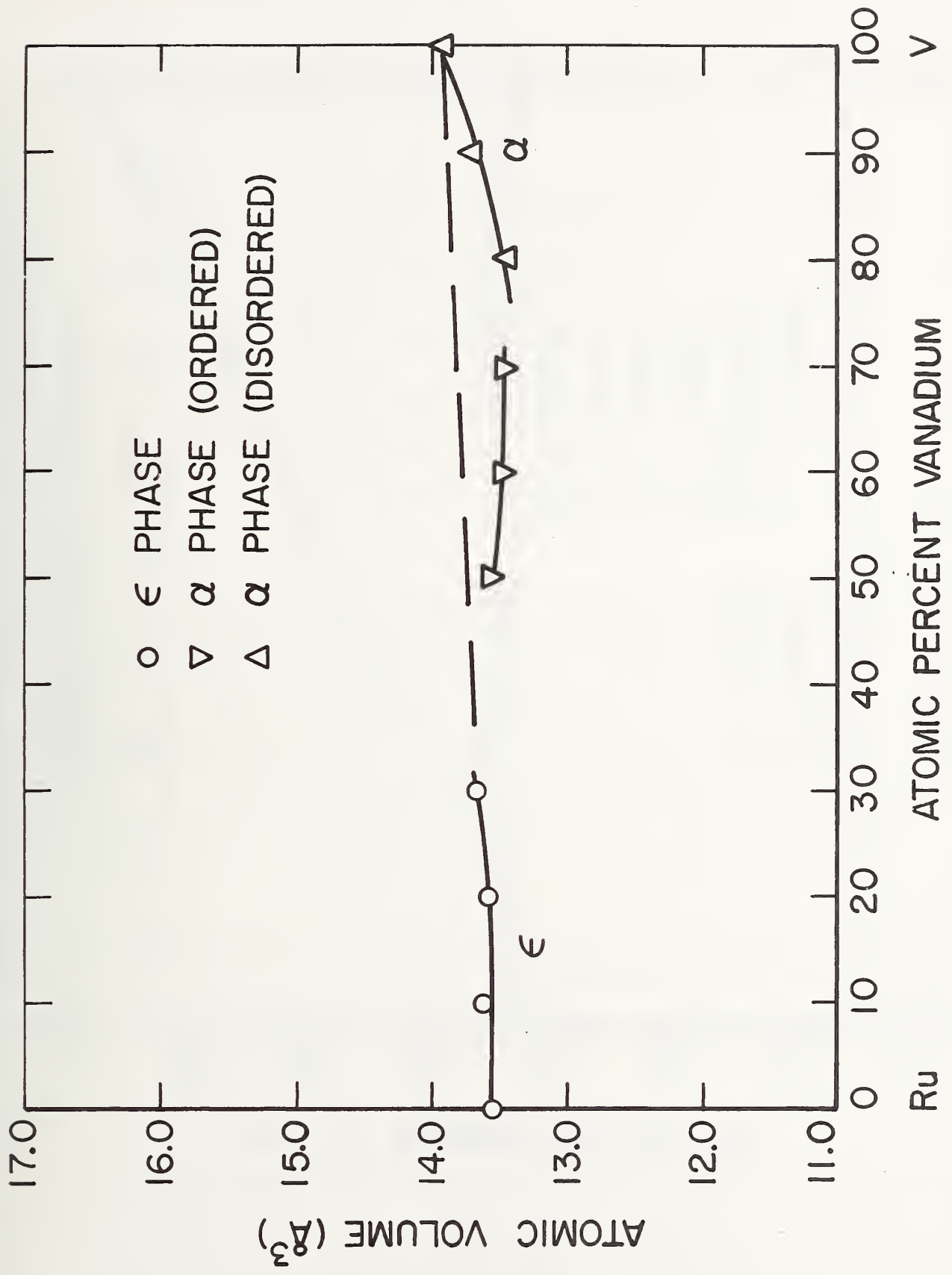


Fig. 37 - Atomic volumes of V-Ru alloys

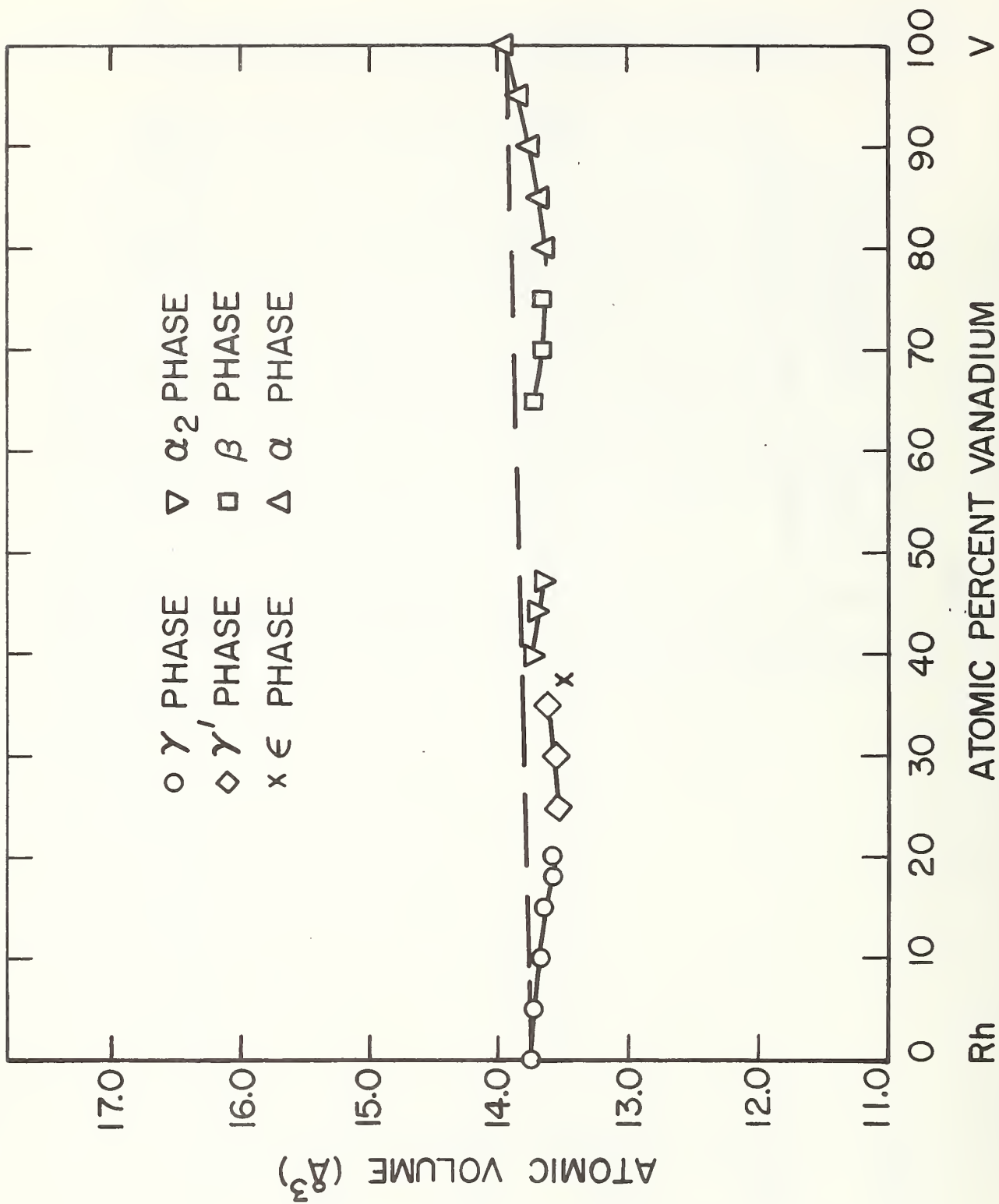


Fig. 38 - Atomic volumes of V-Rh alloys

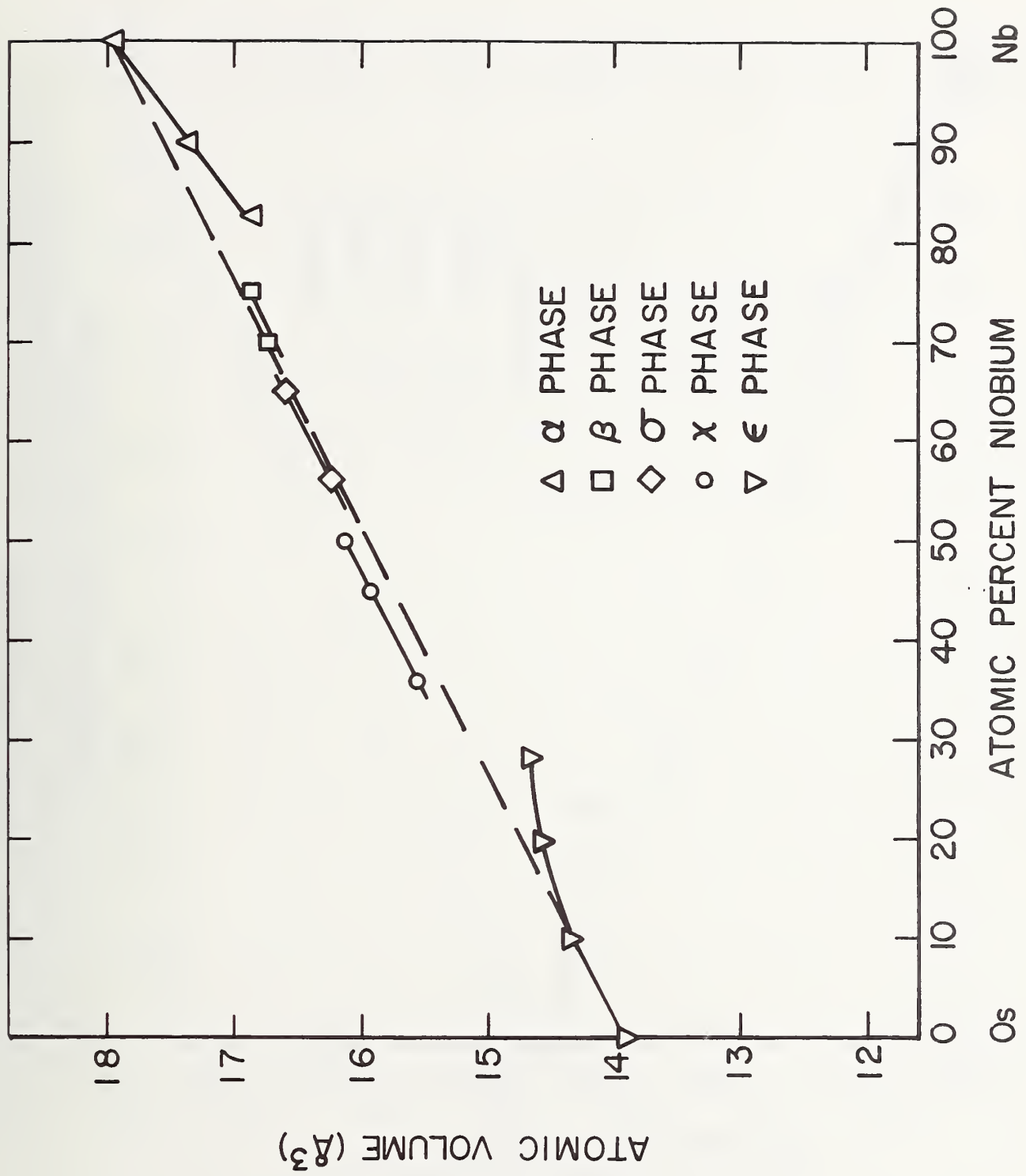


Fig. 39 - Atomic volumes of Nb-Os alloys

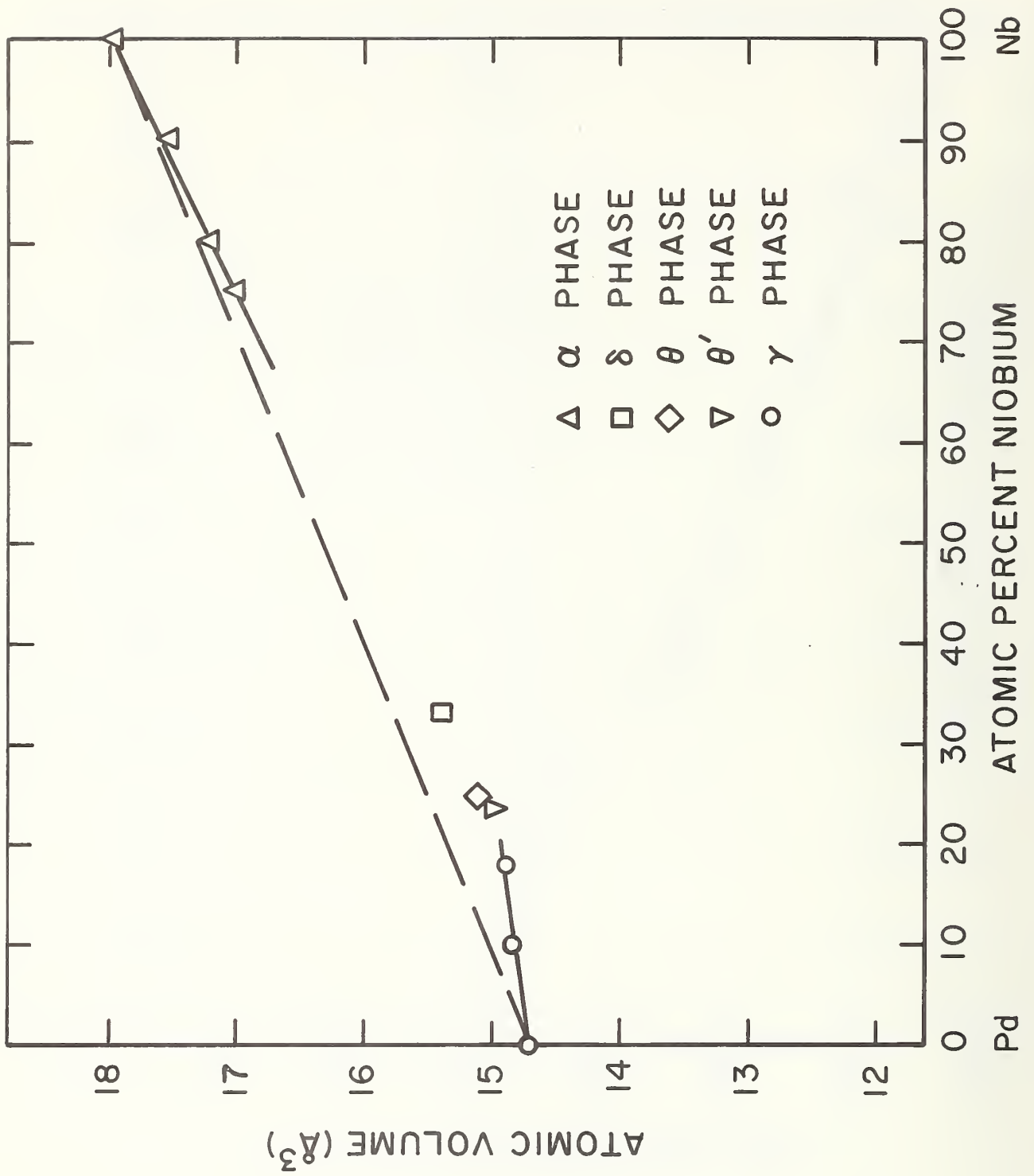


Fig. 40 - Atomic volumes of Nb-Pd alloys

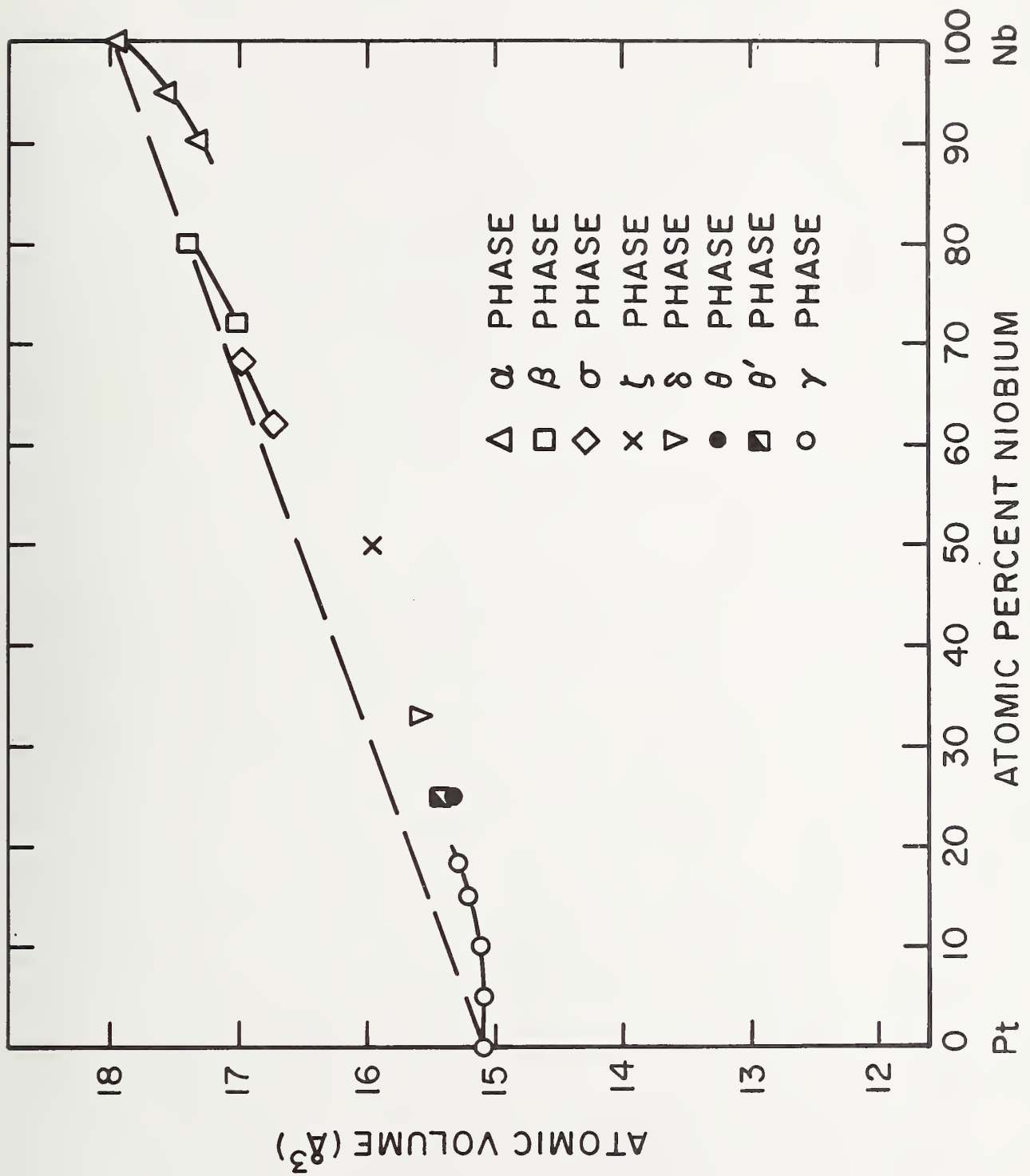


Fig. 41 - Atomic volumes of Nb-Pt alloys

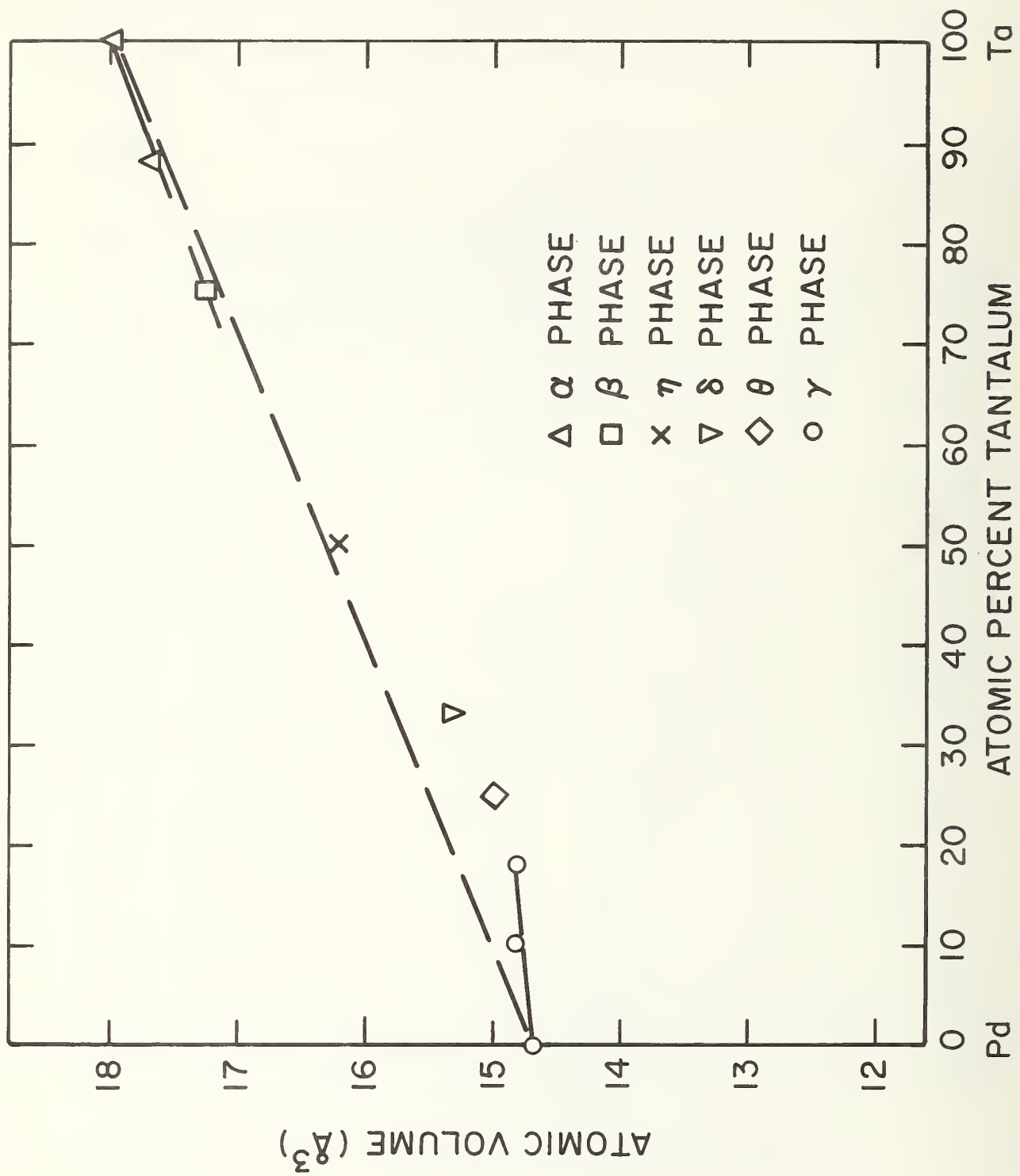


Fig. 42 - Atomic volumes of Ta-Pd alloys



